N°d'ordre NNT : 2022ISAL0116

**THESE de DOCTORAT DE L'INSA LYON,**
**membre de l'UNIVERSITE DE LYON**

délivré en partenariat international avec
**Ecole Nationale d'Ingénieurs de Tunis,**
**membre de l'UNIVERSITE DE TUNIS EL MANAR**

**Ecole Doctorale *MEGA n° 162***

**Spécialité / discipline de doctorat :**
***INGÉNIERIE MÉCANIQUE***

Soutenue publiquement le **06/12/2022**, par :
**Sarra KAROUI**

---

# Contribution to the homogenization of a fibered layer in large deformation: AN ITERATIVE DECOUPLED METHOD

# Contribution à l'homogénéisation d'une nappe fibrée en grande déformation: UNE MÉTHODE ITÉRATIVE DÉCOUPLÉE

---

| | | | |
|---|---|---|---|
| Moez CHAFRA | Professeur | Université de Tunis El Manar (TN) | *Président* |
| Mikaël BARBOTEU | Professeur | Université de Perpignan Via Domitia (FR) | *Rapporteur* |
| Adnane BOUKAMEL | Professeur | Ecole Centrale de Casablanca (MAR) | *Rapporteur* |
| Moez CHAFRA | Professeur | Université de Tunis El Manar (TN) | *Examinateur* |
| Olfa TRABELSI | Maîtresse de conf. | Université de Technologie de Compiègne (FR) | *Examinatrice* |
| Yves RENARD | Professeur | INSA-Lyon (FR) | *Directeur* |
| Makrem ARFAOUI | Maître de conf. | ENIT-UTM (TN) | *Co-Directeur* |
| Khalil MANSOURI | Maître assistant | ENIT-UTM (TN) | *Encadrant* |
| Charlie DOUANLA-LONTSI | Ingénieur | Michelin (FR) | *Encadrant indus.* |
| Thomas HOMOLLE | Ingénieur | Michelin (FR) | *Encadrant indus.* |

# Département FEDORA – INSA Lyon - Ecoles Doctorales

| SIGLE | ECOLE DOCTORALE | NOM ET COORDONNEES DU RESPONSABLE |
|---|---|---|
| CHIMIE | **CHIMIE DE LYON**<br>**https://www.edchimie-lyon.fr**<br>Sec. : Renée EL MELHEM<br>Bât. Blaise PASCAL, 3e étage<br>secretariat@edchimie-lyon.fr | **M. Stéphane DANIELE**<br>C2P2-CPE LYON-UMR 5265<br>Bâtiment F308, BP 2077<br>43 Boulevard du 11 novembre 1918<br>69616 Villeurbanne<br>**directeur@edchimie-lyon.fr** |
| E.E.A. | **ÉLECTRONIQUE, ÉLECTROTECHNIQUE, AUTOMATIQUE**<br>**https://edeea.universite-lyon.fr**<br>Sec. : Stéphanie CAUVIN<br>Bâtiment Direction INSA Lyon<br>Tél : 04.72.43.71.70<br>secretariat.edeea@insa-lyon.fr | **M. Philippe DELACHARTRE**<br>INSA LYON<br>Laboratoire CREATIS<br>Bâtiment Blaise Pascal, 7 avenue Jean Capelle<br>69621 Villeurbanne CEDEX<br>Tél : 04.72.43.88.63<br>**philippe.delachartre@insa-lyon.fr** |
| E2M2 | **ÉVOLUTION, ÉCOSYSTÈME, MICROBIOLOGIE, MODÉLISATION**<br>**http://e2m2.universite-lyon.fr**<br>Sec. : Bénédicte LANZA<br>Bât. Atrium, UCB Lyon 1<br>Tél : 04.72.44.83.62<br>secretariat.e2m2@univ-lyon1.fr | **Mme Sandrine CHARLES**<br>Université Claude Bernard Lyon 1<br>UFR Biosciences<br>Bâtiment Mendel<br>43, boulevard du 11 Novembre 1918<br>69622 Villeurbanne CEDEX<br>**sandrine.charles@univ-lyon1.fr** |
| EDISS | **INTERDISCIPLINAIRE SCIENCES-SANTÉ**<br>**http://ediss.universite-lyon.fr**<br>Sec. : Bénédicte LANZA<br>Bât. Atrium, UCB Lyon 1<br>Tél : 04.72.44.83.62<br>secretariat.ediss@univ-lyon1.fr | **Mme Sylvie RICARD-BLUM**<br>Institut de Chimie et Biochimie Moléculaires et Supramoléculaires (ICBMS) - UMR 5246 CNRS - Université Lyon 1<br>Bâtiment Raulin - 2ème étage Nord<br>43 Boulevard du 11 novembre 1918<br>69622 Villeurbanne Cedex<br>Tél : +33(0)4 72 44 82 32<br>**sylvie.ricard-blum@univ-lyon1.fr** |
| INFOMATHS | **INFORMATIQUE ET MATHÉMATIQUES**<br>**http://edinfomaths.universite-lyon.fr**<br>Sec. : Renée EL MELHEM<br>Bât. Blaise PASCAL, 3e étage<br>Tél : 04.72.43.80.46<br>infomaths@univ-lyon1.fr | **M. Hamamache KHEDDOUCI**<br>Université Claude Bernard Lyon 1<br>Bât. Nautibus<br>43, Boulevard du 11 novembre 1918<br>69 622 Villeurbanne Cedex France<br>Tél : 04.72.44.83.69<br>**hamamache.kheddouci@univ-lyon1.fr** |
| Matériaux | **MATÉRIAUX DE LYON**<br>**http://ed34.universite-lyon.fr**<br>Sec. : Yann DE ORDENANA<br>Tél : 04.72.18.62.44<br>yann.de-ordenana@ec-lyon.fr | **M. Stéphane BENAYOUN**<br>Ecole Centrale de Lyon<br>Laboratoire LTDS<br>36 avenue Guy de Collongue<br>69134 Ecully CEDEX<br>Tél : 04.72.18.64.37<br>**stephane.benayoun@ec-lyon.fr** |
| MEGA | **MÉCANIQUE, ÉNERGÉTIQUE, GÉNIE CIVIL, ACOUSTIQUE**<br>**http://edmega.universite-lyon.fr**<br>Sec. : Stéphanie CAUVIN<br>Tél : 04.72.43.71.70<br>Bâtiment Direction INSA Lyon<br>mega@insa-lyon.fr | **M. Jocelyn BONJOUR**<br>INSA Lyon<br>Laboratoire CETHIL<br>Bâtiment Sadi-Carnot<br>9, rue de la Physique<br>69621 Villeurbanne CEDEX<br>**jocelyn.bonjour@insa-lyon.fr** |
| ScSo | **ScSo***<br>**https://edsciencessociales.universite-lyon.fr**<br>Sec. : Mélina FAVETON<br>INSA : J.Y. TOUSSAINT<br>Tél : 04.78.69.77.79<br>melina.faveton@univ-lyon2.fr | **M. Bruno MILLY**<br>Université Lumière Lyon 2<br>86 Rue Pasteur<br>69365 Lyon CEDEX 07<br>**bruno.milly@univ-lyon2.fr** |

*ScSo : Histoire, Géographie, Aménagement, Urbanisme, Archéologie, Science politique, Sociologie, Anthropologie

*"An Oak tree is a daily reminder that great things often have small beginnings."*

Matshona Dhliwayo

# *Acknowledgements*

These years of thesis were rich in learning, meetings, travels and challenges. But the final result in this manuscript does not reflect the many twists and turns during these years. I would like to thank the people without whom this work would not have been possible.

First of all, I would like to thank Khalil Mansouri for having accompanied me in this adventure until the end of this thesis. I would also like to thank my two thesis directors, Yves Renard and Makrem Arfaoui, for having entrusted me with this subject and for having trusted me to carry out a large part of these four years outside the walls of a single laboratory and initiated me to the research. Last but not least, I am very grateful to all three of you for your advice and help on all aspects of this thesis.

I would also like to thank the Michelin team, Thomas Homolle, Philippe Bussetta and Charlie Douanla-Lontsi for welcoming me during this thesis in the Michelin team as well as the opportunities offered to better understand composite materials.

I thank all my colleagues of the LaMCoS, past and present. My time in the laboratory was always very pleasant thanks to you and your good mood. I would also like to thank my office colleague and my friend Marjolaine who accompanied me during my beautiful and miserable times.

I sincerely thank Saîd Mabchour, Aurelien Saulot, Arnaud Sandel and all the teaching team of the FIMI and Mechanics departments with whom I had the chance to teach and convince me that the life of a teacher is hard.

I also thank Mikaël Barboteu and Adnane Boukamel for accepting to report this work and also the rest of my jury for freeing up time to participate in my defense.

My last thanks go to my aunts, my cousins, my person and my best friend for their encouragement and support. To my mother, who more than any other person, has lived these years of thesis with me, thank you for your presence and support.

# Contents

# List of Figures

# List of Tables

# List of Symbols

TABLE 1: Summary table

| | Definition | Comments |
|---|---|---|
| $\mathbb{1}$ | 2nd-order identity tensor | |
| $\mathbb{I}$ | 4th-order symmetric identity tensor | |
| $X$ | Macro-scale reference position vector | |
| $x$ | Macro-scale current position vector | |
| $Y$ | Micro-scale reference position vector | |
| $y$ | Micro-scale current position vector | |
| $\tilde{u}$ | Macro-scale displacement field | $\tilde{u}(X) = x - X$ |
| $\tilde{\varphi}$ | Macro-scale nonlinear deformation function | $\tilde{\varphi}(X) = X + \tilde{u}(X)$ |
| $\tilde{H}$ | Macro-scale displacement gradient | $d\tilde{u} = \tilde{H}.dX$ ; $\tilde{H}(X) = \nabla_X \tilde{u}(X)$ |
| $u^*$ | Fluctuation displacement | |
| $c$ | Constant vector independent of $Y$ | |
| $w$ | Micro-scale displacement of the unit cell | $w(X;Y) = y - Y = \tilde{H}(X).Y + u^*(X;Y) + c(X)$ |
| $\varphi$ | Micro-scale nonlinear deformation function | $y = \varphi(X;Y) = Y + w(X;Y)$ |
| $\tilde{F}$ | Macro-scale deformation gradient | $dx = \tilde{F}.dX \quad ; \quad \tilde{F} = \mathrm{Grad}_X(x)$ |
| $H$ | Micro-scale displacement gradient | $H(X;Y) = \nabla_Y w(X;Y)$ |
| $F$ | Micro-scale deformation gradient | $F(X;Y) = H(X;Y) + \mathbb{1}$ |
| $J$ | Macro-scale Jacobien | $J = \det(\tilde{F})$ |
| $\tilde{C}$ | Macro-scale Right Cauchy-Green deformation tensor (Lagrangian description) | $\tilde{C} = \tilde{F}^t.\tilde{F}$ |
| $\tilde{E}$ | Macro-scale Green-Lagrange deformation tensor | $\tilde{E} = \frac{1}{2}(\tilde{C} - \mathbb{1}) = \frac{1}{2}(\tilde{H} + \tilde{H}^t + \tilde{H}^t\tilde{H})$ |
| $\tilde{B}$ | Macro-scale Left Cauchy-Green deformation tensor (Eulerian description) | $\tilde{B} = \tilde{F}.\tilde{F}^t$ |
| $\tilde{A}$ | Macro-scale Euler-Almansi deformation tensor | $\tilde{A} = \frac{1}{2}(\mathbb{1} - \tilde{B}^{-1})$ |
| $P$ | Micro-scale first Piola–Kirchhoff stress tensor | $P = \mathcal{F}(F)$ |
| $\tilde{P}$ | Macro-scale first Piola–Kirchhoff stress tensor | $\tilde{P} = \langle P \rangle$ |
| $\tilde{S}$ | Macro-scale second Piola–Kirchhoff stress tensor (Lagrangian description) | $\tilde{S} = \tilde{F}^{-1}\tilde{P}$ |
| $S$ | Micro-scale second Piola–Kirchhoff stress tensor | |
| $\tilde{L}$ | Macro-scale Eulerian velocity gradient tensor | $\tilde{L} = \dot{\tilde{F}}\tilde{F}^{-t}$ |
| $\tilde{D}$ | Macro-scale tensor deformations' rate | $\tilde{D} = (\dot{\tilde{F}}\tilde{F}^{-t})_{sym}$ |

*Next page*

**Table 1 – *Summary table***

| | Definition | Comments |
|---|---|---|
| $N^{[J]}$ | Micro-scale outward unit normal surface $[J]$ vector in the reference configuration | |
| $n^{[J]}$ | Micro-scale outward unit normal surface $[J]$ vector in the current configuration | |
| $T$ | Micro-scale Piola traction vector | |
| | Mixed description | $T^{[J]} = P.N^{[J]}$ |
| | Lagrangian description | $T^{[J]} = S.N^{[J]}$ |
| $\nabla_Y$ | Micro-scale divergence operator | |
| $\nabla_X$ | Macro-scale divergence operator | |
| $\rho_0, \rho$ | Micro-scale mass density in the initial, current configuration | $\rho_0 = J\rho$ |
| $\Longrightarrow$ | **here we do not distinguish the micro- and** | **macro-scale variables below** |
| $\tilde{W}_h$ | Homogenized strain energy density function | |
| $\mathbf{A}, \mathbf{B}$ | Unit vector along the fiber | |
| $I_1$ | *Classical invariants* | $I_1 = tr(C)$ |
| $I_2$ | | $I_2 = \frac{1}{2}\left[(tr(C))^2 - tr(C^2)\right]$ |
| $I_3$ | | $I_3 = J^2 = det(C)$ |
| $I_4$ | | $I_4 = \mathbf{A}.C\mathbf{A}$ |
| $I_5$ | | $I_5 = \mathbf{A}.C^2\mathbf{A}$ |
| $I_6$ | | $I_6 = \mathbf{B}.C\mathbf{B}$ |
| $I_7$ | | $I_7 = \mathbf{B}.C^2\mathbf{B}$ |
| $I_8$ | | $I_8 = (\mathbf{A}.\mathbf{B})\mathbf{A}.C\mathbf{B}$ |
| $\underline{F}$ | Isochoric deformation gradient | $\underline{F} = J^{-1/3}F$ |
| $\underline{C}$ | Isochoric Cauchy-Green strain tensor | $\underline{C} = \underline{F}^t\underline{F} = J^{-2/3}F^tF = I_3^{-1/3}C$ |
| $\underline{I}_i$ | *Isochoric invariants* | $\underline{I}_i = J^{-2/3}I_i$ for $i \in \{1,4,6\}$ |
| $\underline{I}_j$ | | $\underline{I}_j = J^{-4/3}I_j$ for $j \in \{2,5,7,8\}$ |
| $\underline{I}_1$ | | $\underline{I}_1 = tr(\underline{C})$ |
| $\underline{I}_2$ | | $\underline{I}_2 = \frac{1}{2}\left[(tr(\underline{C}))^2 - tr(\underline{C}^2)\right]$ |
| $\underline{I}_4$ | | $\underline{I}_4 = \mathbf{A}.\underline{C}\mathbf{A}$ |
| $\underline{I}_5$ | | $\underline{I}_5 = \mathbf{A}.\underline{C}^2\mathbf{A}$ |
| $\underline{I}_6$ | | $\underline{I}_6 = \mathbf{B}.\underline{C}\mathbf{B}$ |
| $\underline{I}_7$ | | $\underline{I}_7 = \mathbf{B}.\underline{C}^2\mathbf{B}$ |
| $\underline{I}_8$ | | $\underline{I}_8 = (\mathbf{A}.\mathbf{B})\mathbf{A}.\underline{C}\mathbf{B}$ |

*Dedicated to my mom, my family and the one in my heart ...*
*Thank you...*

# General introduction

### Industrial motivation

The design of new tire ranges, for areas such as emerging countries where usage conditions can be particularly severe (overloading, road conditions, humidity, high temperature, etc.) is confronted with the management of complex trade-offs such as the need to reduce material quantities while keeping implicit performance such as endurance at a level equivalent or even superior to what it is on current ranges. Such a design approach implies making significant progress on endurance performance, notably by re-exploring the material modelling strategies currently implemented in our mechanical simulation chain. In this perspective, revisiting the thermomechanical description of the reinforcement plies is an important step.

Reinforcement plies are one of the main components of tires. Therefore, the performance and durability of tires are directly related to the mechanical strength of these plies. These objects are subjected to various extreme stresses (extension/compression, shear or bending) from the manufacturing process to the actual use in tires. In our mechanical simulation chain, the reinforcement plies are modelled as homogenized composite materials, with as main assumption the approximation of the exact geometry of the layer (fig. 1-a) by a two-dimensional geometry (fig. 1-b) which keeps the same volume fraction of reinforcements ([Lig11]). In other words, the cylindrical reinforcements are approximated by straight blocks of the same length as the sheets. If this model correctly accounts for the extensional behaviour of the cables, it does not allow for example to describe the transverse shear stiffening at very large deformations (typically simulation of breaking energy, perforation or pinch shock tests).

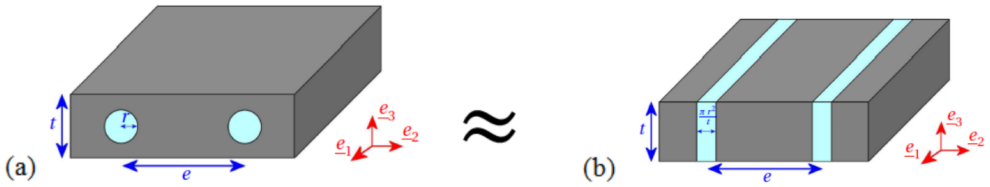


FIGURE 1: Approximation of a unidirectional fiber layer geometry (a) by a two-dimensional geometry (b)

The industrial objective of this thesis will be to propose an approach to improve the current homogenization model of a fibred layer through numerical approaches in order to better predict their behaviour at high deformations.

### Scientific motivation

The existence of fiber-reinforced rubber-like composites in natural and artificial materials and structures has long been known, and several fields, including manufacturing, plants, geomechanics, and biomechanics, have attested to this fact. At

a macroscale observation scale, some fiber reinforced rubber-like composites, such as soft tissues [Fun13], appear homogeneous, yet at a specific microscale length, they exhibit fibrous microstructure behaviour. At a macroscopic observation scale, several other reinforced rubber-like composites, such as the fiber-reinforced layers in the tyres that serve as the subject of this thesis [Lig11], appear heterogeneous. These materials and structures are classified as fiber-embedded composites and can be physically represented as a pliable matrix material with aligned cylindrical stiffer fiber inclusions. Two methodologies can be used to model the mechanical behaviour of these materials: micro-mechanical [NNH13a] and macro-mechanical phenomenology [TN04]. The micro-macro or homogenization technique is useful for comprehending and designing the physical behaviour of materials. However, this method is expensive for commercial use, particularly for nonlinear material behaviour [Gee+17]. The macro-mechanical phenomenological continuum technique, where the model's parameters are calibrated using data from macroscopic experiments, is an effective and straightforward way to construct constitutive equation [TN04]. Despite having these desirable characteristics, these phenomenological models are hampered by a lack of actual knowledge about the microstructure of fiber-reinforced rubber-like composites.

Thus, the scientific objective of this thesis is the development of a mechanical and numerical methodology linking the micromechanical and the macromechanical phenomenological approaches while keeping their advantages and reducing their inconveniences. This is the decoupled homogenization method. To do this, the fiber and the matrix will be considered as hyperelastic materials. This is a first approximation which can be enriched in other works.

Classical homogenization theory [Esh57]; [Esh59]; [HS63]; [SP80]; [SP83]; [BLP11] has long been an essential tool to characterize the behaviour of composite materials with periodic or quasi-periodic microstructures and to derive numerical approximations at reasonable costs, especially in the context of linear materials where homogenized constitutive laws can often be identified with a limited number of parameters to be determined.

In the context of the homogenization of hyperelastic composites [Hil63]; [Hil72]; [Ogd74] apart for very specific situations in terms of constitutive laws used at the microscopic scale and even in terms of loading (see [CH71]; [BO13]; [He99]; [HLQF06]; [DHS06a]; [LPI10]), it is not possible to identify the homogenized law in the nonlinear case which makes the decoupling between the micro and macroscopic scales impossible to reach. This has given rise to the development of the so-called computational homogenization, which has motivated a very large number of studies [DEGA16]; [NZY11]; [MHY11]. We refer for instance to the monograph [Yvo19] and the reference therein for an overview of computational homogenization techniques. A classical numerical strategy to keep the micro-macro coupling is the use of the so called $FE^2$ approximation [RM87]; [SBM98]; [Fey99]; [FC00]; [TK01]. This type of strategy (also called multilevel finite element method) consists in solving a finite element approximation on the RVE (representative volume element of the microstructure) at each integration point of a finite element method for the macroscopic problem. It gives very good results, but is extremely expensive in terms of computational resources, even when model reduction strategies are applied (as proposed for instance in [YH07]; [MYH08]; [Her+14]; [Ekr+22]). A discussion of the extension to second order homogenization for an enhanced accuracy can be found for instance in [OOM18] and the reference therein, however, this kind of strategy is even more computationally expensive which can represent a serious obstacle to its use.

Within this frame of reference, the decoupled numerical method introduced by

Terada et al. [Ter+13a] allows to recover a computational cost comparable to a classical structural mechanics calculation with a homogeneous material (see also [PSK20]; [Sai+21] for further developments). This is at the cost of an additional approximation on the homogenized law whose shape is preselected with a more or less important number of parameters. This law aims at characterizing the global response of the micro-structure at the RVE level, at least in the solicitation range of interest for the macroscopic level. The method can be used either with simple homogenized laws, in the case such a specific simple law can be expected, or either with more complex or even fully parametric laws. A possibility in order to identify a fully parametric law is to take advantage of the approximation property of artificial neural network (see [LYH15]; [Kal+22]). An optimization of the homogenized law parameters is performed off-line on a training set composed of numerical experiments coming from a finite element approximation of the boundary value problem (BVP) defined at the micro-scale on the RVE. The shape of the chosen homogenized law is obviously crucial for the proper functioning and efficiency of the method. Once the parameters of the homogenized law have been identified, it can be used to represent the micro-scale response and then to evaluate the macro-scale response.

In the context of modern continuum mechanics [TN04], Rivlin developed in a series of papers [Riv48c]; [Riv48a]; [Riv48b]; [RS51a]; [Riv51] a formalism for the modelling of large elastic deformations of isotropic materials. The main idea of this theory is based on Georges Green's method established in 1840 [Tru52] by modelling the elastic behaviour with a strain energy function: the elastic material is named hyperelastic material. The effect of fiber reinforced material was first analyzed by resolving some boundary value problems of an isotroipic hyperelastic matrix reinforced with inextensible cords [AR55]. This exact analytical approach uses the semi-inverse method. Another way to model the effect of fiber reinforced material was initiated by [ER97]. The strain energy is assumed to be a function of some strain invariants that are used to model the fibres directions effect with some structural tensors [Spe72]; [Boe79]. This phenomenological approach was used to develop some popular hyperelastic anisotropic models [WMG96a]; [BB98]; [Kal00a]; [HGO00]; [HGO04]; [HS05]. The analysis of the ellipticity, convexity, polyconvexity or other inequality [MH94] of constitutive law was extended to anisotropy in [SN03b]; [Bal+06] among others.

The thesis plan will be presented in the following:

The first chapter is an overview on the different multi-scales and homogenization methods. The first part of this chapter is a survey on the different multi-scales and homogenization approaches existing in the literature. On the other hand, the second part presents in the most explicit way a presentation of coupled and decoupled homogenization in large deformations.

The second chapter is dedicated for the isotropic and anistropic hyperelasticity. Focusing on hyperelastic behaviour, a brief recall is made for the mathematical tools for the modeling of such mechanical behaviour.

The third chapter is devoted to the development of a decoupled computational homogenization methodology. A comparison of some different homogenized tranverse isotropic potentials in term of local error is performed. The original version of the tranverse isotropic potentials from litterature are improved in order to get a better calibration.

In the fourth chapter, tests on the macro-scale of a fiber reinforced layer are performed. A comparison is done both in term of local and global error with a fully

discretized heterogeneous layer. An iterative correction method is developed and tests of its effectiveness in term of local and global error are achieved.

# Chapter 1

# Homogénéisation et approche multi-échelle

## 1.1 Introduction

La modélisation multi-échelle du comportement non linéaire des matériaux est un sujet tellement vaste qu'il est presque impossible de fournir une vue d'ensemble exhaustive de toutes les méthodes développées dans le passé. Nous allons plutôt en donner un bref aperçu, en nous concentrant sur quelques méthodes sélectionnées qui seront discutées plus en détail dans ce chapitre. La mise à l'échelle de la réponse mécanique non linéaire de matériaux hétérogènes est le domaine d'application considéré ici. L'objectif principal de ce chapitre est de résumer les stratégies d'homogénéisation couplée et découplée. Le chapitre est organisé comme suit : La première section présente un survol des différentes méthodes multi-échelle. La section 2 présente l'homogénéisation numérique nonlinéaire trouvée dans les ouvrages de référence. Dans la section 3, on introduit la définition de l'homogénéisation couplée classique en grandes déformations. La section 4 décrit l'homogénéisation computationnelle découplée et un diagramme résumant la méthodologie d'homogénéisation proposée par cette thèse.

## 1.2 Classification des méthodes multi-échelle

Les méthodes multi-échelles ne peuvent pas être classées dans une seule catégorie. Différentes catégories de méthodes multi-échelles peuvent être identifiées d'un point de vue méthodologique, [VE07] [Wei11][Fis06][Fis10a], en fonction de l'emplacement et de la géométrie de l'échelle hétérogène. Trois catégories de problèmes peuvent être mentionnées :

- Problèmes comportant des détails isolés (par exemple, des défauts, des cavités et des fissures) qui doivent être traités avec une résolution et une précision élevées. Le problème à échelle trés petite "fine" est alors contraint à une petite région du domaine global. Ce type de problème est fréquemment appelé "Problème à échelles multiples" plutôt que "Problème multi-échelles".
- Problèmes dans lesquels la réponse macroscopique doit être extraite du comportement sous-jacent à petite échelle dans de grandes parties du domaine. L'échelle macroscopique effective est déterminée en sondant la "micro-échelle".
- Problèmes mixtes, combinant les deux catégories précédentes, dans lesquels une auto-similarité à travers l'échelle est observée [VE07].

Pour une illustration plus complète, le lecteur peut consulter [Fis06]; [Fis10a]. Une autre classification connue dans la littérature est basée sur la "Formulation du problème" [Gee+17].

- **Les méthodes concurrentes** : les méthodes concurrentes formulent le problème tout en traitant simultanément les deux échelles. En général, différentes échelles de temps et de longueur sont appliquées à un domaine unique ou à plusieurs domaines. En réalité, le terme "concurrent" est souvent limité aux procédures où différentes échelles (et méthodologies) sont employées dans différents domaines.

- **Les méthodes hiérarchique** : les deux échelles sont liées de manière hiérarchique, ce qui implique que différentes échelles sont prises en compte et couplées dans la même zone d'un domaine. Le lien hiérarchique peut être créé, par exemple, par la moyenne en volume des variables du domaine ou par la simple identification des paramètres.

- **Les méthodes hybrides** : les méthodes hybrides, telles que les méthodes multigrilles [MB07], les méthodes par éléments finis généralisées [PD15], les méthodes basées sur les ondelettes et les méthodes quasi-continu, révèlent généralement des propriétés de diverses classes

Parmi les méthodes multi-échelles énumérées ci-dessus, une attention particulière sera accordée aux méthodes d'homogénéisation numérique. Cette classe de méthode est considérée comme hiérarchique, même si les processus de résolution du problème non-linéaire sont itératives et imbriqués, c'est-à-dire que l'équilibre aux deux échelles est établi simultanément. Ces méthodes sont essentiellement basées sur l'intégration sur de petites échelles de longueur (par exemple, sur un volume élémentaire représentatif VER microstructurale).

## 1.3 Homogénéisation numérique nonlinéaires

La théorie classique de l'homogénéisation [BLP11]; [SP80]; [SP83] est depuis longtemps considérée comme un outil essentiel pour caractériser le comportement des matériaux composites à microstructures périodiques ou quasi-périodiques. Pour dériver des approximations numériques à des coûts raisonnables, surtout dans le cas des matériaux linéaires où des lois de comportement homogénéisées peuvent souvent être identifiées avec un nombre limité de paramètres.

En dehors de situations très spécifiques en termes de lois de comportement utilisées à l'échelle microscopique et en termes de conditions aux limites (de chargement) [CH71]; [BO13]; [He99]; [HLQF06], il n'est pas possible d'identifier une loi homogénéisée dans le cas non linéaire ce qui rend impossible le découplage entre les échelles microscopique et macroscopique. Ceci a donné lieu au développement de technique d'homogénéisation dite computationnelle ou numérique (Computational Homogenization CH).

Au cours des dernières décennies, des progrès substantiels ont été réalisés dans l'homogéneisation numérique (HN) à deux échelles de solides multiphases complexes [GKB10]. Cette méthode est essentiellement basée sur la résolution imbriquée de deux problèmes aux limites, à chaque échelle (échelle macroscopique-échelle microscopique). Bien que coûteuses en calcul, les procédures développées permettent d'évaluer l'influence macroscopique des paramètres microstructurels de

manière assez directe. La technique du premier ordre de cette méthode est maintenant bien établie et largement utilisée par la communauté scientifique et technique [Suq85]; [GLM96]; [GLR01]; [SBM98]; [MSS99a]; [MSS99b]; [FC00]; [Ter+00]; [KBB01]; [TK01]; [Mie02]. Depuis la fin des années 1990, de nombreuses contributions dans le cadre de l'homogénéisation numérique de différents matériaux ont été développées pour, par exemple, les milieux poreux (Ehlers et al., 2003)[Ehl+03], les matériaux cellulaires (Ebinger et al., 2005)[ESD05], les métaux polycristallins et les matériaux granulaires. Beaucoup d'entre eux se sont concentrés sur des problèmes linéaires, et pour des raisons de compacité, nous limitons cet aperçu aux problèmes non linéaires qui ont été résolus depuis. Plusieurs extensions de la méthode d'homogénéisation numérique HN ont été proposées dans la littérature :

- Homogénéisation numérique d'ordre supérieur : cette variante d'ordre supérieure utilise une description enrichie de la cinématique à l'échelle macro, qui est utilisée pour construire un problème à l'échelle micro plus complexe. L'homogénéisation permet d'extraire le tenseur des contraintes de Cauchy, ainsi que le tenseur des contraintes d'ordre supérieur et toutes les tangentes correspondantes [GKB01]; [GKB03]; [KGB02]; [KGB04a]; [KGB04b]; [Kou04]; [KPB08]; [KPB10]; [BG10]. L'approche dite "Computational Continua" [FK10]; [FFF15] est une variante qui relâche la condition de continuité d'ordre supérieur.

- Homogénéisation-Localisation continue-discontinue : dans cette variante la transition de l'endommagement à la rupture est pris en considération (via la localisation) dans une approche multi-échelle. Elle est étudié par [LB07]; [BLS08]; [HHR08]. Les méthodes récemment développées de ce type reposent sur une solution adéquate pour remédier au manque de séparation d'échelle entre le problème macroscopique et microscopique (c'est-à-dire en prenant explicitement en compte la cinématique à micro-échelle à l'échelle macro). Les propriétés localisées à la micro-échelle doivent être incorporées directement dans la description à la macro-échelle sans moyennage. Des solutions ont été proposées dans lesquelles une bande discrète (discontinuité faible) est utilisée à l'échelle macroscopique [MPG07b]; [MPG07a], ainsi qu'un saut discontinu (discontinuité forte) à l'échelle macroscopique [CKG12a]; [Coe+12]; [Bos+14]; [BKG15]. Dans chaque cas, l'échelle micro est modélisée comme un domaine continu régulier, avec des modèles d'endommagement ou de plasticité appropriés. L'échelle macroscopique est enrichie, par des discontinuités intégrées ou des algorithmes de solution basés sur la méthode X-FEM (méthode des éléments finis étendue) ont été utilisés. Il convient de noter que des approches simplifiées ont été proposées pour établir un couplage volumétrique direct entre la taille d'un élément fini (à l'échelle macroscopique) et le Volume élémentaire représentatif VER localisateur à l'échelle microscopique (Gitman et al., 2008)[GAS08]. Contrairement aux méthodes précédemment citées, cette solution n'est plus vraiment de type homogénéisation et ressemble plutôt à une approche de décomposition de domaine dans laquelle l'échelle fine est intégrée comme un raffinement local.

- Instabilités géométriques microstructural : un autre cas qui viole la séparation d'échelle est induit par des instabilités locales (flambage) au niveau de la microstructure, comme on le rencontre typiquement dans les matériaux cellulaires. Ce cas a reçu une attention particulière dans les travaux de [MK02], et plus récemment dans [Nez+09].

- Homogénéisation numérique thermo-mécanique : ce schéma est un problème couplé, fournissant l'homogénéisation des problèmes thermiques et mécaniques couplés [ÖBG08a]; [ÖBG08b].
- Plaque et coque sous-structurées : l'homogénéisation numérique appliquée aux poutres, aux plaques et coques utilise la cinématique d'ordre supérieur déjà développée pour le schéma du second ordre. Les volumes élémentaires représentatifs VER sont homogénéisés dans le plan (de la plaque et coque) et intégrés dans leur épaisseur. Cette méthode permet de réaliser des homogénéisation numérique non linéaires pour des domaines continus de type plaques et coques [GCK07]; [CKG10]; [Con+15].
- Interfaces multi-échelles ou fissures cohésives : l'homogénéisation numérique des interfaces couple généralement une description de type zone cohésive à l'échelle macroscopique à un VER décrivant l'interfaciale à l'échelle microscopique [MKG08]; [Ver+10]; [Ngu+12]; [MM15].
- Problèmes multiphysiques : l'homogénéisation numérique a été étendu aussi à d'autres problèmes physiques (couplés), par exemple l'électromagnétisme [JCS13]; [ZM13]; [Niy+14]; [KSS14], les problèmes de diffusion [Nil+14], le frittage en phase liquide [ÖLR13], le transfert thermique [LRS10], ou impliquant des couplages chimiques [Yua+14].
- Problèmes de contact et de friction : le contact et la friction à petite échelle impliquent toujours des surfaces rugueuses, pour lesquelles une approche par homogénéisation numérique peut aider à résoudre le problème [DLW13]; [Tem14b].
- Dynamique des matériaux : l'extension du schéma pour intégrer la dynamique de la propagation des ondes et de la microinertie a été réalisée par Pham et al. (2013)[PKG13]. L'homogénéisation numérique a permis d'analyser les phénomènes non linéaires de transmission et d'atténuation des ondes, en intégrant les effets de résonance locale à l'intérieur de la microstructure. Les exemples typiques d'intérêt sont les métamatériaux acoustiques localement résonants.

Autres contributions récentes à la méthode d'homogénéisation numérique pour l'analyse des problème multi-échelles des matériaux peuvent être trouvées dans les ouvrages suivants :

- Milieux poreux, par exemple, Su et al. (2011)[SLR11] et Zhuang et al. (2015)[ZWZ15]
- Matériaux cellulaires, par exemple, Nguyen et Noels (2014)[NN14] et Iltchev et al. (2015)[Ilt+15]
- Matière molle, par exemple, Temizer (2014b)[Tem14a]
- métaux polycristallins, par exemple, Segurado et Llorca (2013)[SL13]
- Textiles techniques, par exemple, Fillep et al. (2015)[FMS15]
- Matériaux granulaires, par exemple, Liu et al. (2014)[Li+14]
- Matériaux biomécanique (os trabéculaire), par exemple, Wierszycki et al. (2014)[Wie+14]

- Plaques composites, par exemple, Helfen et Diebels (2014)[HD14]
- Matériaux pour des cellules de batterie Li-ion, par exemple, Salvadori et al. (2014)[SBG14]

Bien que CH soit une technique multi-échelle extrêmement puissante, elle s'accompagne d'un coût de calcul élevé. Néanmoins, la CH est naturellement parallélisable [MM15] et la méthode a démontré une excellente évolutivité, comme on le verra plus loin dans ce chapitre. Par ailleurs, l'accent est mis de plus en plus sur l'efficacité de cette méthode, qui fait appel à des techniques de calcul avancées et à des modèles d'ordre réduit [YH07]; [FL13]; [FHL14]; [KRB14].

Dans ce contexte, la méthode numérique découplée introduite par Terada et al. [Ter+13a] permet de retrouver un coût de calcul comparable à celui d'un calcul classique de mécanique des structures avec un matériau homogène (voir également [PSK20]; [Sai+21] pour plus de développements). Ceci au prix d'une approximation supplémentaire sur la loi homogénéisée dont la forme est présélectionnée avec un nombre plus ou moins important de paramètres. Cette loi vise à caractériser la réponse globale de la micro-structure au niveau VER, au moins dans le domaine de sollicitation qui intéresse le niveau macroscopique. La méthode peut être utilisée soit avec des lois simples homogénéisées, dans le cas où l'on peut s'attendre à une telle loi simple spécifique, soit avec des lois plus complexes ou même entièrement paramétriques. Une possibilité pour identifier une loi entièrement paramétrique est de tirer parti de la propriété d'approximation des réseaux neuronaux artificiels (voir [LYH15]; [Kal+22]). Une optimisation des paramètres de la loi homogénéisée est effectuée hors ligne sur un ensemble d'entraînement composé d'expériences numériques provenant d'une approximation par éléments finis du problème aux limites [1] défini à l'échelle micro sur le VER. La forme de la loi homogénéisée choisie est évidemment cruciale pour le bon fonctionnement et l'efficacité de la méthode. Une fois les paramètres de la loi homogénéisée sont identifiés, celle-ci peut être utilisée pour représenter la réponse à micro-échelle et ensuite pour évaluer la réponse à macro-échelle.

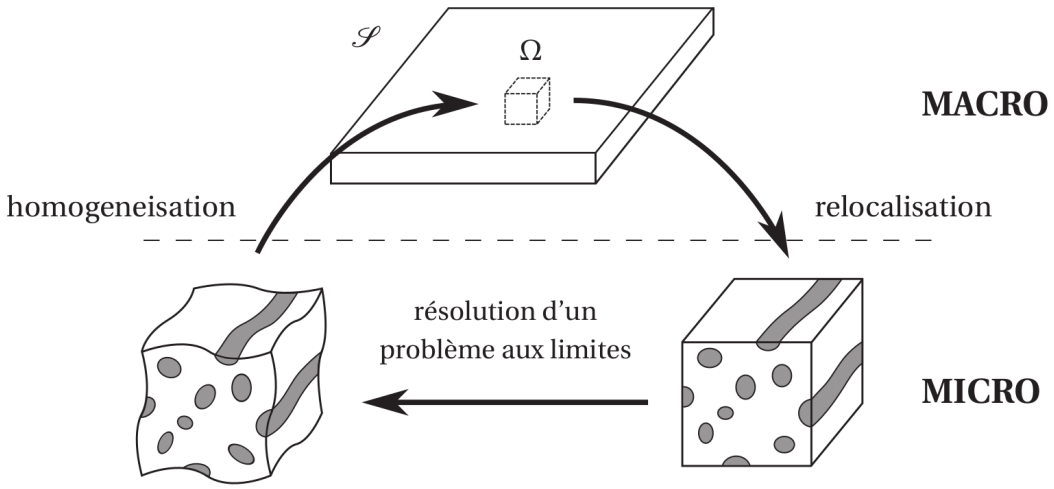


FIGURE 1.1: La méthode d'homogénéisation couplée à deux-échelles

[1] BVP en anglais boundary value problem

## 1.4 Homogénéisation couplée : Application à un problème en grande déformation

Pour contourner les problèmes de coût de calcul liés aux calculs imbriqués dans les méthodes d'homogéinisation numérique tel que FE$^2$ [FC00] figure1.1, des approches alternatives ont été introduites dans le but de développer des méthodes numériques découplées pour l'homogénéisation des matériaux hétérogènes avec des comportements non linéaires ou dépendants du temps.

- Une première approche directe, inspirée des procédures classiques d'identification expérimentale, utilise des tests virtuels sur des VER par le biais de calculs numériques élément finis pour identifier les lois de comportement macroscopiques empiriques [Ter+13b], [Ter+14a].
- Une deuxième approche permettant la construction de lois constitutives efficaces sans connaissance préalable de leur forme est cependant possible, mais dans certains cas restreints. Une deuxième classe de techniques est basée sur la construction d'une carte numérique matérielle entre les contraintes et les déformations effectives [TK95]; [TZO96]; [TW07]; [YGH09]; [YMH13]; [CSY12]; [Tra+11].

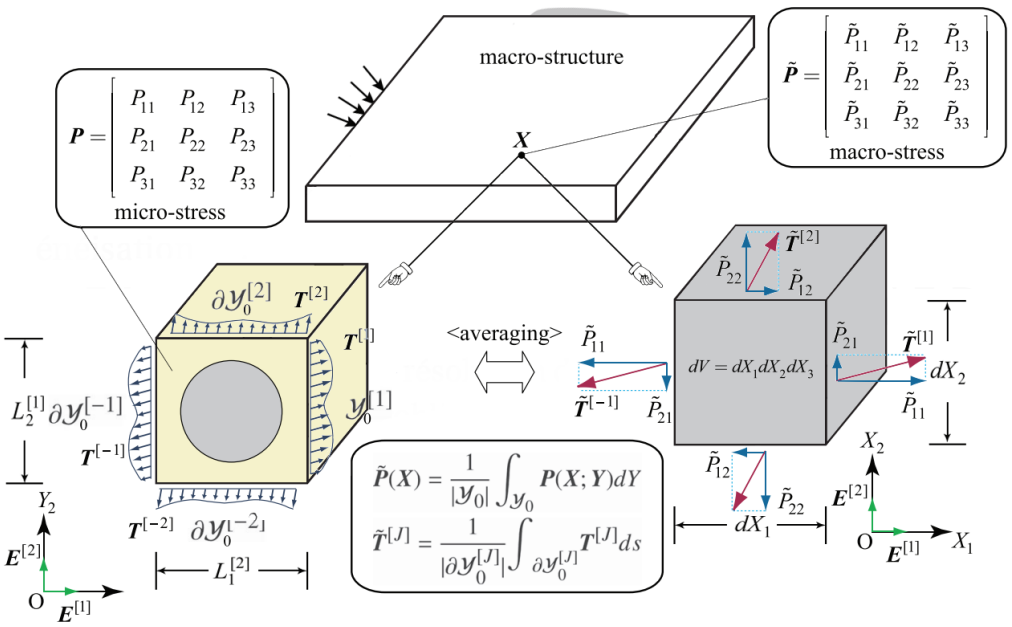


FIGURE 1.2: La méthode d'homogénéisation découplée à deux-échelles

Les deux méthodes ont été appliquées, dans le cas de matériaux hyperélastiques ou pour la viscoélasticité linéaire. Afin d'introduire l'homogénéisation à deux échelles pour la grande déformation d'un matériau composite micro-structuré, nous décrivons d'abord le problème à l'échelle macroscopique, puis à l'échelle microscopique et enfin le couplage entre les deux échelles.

### 1.4.1 Problème macroscopique

Considérons un corps continu qui occupe la configuration de référence $\tilde{\mathcal{B}}_0$ avec un bord noté $\partial\tilde{\mathcal{B}}_0$. Le vecteur normal unitaire extérieur au bord est défini par $\tilde{N}$. Chaque

point est paramétré par le vecteur de position dans la configuration de référence à l'échelle macro $X \in \tilde{\mathcal{B}}_0$. Il est mis en correspondance avec la configuration actuelle $\tilde{\mathcal{B}}_t$ dont le bord est limite $\partial\tilde{\mathcal{B}}_t$. Le vecteur unitaire normal au bord est défini par $\tilde{n}$. Chaque point matériel est paramétré par son vecteur position $x$ dans la configuration actuelle $\tilde{\mathcal{B}}_t$. Ainsi la transformation $\tilde{\varphi}(X)$

$$x = \tilde{\varphi}(X) = \tilde{u}(X) + X \quad \forall X \in \tilde{\mathcal{B}}_0 \tag{1.1}$$

où $\tilde{u}$ est le champ de déplacement à l'échelle macroscopique, (voir fig. 3.1). Sur le plan mathématique, la transformation $\tilde{\varphi}(X)$ est une bijection. Le gradient de la déformation à l'échelle macro

$$\tilde{F} = \nabla_X(\tilde{\varphi}(X)) \tag{1.2}$$

où $\nabla_X()$ désigne l'opérateur gradient par rapport à la configuration initiale. Ainsi le tenseur de transformation $\tilde{F}$ relie un élément $\mathrm{d}X \in \tilde{\mathcal{B}}_0$ dans la configuration initiale à un élément dans la configuration courante $\mathrm{d}x \in \tilde{\mathcal{B}}_t$, par

$$\mathrm{d}x = \tilde{F}.\mathrm{d}X \tag{1.3}$$

En combinant les deux équation (1.1) et (1.3) on peut définir ainsi le tenseur gradient de déplacement macroscopique

$$\tilde{H} = \nabla_X(\tilde{u}(X)) = \tilde{F} - \mathbb{1} \tag{1.4}$$

Pour un corps hétérogène macroscopique, soumis à un chargement et à des contraintes et en l'absence d'effets d'inertie, l'équation d'équilibre à l'échelle macro s'exprime comme suit

$$\nabla_X.\tilde{P} + \tilde{b} = 0 \text{ in } \tilde{\mathcal{B}}_0, \tag{1.5}$$

où

- $\nabla_X$ : désigne l'opérateur de divergence par rapport à la configuration initiale.
- $\tilde{P}$ : est le premier tenseur de contraintes de Piola-Kirchhoff à l'échelle macroscopique.
- $\tilde{b}$ : les forces volumiques appliqués sur le corps dans la configuration initiale

Le corps est soumis à des conditions aux limites de Neumann (efforts imposés) et Dirichlet (déplacements imposés)

$$\begin{aligned} \tilde{P}.\tilde{N} &= \tilde{T}_0 \qquad \text{sur} \quad \partial\tilde{\mathcal{B}}_0^N, \\ \tilde{u} &= \tilde{u}_0 \qquad \text{sur} \quad \partial\tilde{\mathcal{B}}_0^D, \end{aligned} \tag{1.6}$$

où

- $\tilde{T}_0$ : est l'effort appliqué donné sur la configuration de référence
- $\tilde{u}_0$ : le déplacement imposé sur $\partial\tilde{\mathcal{B}}_0^D$
- $\{\partial\tilde{\mathcal{B}}_0^N, \partial\tilde{\mathcal{B}}_0^D\}$ sont une partition (1.7) du bord $\partial\tilde{\mathcal{B}}_0$.

$$\begin{aligned} \partial\tilde{\mathcal{B}}_0^N \cup \partial\tilde{\mathcal{B}}_0^D &= \partial\tilde{\mathcal{B}}_0 \\ \partial\tilde{\mathcal{B}}_0^N \cap \partial\tilde{\mathcal{B}}_0^D &= \varnothing \end{aligned} \tag{1.7}$$

### 1.4.2 Problème microscopique

Le comportement mécanique de la micro-structure du matériau est identifié par un Volume Élémentaire Représentatif (VER [2]). Idéalement, ce VER doit inclure un échantillonnage représentatif de toutes les hétérogénéités micro-structurelles qui se produisent dans le matériau à une échelle de longueur qui devrait être plus petite que la longueur caractéristique de la variation de champ macroscopiquement, mais suffisamment grande que la physique à micro-échelle. En particulier, il est très important dans l'homogénéisation d'un matériau fibreux que le rapport fibre/matrice soit maintenu aux deux échelles, voir les manuels classiques sur la théorie de l'homogénéisation : [NNH13b]; [Fis10b].
En raison de l'indépendance d'échelle de l'équation d'équilibre et des conditions aux limites, le VER est généralement considéré comme étant la cellule unitaire. Ainsi chaque point matériel du VER est paramétré par son vecteur position $Y$ dans la configuration initiale $\mathcal{B}_0$. Dans la configuration actuelle $\mathcal{B}_t$ ce point matériel est paramétré par son vecteur position $y$. Ainsi l'évolution de la position $y$ d'un point matériel

$$y = \varphi(X;Y) = Y + w(X;Y), \tag{1.8}$$

où $w(X;Y)$ est le déplacement à micro-échelle de la cellule unitaire (VER) est défini par

$$w(X;Y) = \tilde{H}(X).Y + u^*(X;Y) + c(X), \tag{1.9}$$

- $\tilde{H}$ est le gradient de déplacement à macro-échelle défini par (1.4).
- $u^*$ désigne le déplacement de fluctuation (voir section suivante)
- $c$ est un vecteur constant indépendant de $Y$, dérivé de l'intégration du gradient de déformation à micro-échelle défini par

$$F(X;Y) = \nabla_Y \varphi(X;Y) = \nabla_Y w(X;Y) + \mathbb{1} = H(X;Y) + \mathbb{1}, \tag{1.10}$$

où $\mathbb{1}$ est le tenseur d'identité (métrique) et $H$ est le gradient de déplacement à l'échelle microscopique donné par

$$H(X;Y) = \nabla_Y w(X;Y) = \tilde{H}(X) + \nabla_Y u^*(X;Y), \tag{1.11}$$

où $\tilde{H} = \frac{1}{|\mathcal{B}_0|}\int_{\mathcal{B}_0} H dV$ et $|\mathcal{B}_0|$ est le volume de référence de le VER (dans notre cas, $|\mathcal{B}_0| = 1$).

Le tenseur de déformation macro-homogène $\tilde{F}$ est lié au tenseur de gradient de déformation à micro-échelle pour chaque point à micro-échelle par

$$F(X;Y) = \tilde{F}(X) + \nabla_Y u^*(X;Y). \tag{1.12}$$

En l'absence de forces volumiques, l'équation d'auto-équilibre à micro-échelle pour la cellule unitaire VER en termes de premier tenseur de contraintes de Piola-Kirchhoff à micro-échelle $P$ et de sa fonction de réponse $\mathcal{F}(F)$ est donnée par

$$\begin{cases} \nabla_Y.P = 0 & \forall Y \in \mathcal{B}_0 \\ P = \mathcal{F}(F) & \forall Y \in \mathcal{B}_0 \end{cases} \tag{1.13}$$

[2] RVE en anglais pour Representative Volume Element

### 1.4.3 Couplage Macro-micro : cinématique

L'homogénéisation par couplage au premier ordre est basée sur l'idée que les quantités microscopiques sont reliées à leurs contreparties macroscopiques par le biais d'une moyenne volumique sur le VER : [Hil72]; [Ogd74]. L'une des relations de transition d'échelle les plus couramment utilisées pour établir le couplage macro-micro est la relation de moyenne cinématique. Elle exige que la moyenne volumique [3] du tenseur gradient de transformation à l'échelle microscopique $F$ soit égale au tenseur de gradient de transformation $\tilde{F}$ à l'échelle macroscopique correspondante(1.10), c'est-à-dire

$$\tilde{F} = \frac{1}{|\mathcal{B}_0|}\int_{\mathcal{B}_0} F dV = \tilde{H} + \mathbb{1}. \tag{1.14}$$

L'insertion du tenseur de gradient de déformation à micro-échelle (1.12) dans (1.14) conduit à

$$\begin{aligned}\frac{1}{|\mathcal{B}_0|}\int_{\mathcal{B}_0} F dV &= \tilde{F} + \frac{1}{|\mathcal{B}_0|}\int_{\mathcal{B}_0} \nabla_Y u^*(X;Y) dV \\ &= \tilde{F} + \frac{1}{|\mathcal{B}_0|}\int_{\partial\mathcal{B}_0} u^*(X;Y) \otimes N dA,\end{aligned} \tag{1.15}$$

où nous utilisons le théorème de divergence pour transformer l'intégrale de volume en intégrale de surface sur la frontière non déformée $\partial\mathcal{B}_0$ du VER avec le vecteur normal extérieur $N$. Pour satisfaire la relation de transition d'échelle, les conditions aux limites sur le VER doivent être choisies de manière à faire disparaître la contribution du champ de microfluctuation $u^*$ dans l'équation (1.15). Ceci peut être réalisé de différentes manières. Voici quelques-unes présentées et utilisées dans la littérature :

1. Éliminer les fluctuations $u^*$ microstructurelles dans le VER

$$u^* = 0, \quad \forall Y \in \mathcal{B}, \tag{1.16}$$

   Cette condition oblige le volume entier à se déformer selon la macro-transformation prescrite $\tilde{F}$ (connue sous le nom d'hypothèses de Taylor/Voight).

$$F = \tilde{F}, \quad \forall Y \in \mathcal{B}, \tag{1.17}$$

2. Éliminer les fluctuations $u^*$ sur le bord du VER $\partial\mathcal{B}_0$ uniquement, tout en laissant les changements microstructurels du volume inconnu du problème.

$$u^* = 0, \quad \forall Y \in \partial\mathcal{B}_0 \tag{1.18}$$

   L'équation (1.15) sera transformée en

$$y = \tilde{F} \cdot Y \quad \forall Y \in \partial\mathcal{B}_0 \tag{1.19}$$

   Cette condition est connue sous le nom de condition de déplacement uniforme. Les déplacements de la frontière VER sont complètement dictés par la transformation $\tilde{F}$ à l'échelle macroscopique.

[3] Sur le VER

3. Dans le cas d'un VER avec une frontière géométriquement périodique, le bord peut être divisé en parties " + " et " − " définies par des vecteurs normaux extérieurs opposés définis par ce qui suit

$$N^{+} = -N^{-} \tag{1.20}$$

La condition aux limites dans ce cas est connue sous le nom de condition aux limites périodique. Elle est imposée en exigeant la périodicité du champ de fluctuation. Dans notre cas avec un VER tridimensionnel cubique

$$u^{*}|_{\partial\mathcal{B}_0^{[J]}} = u^{*}|_{\partial\mathcal{B}_0^{[-J]}} \quad (J = 1,2,3). \tag{1.21}$$

où $J$ désigne la paire constituée des faces opposées du VER. Sur le bord les deux équations (1.8) et (1.9)

$$y|_{\partial\mathcal{B}_0^{[J]}} - y|_{\partial\mathcal{B}_0^{[-J]}} = \tilde{F} \cdot \left( Y|_{\partial\mathcal{B}_0^{[J]}} - Y|_{\partial\mathcal{B}_0^{[-J]}} \right) \tag{1.22}$$

4. La condition limite la plus faible possible, connue sous le nom de "conditions limites cinématiques minimales" introduite par [MP05]

$$\int_{\partial\mathcal{B}_0} u^{*} \otimes N d\partial\mathcal{B}_0 = 0 \tag{1.23}$$

Deux autres conditions aux limites simples sont parfois utilisées dans la la littérature, mais qui ne s'inscrivent pas directement dans la la transition macro-micro cinématique :

5. une condition de contrainte aux limites connue sous le nom d'hypothèse de Sachs ou de Reuss. Dans ce cas, on suppose une contrainte constante identique comme suit

$$P = \tilde{P}, \quad \forall Y \in \mathcal{B}, \tag{1.24}$$

6. La dernière est connue sous le nom de conditions limites de traction uniforme. Elle consiste à prescrire des tractions sur le VER en fonction d'une contrainte macroscopique donnée $\tilde{P}$.

$$p = \tilde{P}.\tilde{N}, \quad \forall Y \in \partial\mathcal{B}_0 \tag{1.25}$$

D'autres approches pour imposer les conditions aux limites nécessitent de résoudre le problème aux limites sur le VER tout en permettant l'intégration des caractéristiques microstructurelles locales. L'application de conditions aux limites de déplacement uniforme sur une cellule microstructurale conduit généralement à une surestimation des propriétés effectives, tandis que les conditions aux limites cinématiques minimales et les conditions aux limites de traction uniforme conduisent à une sous-estimation de ces propriétés. Les conditions aux limites (5) et (6) sont connues pour être sensibles à des détails microstructuraux particuliers près du bord de VER. Les conditions aux limites périodiques sont connues pour fournir la meilleure estimation des propriétés globales [Slu+00], [Ter+00], [MK02], [Kan+03], [Kan+06], [KOS06], [Per+11]. Des types avancés de BC sur RVE ont été développés pour des problèmes spécifiques basés sur la combinaison des BC ci-dessus [Lar+11], [CKG12b].

### 1.4.4 Couplage micro-macro : Condition de Hill-Mandel

La relation de transition entre les échelles micro et macro est généralement établie sur la base de la condition dite de Hill-Mandel ou condition de macrohomogénéité ([Hil63], [Suq85]). Cette condition exige que la moyenne en volume de l'incrément (ou de la variation) du travail effectué sur le VER soit égale à l'incrément (ou à la variation) du travail local à l'échelle macroscopique. Formulé en termes d'un ensemble conjugué de travail, c'est-à-dire, le gradient de déformation et du premier tenseur de contraintes de Piola-Kirchhoff, la condition de Hill-Mandel est la suivante

$$\frac{1}{|\mathcal{B}_0|}\int_{\mathcal{B}_0} P : \delta F^T dV = \tilde{P} : \delta \tilde{F}^T. \tag{1.26}$$

A partir de l'équations d'équilibre à l'échelle microscopique (1.13), on peut obtenir facilement en utilisant le théorème de divergence, la moyenne volumique du travail virtuel à l'échelle microscopique qui peut être exprimée en termes de quantités de surface du VER. Ainsi, le premier tenseur de contrainte de Piola-Kirchhoff à l'échelle macroscopique $\tilde{P}$ peut être défini comme la moyenne volumique de la contrainte correspondante à l'échelle microscopique $P$ sur la cellule unitaire VER [Gee+17], comme suit

$$\tilde{P} = \frac{1}{|\mathcal{B}_0|}\int_{\mathcal{B}_0} P dV. \tag{1.27}$$

En considérant la condition de périodicité (1.21), le vecteur de traction micro Piola $T$ satisfait une condition d'antipériodicité sur la limite de la cellule unitaire $\partial\mathcal{B}_0$ avec $N$ étant le vecteur normal unitaire extérieur sur la surface correspondante dans la configuration de référence

$$T^{[J]} + T^{[-J]} = 0 \qquad \text{où } T^{[J]} = P.N^{[J]}, \tag{1.28}$$

à partir duquel le vecteur de traction moyen de Piola peut être dérivé

$$\begin{aligned} \tilde{T}_i^{[J]} &= \tilde{P}_{iJ} = N^{[i]}.\tilde{T}^{[J]} = N^{[i]}.(\tilde{P}.N^{[J]}) \\ &= N^{[i]}.\left(\frac{1}{|\partial\mathcal{B}_0|}\int_{\partial\mathcal{B}_0} P.N^{[J]} dA\right) = \frac{1}{|\partial\mathcal{B}_0^{[J]}|}\int_{\partial\mathcal{B}_0^{[J]}} T_i^{[J]} ds, \end{aligned} \tag{1.29}$$

où $|\partial\mathcal{B}_0^{[J]}|$ est l'aire de la limite du VER $\partial\mathcal{B}_0^{[J]}$ et $\tilde{P}_{iJ}$ est la composante iJ du premier tenseur de contrainte de Piola-Kirchhoff à l'échelle macro, la moyenne surfacique du vecteur de traction de Piola à micro-échelle correspondant $T_i^{[J]}$ à la limite de la cellule unitaire $\partial\mathcal{B}_0^{[J]}$. Cette relation est d'un grand intérêt pour le calcul numérique de $\tilde{P}$ .

Les conditions aux limites du VER satisfont la condition de Hill-Mandel d'où elles sont déterminées à l'aide du lemme de Hill

$$\frac{1}{|\mathcal{B}_0|}\int_{\mathcal{B}_0} P : \delta F^T dV - \tilde{P} : \delta \tilde{F}^T = \int_{\partial\mathcal{B}_0} [\delta\varphi - \delta\tilde{F}.Y].[P.N - \tilde{P}.N] dA. \tag{1.30}$$

Dans notre cas, les conditions aux limites de déplacement périodiques(1.21), de traction antipériodique et (1.27) sont suffisantes pour satisfaire la condition de Hill-Mandel (d'homogéinisation). Ainsi le problème couplé micro-macro-homogénéisé peut être résumé comme suit ; le problème aux valeurs limites à l'échelle micro doit être résolu pour chaque $X \in \tilde{\mathcal{B}}_0$ pour l'ensemble des solutions $w$, $F$, $H$ qui satisfont

l'équation d'équilibre à l'échelle micro (1.13) avec la condition de périodicité (1.21), tandis que le problème aux valeurs limites à l'échelle macro est résolu pour $\tilde{F}$, $\tilde{P}$ qui satisfait (1.14), (1.27) et (1.5). Il est à noter que le problème aux valeurs limites à l'échelle micro ne peut être résolu que si la solution à macro-échelle est donnée et vice versa. Cette méthode d'homogénéisation couplée permet de définir le comportement effectif analytique des matériaux hétérogènes pour des classes simples et spéciales de conditions aux limites uniformes et des modèles de comportements des constituants des matériaux. Ces résultats analytiques ont une importance à la fois théorique et pratique et seront utilisés dans ce travail. Pour les situations complexes, des méthodes de calcul ont été développées (voir une revue intéressante dans [Gee+17]) mais elles restent très coûteuses pour les applications industrielles.

## 1.5 Méthode découplé proposée

Pour la méthode que nous proposons la condition préalable au découplage[4] est que nous soyons en mesure de prendre un modèle constitutif (potentiel hyperélastique anistrope) pour caractériser correctement le comportement du matériaux à l'echelle macro qui est obtenu à partir de l'analyse numérique par la méthode des éléments finis d'un problème aux valeurs limites à l'échelle micro. Il est à noter que, d'un point de vue pratique (industriel), les modèles constitutifs approximatifs permettent des alternatives, car il se peut qu'il n'y ait pas de modèle rigoureux disponible selon le type de matériaux composites. Une fois que la forme fonctionnelle d'une équation constitutive macro appropriée est supposée, plusieurs analyses numériques à l'échelle micro sont effectuées sur un VER afin d'obtenir les paramètres du matériau homogénéisé via des procédures d'optimisation. L'ensemble des analyses numériques par la méthodes des éléments finis à l'échelle micro à cette fin peut être considéré comme test numérique des matériaux. Les étapes de la procédure de la méthode (figure 1.3) sont décrites comme suit :

(**E0**): On suppose un modèle constitutif "potentiel hyperélastique anistrope" approprié pour le comportement macroscopique du matériau considéré.

(**E1**): Une série de test est effectuée sur un modèle de VER (maillage élément finis), qui est considéré comme un "spécimen numérique", pour obtenir le comportement homogénéisé ou macroscopique du matériau. Notez bien que différentes conditions aux limites cinématiques sont utilisées.

(**E2**): Les paramètres du matériau du modèle constitutif supposé sont identifiés au moyen des données obtenues à partir des test numérique réalisés sur le VER et d'une procédure d'optimisation approprié. Notez bien que les critéres de convergence des procedures d'optimisation sont basés sur des erreurs des composantes de tenseur des contraintes.

(**E3**): Des analyses par éléments finis sont effectuées pour résoudre le problème aux valeurs limite l'échelle macro (nappe fibré) en utilisant le modèle constitutif supposé avec les paramètres des matériaux identifiés.

(**E4**): Vérification du modèle sur des calculs effectué à l'échelle macro (sur nappe) via des calcul sur des VER locaux à la nappe. Correction des paramètres par des procédure d'optimisation si le critère de convergence n'est pas assuré

[4] découplage micro macro

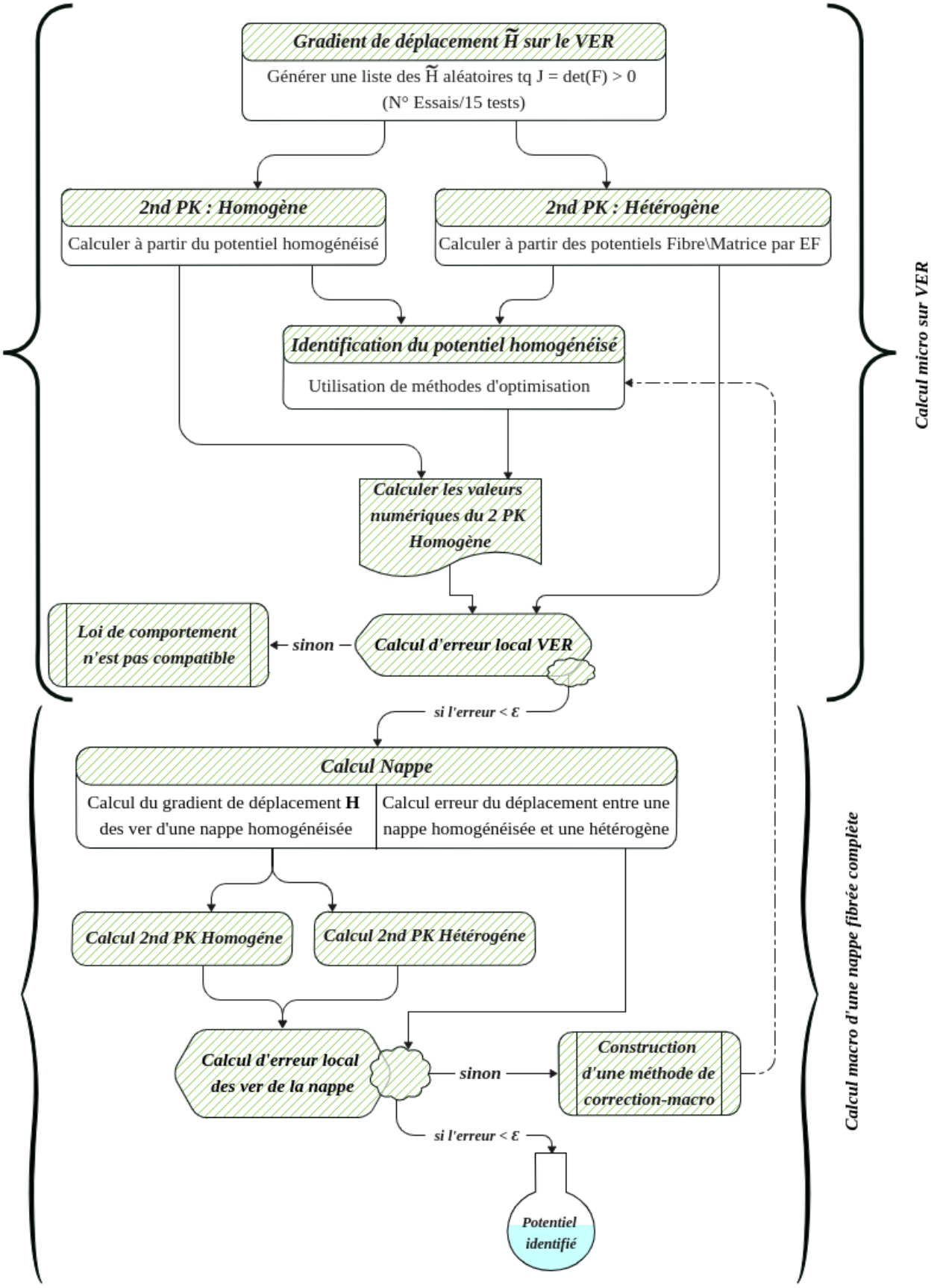


FIGURE 1.3: Flowchart de la procédure proposée

## 1.6 Conclusion

Dans ce chapitre, nous avons résumé les différentes approches d'homogénéisation. Dans une première partie, une brève classification des méthodes multi-échelle est proposée. Puis dans une seconde partie un survol bibliographique des méthodes homogénéisation numérique non-linéaires a été proposé. La troisième partie a été consacrée à l'application de ces méthodes, principalement la méthode découplée, dans un cadre non-linéaire en grande déformation. Dans la dernière partie nous avons détaillé schématiquement la méthode proposée afin de faciliter la lecture des chapitres 3 et 4 qui présentent en détails l'application de cette méthode pour identifier des potentiels anisotropes hyperélastiques.

# Chapter 2

# Isotropic and anisotropic hyperelasticity

## 2.1 Introduction

The following chapter is devoted to the introduction of the mechanical framework of the thesis. In the first part we introduce the equilibrium for a deformable body undergoing a finite deformation. Physically hyperelastic media are in general rubber-like materials bodies, so a survey is dedicated to the physical properties of these materials in the second part of the chapter. Both incompressible and compressible class of material behaviour are presented in this second part. In the last one a literature survey of anisotropic hyperelastic class of behaviour is presented. Some anisotropic potential will be used to test homogenization method proposed in this work.

## 2.2 Nonlinear elasticity equilibrium problem

### 2.2.1 Kinematics

In order to derive the equilibrium equation, let a body occupying a reference configuration $\mathcal{B}_0$ and each point $\mathbf{M}$ of the body in $\mathcal{B}_0$ is labelled by $X = (X_1, X_2, X_3)$ in a cartesian coordinate systems. If the body is deformed quasi-statically from $\mathcal{B}_0$ to $\mathcal{B}$ (Figure 2.1) the deformation of the body can be described by

$$u(X,t) = x(X,t) - X, \tag{2.1}$$

where $x(X,t) = (x_1, x_2, x_3)$ is the position vector of the point $\mathbf{M}$ in $\mathcal{B}$ and $u(X,t)$ denote the displacement vector. To describe the deformation, the second order tensor $F$ can be written

$$F = Grad_X(x) \quad F_{iJ} = \frac{\partial x_i}{\partial X_J}, \tag{2.2}$$

$Grad_X$ in (2.2) being the gradient operator in $\mathcal{B}_0$. The transformation tensor $F$ should be non-singular to assure the invertibility of the transformation between the two configurations $\mathcal{B}_0$ and $\mathcal{B}$ of the body. Then we adopt the usual convention that

$$J = det(F) > 0. \tag{2.3}$$

Equation (2.1) written in the form

$$dx = FdX \tag{2.4}$$

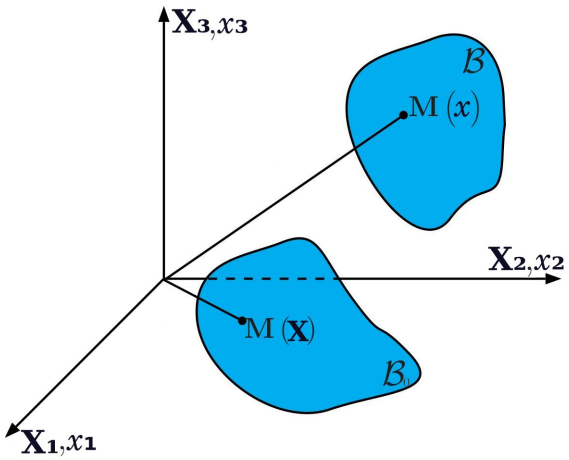


FIGURE 2.1: 3D body deformation

describes the linear transformation of an infinitesimal line element $dX$ at the point $\mathbf{M}(X)$ into the line element $dx$ at $\mathbf{M}(x)$. Surface transformation can be deduced using the Nanson's formula and a vector surface element $NdS_0$ in the undeformed configuration $\mathcal{B}_0$ is transformed to $ndS$

$$ndS = JF^{-T}NdS_0, \tag{2.5}$$

where $F^{-T} = \left(F^{-1}\right)^T$ denote the transpose of the inverse of the deformation tensor. If $dV_0$ denote volume elements in $\mathcal{B}_0$, the volume change to $dV$ on $\mathcal{B}$ can be deduced

$$dV = JdV_0. \tag{2.6}$$

To define a general measure of deformation, let $dX_a$ and $dX_b$ be two elementary vectors that deform to $dx_a$ and $dx_b$, respectively. The deformation can be decomposed into two different deformations ;

- Stretching: change in length.
- Changes in the enclosed angle between the two vectors $(\widehat{dX_a, dX_b})$.

The scalar product in the deformed configuration $dx_a \cdot dx_b$ can be found in terms of the vectors $dX_a$ and $dX_b$ in the undeformed configuration

$$\begin{aligned} dx_a \cdot dx_b = (F \cdot dX_a) \cdot (F \cdot dX_b) &= dX_a^T \cdot \left(F^T \cdot F\right) \cdot dX_b \\ &= dX_a^T \cdot C \cdot dX_b, \end{aligned} \tag{2.7}$$

where $C$ is the right Cauchy-Green tensor. Conversely, the scalar product $dX_a \cdot dX_b$ in the initial configuration $\mathcal{B}_0$ can be obtained in term of the left Cauchy-Green tensor $B = F \cdot F^T$

$$dX_a \cdot dX_b = dx_a^T \cdot B^{-1} \cdot dx_b. \tag{2.8}$$

To assess the change in scalar product in terms of material vectors $dX_a$ and $dX_b$ the Lagrange [1] strain tensor $E$

$$E = \frac{1}{2}(C - I) \tag{2.9}$$

[1] Also called Green tensor.

and then

$$dx_a \cdot dx_b - dX_a \cdot dX_b = 2dX_a \cdot E \cdot dX_b. \tag{2.10}$$

The same change can be expressed in terms of spatial vectors $dx_a$ and $dx_b$ and the Almansi strain tensor [2]

$$dx_a \cdot dx_b - dX_a \cdot dX_b = 2dx_a \cdot A \cdot dx_b, \tag{2.11}$$

where the spatial tensor $A$

$$A = \frac{1}{2}\left(I - B^{-1}\right). \tag{2.12}$$

The tensor $F$ can be decomposed into rotational and stretching part

$$F = R.\,U = V.\,R \tag{2.13}$$

Equation (2.13) is called the polar decomposition of tensor $F$. Where $R$ the rotation tensor is orthogonal $R^T = R^{-1}$ and $U$, $V$ denote respectively right (material), left (spatial) stretch tensor. It can be shown easily that $U$ and $V$ are two positive definite tensors. Right and left Cauchy-Green tensors $C$ can be written

$$C = U^2, \tag{2.14}$$

$$B = V^2. \tag{2.15}$$

From equations (2.14) and (2.15) we can deduce that Lagrange strain tensor $E$ and Almansi strain tensor $A$ do not include information about rotation. In practical case to obtain the tensor $U$ from equation (2.14) an eigenvalue problem should be solved. Let $\{N_i\}_{i=1,2,3}$ denote the triad eigenvector of tensor $C$ and $\{\lambda_i^2\}_{i=1,2,3}$ are their corresponding eigenvalues. Then we can write

$$C = \sum_{i=1}^{3} \lambda_i^2 N_i \otimes N_i. \tag{2.16}$$

Bearing in mind the symmetry of tensor $C$, the triad $\{N_i\}_{i=1,2,3}$ are orthogonal vectors. Then, combining the two equations (2.14) and (2.16) the stretch tensor $U$ can be obtained by the following equation

$$U = \sum_{i=1}^{3} \lambda_i N_i \otimes N_i. \tag{2.17}$$

After determining the stretch tensor $U$, using equation (2.13) the rotation tensor $R$ can be easily evaluated using the following relation

$$R = F\,U^{-1}. \tag{2.18}$$

Combining the deformation (2.1) and the polar decomposition equation (2.13)

$$dx = F\,dX = R\,(U\,dX). \tag{2.19}$$

In the above equation the vector $U\ dX$ can be considered as a material stretched vector rotated to the spatial configuration by $R$.

[2] Also called Euler tensor.

### 2.2.2 Stress tensors

In continuum mechanics, stress denote a physical quantity expressing the internal forces between particles. The stress has the physical dimension of force per unit area and for every surface a stress vectors $t$ and $T$ can be defined for static problem (steady state problem). Then, let $df$ denote an element of force acting in an element of area $ds$ in the spatial (current) configuration $\mathcal{B}$

$$df = t\,(x, n)\,.ds = T\,(X, N)\,.dS \tag{2.20}$$

Where

- $t$ represents the Cauchy traction vector (force measured per unit surface area defined in the current configuration $\mathcal{B}$).
- $T$ represents the first Piola-Kirchhoff traction vector (force measured per unit surface area defined in the reference configuration $\mathcal{B}_0$).
- $n$, $N$ are the outward normal vectors of $ds$ (surface element in the current configuration $\mathcal{B}$) and $dS$ (surface element in the reference configuration $\mathcal{B}_0$), respectively.

The pseudo traction vector $T$ does not describe the actual intensity. It describes the internal forces acting in the current configuration in terms of the reference configuration position $X$ and the outward normal vector $N$. Using the introduced traction vectors in (2.20) Cauchy's stress tensor and first Piola-Kirchhoff stress tensor can be written

$$t = t\,(x, n) = \sigma \cdot n, \tag{2.21}$$

$$T = T\,(X, N) = \tau \cdot N. \tag{2.22}$$

Using Nanson's formula (2.5) the relation between Cauchy stress tensor and first Piola-Kirchhoff can be derived

$$\sigma = \frac{1}{J}\tau \cdot F^T, \qquad \tau = J\sigma \cdot F^{-T}. \tag{2.23}$$

It can be shown that $\sigma$ is a symmetric tensor (from balance laws) and $\tau$ is asymmetric and satisfy the following relation

$$\tau \cdot F^T = F \cdot \tau^T. \tag{2.24}$$

The tensor $\tau$ is an unsymmetric two-point tensor and is not completely considered as a material configuration tensor. It is possible to derive a totally symmetric stress tensor known as the second Piola-Kichhoff stress tensor by pulling back the spatial element of force $f$ in the equation (2.20). Then a material stress vector $f_0$ will be obtained

$$df_0 = F^{-1} \cdot df. \tag{2.25}$$

Then, combining equations (2.23), (2.20) and (2.25) and the second Piola-Kirchhoff stress tensor can be obtained as

$$S = J\,F^{-1} \cdot \sigma \cdot F^{-T}. \tag{2.26}$$

After defining stress concept for a deformable body, conservation of mass , translational and rotational equilibrium equations will be derived in the next section.

### 2.2.3 Equilibrium equations

#### 2.2.3.1 Mass conservation

The mass of a deformable body undergoing a finite deformation process remains unchanged. To derive an expression for the conservation of mass; let $\rho_0$ and $\rho$ denote respectively the density in the reference $\mathcal{B}_0$ and current configuration. Then the mass of the body can be obtained in both configurations by the following equality

$$m_0 = \int_{\mathcal{B}_0} \rho_0 \cdot dV = \int_{\mathcal{B}} \rho \cdot dv = m. \tag{2.27}$$

Thus, for isotropic body the local formulation of the conservation of mass can be written as

$$\rho_0 = J \cdot \rho. \tag{2.28}$$

#### 2.2.3.2 Translational static equilibrium

To derive the static equilibrium equation let $v$ and $\partial v$ denote respectively the element volume and the element surface of a deformable body in its current configuration. Assuming that the body is under the action of body forces $f$ and stress vector $t$. The translational equilibrium implies that the sum of $t$ and $f$ vanishes

$$\int_{\partial v} t ds + \int_v f dv = 0. \tag{2.29}$$

Using relation (2.21), the equilibrium equation can be expressed in terms of the Cauchy stress tensors

$$\int_{\partial v} \sigma \cdot n ds + \int_v f dv = 0. \tag{2.30}$$

Using the Gauss theorem the previous equation

$$\int_v (div\sigma + f)\, dv = 0. \tag{2.31}$$

The above equation can be equally applied to any enclosed region of the body. In fact the integrand function must vanish

$$div\sigma + f = 0. \tag{2.32}$$

#### 2.2.3.3 Rotational static equilibrium

Symmetry of the Cauchy stress is established by considering the rotational equilibrium of the body under the action of internal forces $t$ and body forces $f$. This implies that the total moment of forces about any arbitrary point must vanish. The total moment of forces about any arbitrary point should vanish. In the origin point the rotational equilibrium give us

$$\int_{\partial v} x \times t ds + \int_v x \times f dv = 0. \tag{2.33}$$

where cross product $\times$ of a force with a position vector $x$ yields the moment of that force about the origin. Using relation (2.21) the above equation can be rewritten

$$\int_{\partial v} x \times (\sigma \cdot n)\, ds + \int_v x \times f dv = 0. \tag{2.34}$$

Using the Gauss theorem and Levi-Civita symbol $\mathcal{E}$ equation (2.34) becomes

$$\int_v x \times (div(\sigma))\, dv + \int_v \mathcal{E} : \sigma^T dv + \int_v x \times f dv = 0. \tag{2.35}$$

So the vector $\mathcal{E} : \sigma^T$ is

$$\mathcal{E} : \sigma^T = \begin{bmatrix} \sigma_{32} - \sigma_{23} \\ \sigma_{13} - \sigma_{31} \\ \sigma_{21} - \sigma_{12} \end{bmatrix} \tag{2.36}$$

Rearranging terms in equation (2.35) and take into account the translational equilibrium (2.30). For any enclosed of the body this equality is obtained

$$\mathcal{E} : \sigma^T = 0 \tag{2.37}$$

Then, in view of (2.36), equation (2.37) implies the symmetry of the Cauchy stress tensor $\sigma$.

### 2.2.4 Homogeneous Hyperelasticity

For hyperelastic material the constitutive behaviour is only a function of the current state of deformation. To define the basic materials stress-strain relationships, the deformation gradient $F$ and its conjugate first Piola-Kirchhoff stress measure $\tau$ can be used

$$\tau = \tau(F, X) \tag{2.38}$$

The direct dependency of the first Piola-Kirchhoff stress tensor $\tau$ on $X$ can translate an inhomogeneity. For hyperelastic material admit a path-independent behaviour and then we can write

$$\mathcal{W}(F, X) = \int_{t_0}^{t} \tau(F, X) : \dot{F} dt \tag{2.39}$$

where $\dot{F}$ denotes the time derivative of deformation tensor. Giving the stored elastic energy $\mathcal{W}(F, X)$ the Piola-Kirchhoff stress tensor

$$\tau = \frac{\partial \mathcal{W}(F)}{\partial F}, \qquad \tau_{iJ} = \frac{\partial \mathcal{W}}{\partial F_{iJ}} \quad \forall \{i, J\} \in \{1, 2, 3\} \tag{2.40}$$

The above equation can be rewritten in spatial (current) configuration $\mathcal{B}$

$$\sigma = J^{-1} \frac{\partial \mathcal{W}(F)}{\partial F} \cdot F^T \tag{2.41}$$

According to objectivity the stored energy $\mathcal{W}$ must remain invariant when a rigid body rotation is applied. This implies that $\mathcal{W}$ depends on $F$ [3] only via the stretch tensor $U$. Recalling the right Cauchy-Green deformation tensor, which is given in terms of the deformation gradient $F$

$$C = F^T F = U^T R^T R\, U = U^T U \tag{2.42}$$

[3] The tensor $F$ can be expressed as the product of a rotation tensor $R$ times a stretch tensor $U$, $F = R\, U$

Where $R$ is an orthogonal tensor $R^T R = \underline{\underline{I}}$. For convenience, the energy function $\mathcal{W}$ is expressed as a function of the right Cauchy-Green deformation tensor (2.42)

$$\mathcal{W}\left(F\left(X\right), X\right) = \mathcal{W}\left(C\left(X\right), X\right) \tag{2.43}$$

The second Piola-Kirchoff stress tensor [BW08] can be obtained

$$S = 2\frac{\partial \mathcal{W}}{\partial C} \tag{2.44}$$

#### 2.2.4.1 Incompressible isotropic hyperelasticity

The isotropy implies that the relationship between $\mathcal{W}$ and $C$ must be independent of the material axes chosen and consequently, $\mathcal{W}$ must only be a function of the $C$ invariants

$$I_1 = tr\left(C\right) \tag{2.45a}$$

$$I_2 = \frac{1}{2}\left\{tr\left(C\right)^2 - tr\left(C^2\right)\right\} \tag{2.45b}$$

$$I_3 = det\left(C\right) = det\left(C^2\right) = J^2 \tag{2.45c}$$

Then in the case of isotropy (2.43),

$$\mathcal{W}\left(F\left(X\right), X\right) = \mathcal{W}\left(C\left(X\right), X\right) = \mathcal{W}\left(I_1, I_2, I_3, X\right) \tag{2.46}$$

Then, the second Piola-Kirchhoff stress tensor can be rewritten under the restriction of isotropy

$$S = 2\frac{\partial \mathcal{W}}{\partial C} = 2\frac{\partial \mathcal{W}}{\partial I_1}\frac{\partial I_1}{\partial C} + 2\frac{\partial \mathcal{W}}{\partial I_2}\frac{\partial I_2}{\partial C} + 2\frac{\partial \mathcal{W}}{\partial I_3}\frac{\partial I_3}{\partial C} \tag{2.47}$$

Expression (2.47) of the second Piola-Kirchhoff stress tensor can be evaluated as [4]

$$S = 2\underline{\underline{I}}\,\frac{\partial \mathcal{W}}{\partial I_1} + 4C\,\frac{\partial \mathcal{W}}{\partial I_2} + 2J^2 C^{-1}\,\frac{\partial \mathcal{W}}{\partial I_3} \tag{2.48}$$

In practice the Cauchy-stresses that are of engineering significance are used. This can be obtained indirectly by using the following transformation

$$\underline{\underline{\sigma}} = J^{-1}\,F \cdot S \cdot F^T \tag{2.49}$$

For incompressible hyperelastic materials $det\left(F\right) = 1$, equations (2.45) to (2.49) are reduced and then

$$\begin{aligned} I_3 = det\left(C\right) = J^2 = 1\ , \qquad & \mathcal{W}\left(C\left(X\right), X\right) = \mathcal{W}\left(I_1, I_2, X\right) \\ S = 2\underline{\underline{I}}\,\frac{\partial \mathcal{W}}{\partial I_1} + 4C\,\frac{\partial \mathcal{W}}{\partial I_2}\ , \qquad & \underline{\underline{\sigma}} = \frac{\partial \mathcal{W}}{\partial F} \cdot F^T - p\ I \end{aligned} \tag{2.50}$$

and the first Piola-Kirchhoff stress tensor can be obtained using equation (2.23)

$$\tau = \frac{\partial \mathcal{W}}{\partial F} - pF^{-T} \tag{2.51}$$

[4] For more details, refer to [BW08]

where $p$ denote a scalar representing a Lagrange multiplier that elucidate the incompressibility constraint. After exposing relation between stress tensors and deformation tensors in (2.50) and (2.51), some constitutive models[5] are presented in the following section.

#### 2.2.4.2 Constitutive models for incompressible hyperelacticity

For constitutive model only strain energy model for incompressible material will be presented. One of the first and simplest constitutive model was the neo-Hookean model [Riv48c]. Its strain energy function is

$$\mathcal{W}(I_1, I_2, I_3) = W(I_1) = \frac{\mu}{2}(I_1 - 3) \tag{2.52}$$

where $\mu > 0$ denote the shear modulus. The neo Hookean model is considered a reliable strain energy function for the non-linear deformation, although the model involve only a single parameter. Noting that the neo-Hookean model can be derived from a micromechanics point of view and the shear modulus $\mu$ is determined by

$$\mu = nkT \tag{2.53}$$

To improve the fitting to experimental data, the previous model was enriched by the second invariant $I_2$. And a purely phenomenological model [Moo40a]; [Riv48b]; [Riv49b]; [Riv49a] known as the **Mooney-Rivlin** model was introduced

$$\mathcal{W}(I_1, I_2) = C_{01}(I_1 - 3) + C_{10}(I_2 - 3). \tag{2.54}$$

Where the shear modulus $\mu = 2(C_{01} + C_{10})$. It has been shown by [Moo40a] that the form represented by (2.54) reflects the undeformed state for large deformations of an incompressible isotropic hyperelastic material. Others authors proposed a generalized neo-Hookean strain energy functions[6]. A generalized neo-Hookean model has the the following form

$$\mathcal{W}(F) = \mathcal{W}(I_1). \tag{2.55}$$

From the phenomenological point of view neo-Hookean models can be devided in two classes:

- Limiting chain extensibility models.
- Power-law chain models.

For the first class of models, [Gen96] proposed the following strain energy density

$$\mathcal{W}(I_1) = -\frac{\mu}{2b_G} ln\left[1 - b_G(I_1 - 3)\right]. \tag{2.56}$$

Where $\mu$ denote the shear modulus and $b_g > 0$ a constant parameter representing polymeric chain extensibility limit. In biomechanics and for soft tissues, a widely used model was proposed by [Fun67]

$$\mathcal{W}(I_1) = \frac{\mu}{2b_F} exp\left[b_F(I_1 - 3) - 1\right] \tag{2.57}$$

here $b_F > 0$ a dimensionless constant reflecting stiffening and $\mu$ is the shear modulus. For small deformation and small value of $b_G$ and $b_F$ Both models behave like

[5] Incompressible constitutive models

[6] We call generalized neo-Hookean models all strain energy form depending in $I_1$ only.

neo-Hookean solids. For carbon filled rubber [Yeo90] proposed a generalized neo-Hookean strain energy function

$$\mathcal{W}(I_1) = C_{10}(I_1 - 3) + C_{20}(I_1 - 3)^2 + C_{30}(I_1 - 3)^3. \tag{2.58}$$

Higher order terms in (2.58) improved the ability to capture moderate and large deformations. Another power model to describe both stiffening and softening effects in biological tissues and rubber-like materials, was proposed by [Kno77] as follows

$$\mathcal{W}(I_1) = \begin{cases} \frac{\mu}{2\alpha\beta}\left[(1+\beta(I_1-3))^{\alpha} - 1\right] & \text{if } \alpha \neq 0 \text{ and } \beta \neq 0 \\ \frac{\mu}{2\beta} log\left(1+\beta(I_1-3)\right) & \text{if } \alpha = 0 \text{ and } \beta \neq 0 \\ \frac{\mu}{2}(I_1-3) & \text{if} \beta = 0, \forall\alpha \end{cases} \tag{2.59}$$

Many experimental data suggest that generalized neo-Hookean models have a limited applicability in the engineering application, nevertheless their application to obtain analytical solution for many problems facilitate understanding of mechanical properties of elastomeric solids and leads to benchmarks problems for complex numerical solutions. Other authors [VL67] proposed strain energy function expressed in term of principle streches

$$\mathcal{W}(\lambda_1, \lambda_2, \lambda_3) = w_1(\lambda_1) + w_2(\lambda_2) + w_3(\lambda_3), \tag{2.60}$$

where functions $w_i(\lambda_i)$ are the same by symmetry for each extension ratios. **Ogden** in [Ogd73] proposed a general form of incompressible hyperelasticity to model the behaviour of rubber, polymers and biological tissues. The strain energy $\mathcal{W}$ in terms of principal stretches:

$$\mathcal{W}(\lambda_1, \lambda_2, \lambda_3) = \sum_{i=1}^{n} \frac{\mu_i}{\alpha}\left[\lambda_1^{\alpha_i} + \lambda_2^{\alpha_i} + \lambda_3^{\alpha_i} - 3\right]. \tag{2.61}$$

Shear modulus $\mu$ can be obtained by the following equation

$$\mu = \frac{1}{2}\sum_{i=1}^{n} \mu_i \alpha_i. \tag{2.62}$$

Many strain energy form can be deduced from the generalized form (2.61) ; for example Mooney-Rivlin model (2.54) can be deduce from (2.61) by taking: $N = 2$ , $\alpha_1 = 2$ and $\alpha_2 = -2$, and replacing $\lambda_i$ with $I_i$ [7].

#### 2.2.4.3 Compressible isotropic hyperelasticity

For compressible hyperelastic materials, the development of strain energy function is subjected to more constraints than those cited below. In fact, the constitutive model $W(I_1, I_2, I_3)$ must approach infinity if the local volume tends to infinity or zero, i.e., to expand a body infinitely or to compress it to a point an infinite energy is necessary. These constraints are called commonly Growth Condition.

[7] Mooney-Rivlin parameter ; $C_{01} = \frac{\mu_1}{2}$, $C_{10} = -\frac{\mu_2}{2}$

One class of rigorously mathematical developed model concerns the so-called Hadamard hyperelastic models introduced by [HG03] and named by [Joh66] characterized by its capacity to propagate infinitesimal longitudinal waves in every direction under an arbitrary state of finite static homogeneous deformation. This strain energy is defined by:

$$W_H(I_1, I_2) = \frac{\mu(1-\varepsilon)}{2}(I_1 - 3) + \frac{\mu\varepsilon}{2}(I_2 - 3) + h(I_3) \tag{2.63}$$

To satisfy the strong ellipticity condition, the growth condition and to recover the infinitesimal behaviour law, the functional $h(I_3)$ should verify the following requirements [JK88]:

$$\begin{aligned} &h^{'}(I_3) + 2I_3 h^{''}(I_3) \geqslant 0 \quad \forall I_3 \in ]0, +\infty[ \quad \text{with} \quad h(I_3 \to 0) \to +\infty \\ &\text{and} \quad h(I_3 \to +\infty) \to +\infty \quad h^{'}(1) = -\frac{\mu}{2}(1+\varepsilon) \quad \text{and} \quad h^{''}(1) = \frac{\mu}{2} + \frac{\lambda}{4} \end{aligned} \tag{2.64}$$

If the parameter $\varepsilon = 0$, the strain energy defined by (2.64) governs a compressible material behaviour and corresponds to the special cases of the Hadamard materials called reduced order Hadamard hyperelastic potential (compressible Neo-Hookean potential) and studied extensively by [Joh66]. A particular and a popular mathematical Hadamard hyperelastic potential is the Ciarlet-Geymonat hyperelastic potential by setting a particular choice for the function $h(I_3)$:

$$h_{CG}(I_3) = \left(\frac{\mu\varepsilon}{2} + \frac{\lambda}{4}\right)(I_3 - 1) - \left(\mu + \frac{\lambda}{2}\right)\ln\left(I_3^{1/2}\right) \tag{2.65}$$

Others particular functions of $h(I_3)$, which do not necessary verify the Growth Conditions constraints, are introduced in the literature as:

$$\begin{aligned} h(I_3) &= A\left(I_3^{1/2} - 1\right)^2 \\ h(I_3) &= B\,\ln\left(I_3^{1/2}\right) \\ h(I_3) &= C\left(\ln\left(I_3^{1/2}\right)\right)^2 \end{aligned} \tag{2.66}$$

The second constitutive model is the Blatz-Ko hyperelastic model developed for highly compressible foam rubber like materials [BK62]. Their experimental data has shown that the axial and lateral stretches under uniaxial tension can be related by a power law relationship and then the model of general behaviour of a hyperelastic material is based on its response to uniaxial tension. Its strain energy density function, which is based on a coupled function of volumetric and isochoric parts, is given by:

$$W_{BK}(I_1, I_2, I_3) = \frac{\mu(1-\varepsilon)}{2}\left[(I_1 - 3) + \frac{1}{\eta}(I_3^{-\eta} - 1)\right] + \frac{\mu\varepsilon}{2}\left[\left(\frac{I_2}{I_3} - 3\right) + \frac{1}{\eta}(I_3^{\eta} - 1)\right], \tag{2.67}$$

where $\eta = \dfrac{\nu}{1-2\nu}$ and $\nu$ is the Poisson coefficient such that $\nu \in ]0, \frac{1}{2}[$. [BS86] have shown that the Blatz-Ko material is the unique hyperelastic potential where the response of the Cauchy stress $\sigma$ versus the deformation $B$ depends only on volume changes, i.e., through the local volume ratio $J$. A generalization of this model to auxetic materials was done by [CS14]. A subclass of the Blatz-Ko hyperelastic model

(2.67) when $\eta = \frac{}{2}$ and $\nu = \frac{1}{4}$ will be used in this work. Further original investigations of the of Blatz–Ko material properties can be found in [BS86] and in the review article by [Bea87].

One of the main differences between the Ciarlet-Geymonat and Blatz-Ko hyperelastic potentials can be investigated by calculating these models mechanical responses for a state of uni-axial large stretch tension in a pure homogeneous plane deformation. The local volume variation $J = \det(F)$ is then determined:

$$J_{CG} \to J_0 = cst \quad \text{and} \quad J_{BK} \to +\infty \tag{2.68}$$

## 2.3 Anisotropic Hyperelasticity

### 2.3.1 Transversely isotropic hyperelasticity

In this thesis, the fiber reinforced composites are composed of a matrix material and one family of fibers and have one single preferred direction. The induced anisotropy is the simplest one called transversely isotropic, i.e., the properties of the material in the transverse direction are isotropic. From mechanical behaviour viewpoint, the stiffness of the material effective behaviour in the preferred direction is much greater than in the direction orthogonal to the fibers. Hence, the local macroscopic constitutive law modelling the effective RVE behaviour depends on the transformation gradient $F$ and on the fiber direction defined by a unit vector $\mathbf{A}$ in the reference configuration figure 2.2. Therefore, the material response remains unaffected under

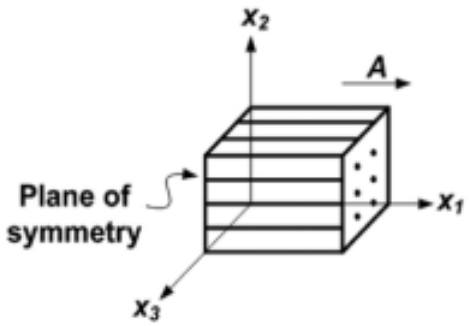


FIGURE 2.2: Transversely isotropic material

arbitrary rotations about the direction $\mathbf{A}$ and by interchange of $\mathbf{A}$ and **-A**. Hence, the constitutive law can be characterized by the gradient transformation $F$ and the structure tensor $\mathbf{A} \otimes \mathbf{A}$ where the operator $\otimes$ represents the outer products. For hyperelastic behaviour and exploiting the objectivity principle, the strain energy is defined of as an isotropic functional of the right Cauchy-Green deformation tensor $C$ and the structure tensor $\mathbf{A} \otimes \mathbf{A}$:

$$W = W(C, \mathbf{A} \otimes \mathbf{A}). \tag{2.69}$$

According to the invariant theory [Spe72]; [Spe84] and for unconstrained behaviour, the hyperelastic potential (2.69) is expressed as:

$$W = W(I_1, I_2, I_3, I_4, I_5), \tag{2.70}$$

where the invariants $(I_1, I_2, I_3)$ characterize the isotropic material response and the new invariants $(I_4, I_5)$ describe the anisotropic material response, i.e., the properties of the fiber family and its interaction with the other material constituents:

$$I_4 = \mathbf{A}C\mathbf{A} \quad , \quad I_5 = \mathbf{A}C^2\mathbf{A}. \tag{2.71}$$

Here, the invariant $I_4$ has a physical sense and is equal to the square of the stretch $\lambda$ in the fiber direction. Therefore, the material is in extension if $I_4 > 1$ and in compression if $I_4 < 1$. The invariant $I_5$ has, in general, no simple interpretation. Holzapfel, Merodio and Ogden have shown in [MO02] and [HO10] that in some choices of the preferred direction $\mathbf{A}$ and the deformation $C$, $I_5$ may be regarded to model the shearing deformation on the preferred direction.

### 2.3.2 Incompressible transversely isotropic hyperelastic models

For incompressible behaviour, $I_3 = 1$, the hyperelastic potential (2.69) is expressed as:

$$W = W(I_1, I_2, I_4, I_5), \tag{2.72}$$

and the Cauchy stress tensor is given by:

$$\sigma = -p\mathbb{1} + 2\frac{\partial W}{\partial I_1}B + 2\frac{\partial W}{\partial I_2}(I_1 B - B^2) + 2\frac{\partial W}{\partial I_4}F\mathbf{A}\otimes F\mathbf{A} + 2\frac{\partial W}{\partial I_5}(F\mathbf{A}\otimes BF\mathbf{A} + BF\mathbf{A}\otimes F\mathbf{A}). \tag{2.73}$$

The incompressible transversely isotropic hyperelastic constitutive law composed by the strain energy (2.72) and the Cauchy stress tensor (2.73) should respect some conditions. Firstly, in the reference stress free configuration, the strain energy (2.72) and the Cauchy stress (2.73) are identically zero. It will be required:

$$W^0 = 0 \quad , \quad 2\frac{\partial W^0}{\partial I_1} + 4\frac{\partial W^0}{\partial I_2} = p^0 \quad , \quad \frac{\partial W^0}{\partial I_4} + 2\frac{\partial W^0}{\partial I_5} = 0, \tag{2.74}$$

where the 0 superscript indicates evaluation for $I_1 = I_2 = 3, I_4 = I_5 = 1$ and $p^0$ is the value of Lagrange multiplier in the reference configuration.

Secondly, in the case of infinitesimal deformation, this incompressible transversely isotropic hyperelastic constitutive law composed by the strain energy (2.72) and the Cauchy stress tensor (2.73) should be compatible with the incompressible transversely isotropic linear elastic constitutive law [Spe72]; [Spe84] given by:

$$W = \mu_T \mathrm{tr}(\varepsilon^2) + 2(\mu_L - \mu_T)\mathbf{A}(\varepsilon^2\mathbf{A}) + \frac{1}{2}(E_L - 4\mu_L + \mu_T)(\mathbf{A}(\varepsilon\mathbf{A}))^2, \tag{2.75}$$

$$\sigma = -p\mathbb{1} + 2\mu_T\varepsilon + 2(\mu_L - \mu_T)(\varepsilon\mathbf{A}\otimes\mathbf{A} + \mathbf{A}\otimes\varepsilon\mathbf{A}) + (E_L - 4\mu_L + \mu_T)(\mathbf{A}(\varepsilon\mathbf{A}))\mathbf{A}\otimes\mathbf{A}. \tag{2.76}$$

Here, $\varepsilon$ denotes the infinitesimal deformation tensor. Notice that the theory of linear, incompressible, transversely isotropic elasticity governed by relations (2.75) and (2.76) is a three constant theory: the Young's modulus in the longitudinal (preferred) direction $E_L$ and the infinitesimal shear moduli for shearing along the fiber direction and in plane normal to the fiber $(\mu_L, \mu_T)$ respectively.

By linearizing the incompressible transversely isotropic hyperelastic constitutive law composed by the strain energy (2.72) and the Cauchy stress tensor (2.73)

and identifying it with the incompressible transversely isotropic linear elastic constitutive law, some required conditions are deduced: (see extended discussions in [Mur13]; [MS15]; [Sac15]; [HMS18]; [HM21]):

$$p = -2\Big(\frac{\partial W^0}{\partial I_1} + \frac{\partial W^0}{\partial I_2}\Big)(\varepsilon \mathbf{A})\mathbf{A} \tag{2.77}$$

$$E_L = 6\frac{\partial W^0}{\partial I_1} + 6\frac{\partial W^0}{\partial I_2} + 4\frac{\partial^2 W^0}{\partial^2 I_4} + 16\frac{\partial^2 W^0}{\partial I_4 \partial I_5} + 16\frac{\partial^2 W^0}{\partial^2 I_5} + 8\frac{\partial W^0}{\partial I_5} \tag{2.78}$$

$$\mu_L = \Big(\frac{\partial W^0}{\partial I_1} + \frac{\partial W^0}{\partial I_2} + \frac{\partial W^0}{\partial I_5}\Big) \tag{2.79}$$

$$\mu_T = 2\Big(\frac{\partial W^0}{\partial I_1} + \frac{\partial W^0}{\partial I_2}\Big) \tag{2.80}$$

The choice of the independent material properties of the three constants incompressible transversely isotropic linear elasticity theory is not unique [HM21]. Another triads are commonly exploited [HM21]: $(E_L, E_T, \mu_T)$ and $(\mu_L, \mu_T, \mu_{TT})$ among others where $E_T$ is the Young's modulus in the plane normal to the fibers and $\mu_{TT}$ is the Poisson ratio. Notice from relations (2.79) and (2.80) that if the strain energy (2.72) is independent from the invariant $I_5$, i.e., $W = W(I_1, I_2, I_{54})$ which is a classical assumption adopted in [HY87]; [HSY90], the longitudinal $\mu_L$ and the transverse $\mu_T$ infinitesimal shear modulus are equal. This is clearly an unphysical prediction.

Thirdly, the strain energy should respect some classical inequalities to ensure the existence and the uniqueness of the local and the global solution and to ensure a physically meaningful material behaviour: Baker-Ericksen, strong ellipticity and strict polyconvexity inequalities [MH94]. For incompressible transversely isotropic hyperelastic potential, the strong ellipticity is assured by the following conditions [WW03]:

$$\begin{cases} \dfrac{\partial W}{\partial I_k^*} > 0 \quad \text{for} \quad k = 1, 2, 4, 5 \\ \dfrac{\partial W}{\partial I_1^*} + \gamma \dfrac{\partial W}{\partial I_4^*} \geqslant 0 \quad \forall \gamma > 4 \\ \det\Big(\dfrac{\partial^2 W}{\partial I_k^* \partial I_I^*}\Big) > 0 \end{cases} \tag{2.81}$$

where the new invariants $I_k^* (k = 1, 2, 4, 5)$ are defined as:

$$I_1^* = \frac{I_1}{2} \quad , \quad I_2^* = \frac{I_1^2}{2} - I_2 \quad , \quad I_4^* = I_4 \quad , \quad I_5^* = I_5. \tag{2.82}$$

The art of constructing a strain energy density (2.72) respecting the conditions listed below and modelling the material behaviour is crucial to design complex hyperelastic structures. Since the appearing of the Rivlin's series [RS51b] and later the Ogden model [Ogd72] based on elongations and a power law development, the development of anisotropic hyperelastic models has been formulated in different ways based in various functional forms such as a series of polynomials or exponentials within the framework of invariant theory. Two general models, coupling the effect and the interaction of the different invariants, are of the form [JT01]:

$$W = \sum_{k,l,m,n} C_{klmn}(I_1 - 3)^{a_k}(I_2 - 3)^{b_l}(I_4 - 1)^{c_m}(I_5 - 1)^{d_n}, \tag{2.83}$$

$$W = \sum_{k,l,m,n} C_{klmn}(I_1^{a_k} - 3^{a_k})(I_2^{b_l} - 3^{b_l})(I_4^{c_m} - 1)(I_5^{d_n} - 1), \tag{2.84}$$

where $(C_{klmn}, a_k, b_l, c_m, d_n)$ are material parameters whose identification is complex. Some way to simplify these models (2.83) and (2.84) is to decouple the invariants effect:

$$W = \sum_k A_k(I_1 - 3)^{a_k} + \sum_l B_l(I_2 - 3)^{b_l} + \sum_m C_m(I_4 - 1)^{c_m} + \sum_n D_n(I_5 - 1)^{d_n}, \tag{2.85}$$

$$W = \sum_k A_k(I_1^{a_k} - 3^{a_k}) + \sum_l B_l(I_2^{b_l} - 3^{b_l}) + \sum_m C_m(I_4^{c_m} - 1) + \sum_n D_n(I_5^{d_n} - 1), \tag{2.86}$$

where $(A_k, a_k, B_l, b_l, C_m, c_m, D_n, d_n)$ are material parameters. The hyperelastic potentials (2.85) and (2.86) verify the strong ellipticity conditions if the materials parameters are strictly positives. It is to be noted that a variant of hyperelastic model (2.85) known as Kaliske's model [Kal00b] will used as a "candidate" for a homogenized hyperelastic model in the third and fourth chapters.

The exponential development of hyperelastic model is a key property of the constitutive modelling of soft tissues which are fibres-reinforced composites "per excellence". The pioneering work of Fung [Fung, 1967][Fun67] was used by numerous researchers to develop more sophistically models, see [WMG96b]; [HGO00]; [Hel+10a] among others. Here, the Holzapfel-Gasser-Ogden (HGO) model [HGO00], which is based on a micro-mechanically formulation, is specified for transversely isotropic behaviour:

$$W = \frac{\mu}{2}(I_1 - 3) + \frac{k_1}{2k_2}\Big[\exp(k_2(I_4 - 1)^2) - 1\Big], \tag{2.87}$$

where $\mu$ is the infinitesimal shear modulus and $(k_1, k_2)$ are material parameters. The strain energy form (2.87) belongs to the uncoupled isotropic/anisotropic hyperelastic model class:

$$W(I_1, I_2, I_4, I_5) = W_{iso}(I_1, I_2) + W_{aniso}(I_4, I_5). \tag{2.88}$$

This class of hyperelastic model (2.88) decouples the energy contributions of the matrix and the fibers. In this case, the coupling influence and interaction between the fibers and the matrix is neglected.

Another way to construct incompressible transversely isotropic hyperelastic model is to exploit the corresponding linear theory. This idea is not new and the isotropic Saint-Venant Kirchoff model is an example of generalization of the Hooke's law for large deformation. The key point of the methodology is to replace the infinitesimal strain $\varepsilon$ in the constitutive law of incompressible transversely isotropic linear elasticity, for example (2.75) or (2.76) which are based on the linear material properties triad $(E_L, \mu_L, \mu_T)$, by a nonlinear strain measure. The resulting hyperelastic model depends on the choice of the linear material properties triad, the strain measure and the linear constitutive law to be used in the substitution of the infinitesimal strain $\varepsilon$ by an appropriate nonlinear strain measure (Cauchy stress, second Piola-Kirchoff stress or strain energy) [MS15]; [HM21]. To illustrate this methodology, two examples will be analyzed. In the first example, the Green-Saint Venant strain tensor $E = \frac{1}{2}(C - 1)$ replaces the infinitesimal strain $\varepsilon$ in the strain energy (2.75). The

corresponding Cauchy stress tensor is obtained from stress-strain relation (2.73):

$$\begin{aligned}\sigma = -p\mathbb{1} + \mu_T(B^2 - B) + \frac{1}{2}[(E_L - 4\mu_L + \mu_T)I_4 - E_L + 3\mu_T]F\mathbf{A}\otimes F\mathbf{A} \\ +(\mu_L - \mu_T)(F\mathbf{A}\otimes BF\mathbf{A} + BF\mathbf{A}\otimes F\mathbf{A}).\end{aligned} \tag{2.89}$$

In the second example, the Eulerian strain measure tensor $d = \frac{1}{2}(1 - B^{-1})$ replaces the infinitesimal strain $\varepsilon$ in the Cauchy stress tensor (2.76):

$$\begin{aligned}\sigma = -p\mathbb{1} - \mu_T B^{-1} - \frac{1}{2}[(E_L - 4\mu_L + \mu_T)I_4^{-1} - E_L + 3\mu_T]I_4^{-1}F\mathbf{A}\otimes F\mathbf{A} \\ -(\mu_L - \mu_T)I_4^{-1}(F\mathbf{A}\otimes B^{-1}F\mathbf{A} + B^{-1}F\mathbf{A}\otimes F\mathbf{A}).\end{aligned} \tag{2.90}$$

It is clear that these two examples give two different Cauchy stress tensors and show the complexity of an anisotropic hyperelastic modelling.

All the anisotropic hyperelastic models listed in this chapter and in the references are phenomenological and have developed to model the directional homogenized responses of the fiber-reinforced composites. These phenomenological models could eventually simulate the effects fibers reinforcement. However, these models generally lack of the microstructural constituents informations. In the papers of [CRF15]; [Cha+17]; [Hel+10a]; [Fen+16]; [Aça21]; [Dal+22]; [CMO22], more interesting reviews and critics about these anisotropic hyperelastic models are done.

To overcome the deficiency of the phenomenological approach, the micromechanical modelling approach is widely used. Its objective is to connect the composite structure microscale response to its macroscale directional homogenized response [Fis10a]; [NNH13a]. In the case an RVE composed by a matrix and a fiber modelled by two different NewHookean potentials, an explicit analytical expression for the homogenized hyperelastic potential was given [DHS06a]:

$$W = \frac{\mu_1}{2}(I_1 - 3) + \frac{\mu_2 - \mu_1}{2}\left(I_4 + \frac{2}{\sqrt{I_4}} - 3\right), \tag{2.91}$$

where $(\mu_1, \mu_2)$ are two homogenized material parameters depending on the matrix and fiber shear modulus.

### 2.3.3 Standard slight compressible transversely isotropic hyperelastic models

On way to develop hyperelastic models is to extend existing incompressible hyperelastic models to compressible behaviour. This is done by assuming an additive split of the strain energy into two parts: a volumetric $W_{vol}$ strain energy depending on volume change invariant $J$ and a isochoric (deviatoric) $W_{isc}$ one function of isochoric strain $\underline{C}$. This is inspiring by the multiplicative decomposition of the deformation gradient introduced by [Flo61a]:

$$W(J, \underline{C}; \mathbf{A}) = W_{vol}(J) + W_{isc}(\underline{C}; \mathbf{A}), \tag{2.92}$$

where the isochoric unimodular are defined by

$$\underline{F} = J^{-1/3}F \quad , \quad \underline{C} = J^{-2/3}C, \tag{2.93}$$

and the corresponding invariants:

$$\underline{I}_1 = I^{-2/3} I_1 \quad , \quad \underline{I}_2 = I^{-4/3} I_2 \quad , \quad \underline{I}_4 = I^{-2/3} I_4 \quad , \quad \underline{I}_5 = I^{-4/3} I_5. \tag{2.94}$$

Thus, the decomposition can be expressed as:

$$W(J, \underline{C}; \mathbf{A}) = W_{vol}(J) + W_{isc}(\underline{I}_1, \underline{I}_2, \underline{I}_4, \underline{I}_5). \tag{2.95}$$

This decomposition (2.92), originally proposed for isotropic behaviour when the hydrostatic Cauchy stress is a function only of J [Ogd78a]; [HM09], should verify some constraints. For incompressible behaviour $J = 1$, the strain energy $W(J = 1, \underline{C}, \mathbf{A})$ should recover a known incompressible hyperelastic model with the constraint $W_{vol}(J = 1) = 0$. In the case of linear behaviour, the strain energy (2.92) should be compatible with the linear elasticity theory. Notice that the split into bulk and deviatoric strain energies (2.92) has the convenience of facilitating material identification through bulk and shear responses. This decoupled sum of strain energies is also crucial for improving the finite element implementation to avoid numerical locking problems for nearly incompressible analysis [STP85a]. Attention should be made for material behaviour that is not nearly incompressible, the decomposition leads to unphysical responses [EE98a].

The key question addressed here is if the decomposition (2.92), assumed by [WMG96b]; [HGO00], is also available for anisotropic behaviour. For the moment, the strain energy decoupled form (2.92) is adopted since this assumption is used by commercial Finite Element codes.

In fact, it seems that the decomposition (2.92) was generalized to anisotropic behaviour [WMG96b]; [HGO00] without theoretical, numerical and experimental analysis. Firstly, it is shown that the fibers play no role for a cube or a sphere under hydrostatic tension [Hel+10a]; [NA+13a]; [Ver+13a]; [Nol+14a]; [Gil+14a]; [Pie+16a]. Secondly, the decomposition (2.92) is not compatible with anisotropic linear elastic theory [San08a]; [Fed10a]; [Pen14a]; [MR18a] as it is expected to be for any nonlinear theory [QS07a].

To overcome these drawbacks, different approaches was formulated. The first one is based on the enrichment of volumetric strain energy in (2.92) with anisotropic invariants:

$$W(J, \underline{C}; \mathbf{A}) = W_{vol}(J, I_4, I_5) + W_{isc}(\underline{I}_1, \underline{I}_2, \underline{I}_4, \underline{I}_5). \tag{2.96}$$

Notice this enrichment was proposed in [Gil+14a] by assuming that the hydrostatic Cauchy stress is a function of volume change and anisotropic invariants. The second approach consists on the substitution of the isochoric anisotropic invariants by classical ones:

$$W(J, \underline{C}; \mathbf{A}) = W_{vol}(J) + W_{isc}(\underline{I}_1, \underline{I}_2, I_4, I_5) \tag{2.97}$$

This enrichment of the anisotropic part of hyperelastic model (2.97) was first proposed in [Nol+14a]; [WL18] and its prediction capability was attested in [NM16a]. There are also others theoretical contributions to overcome the drawback of the volumetric/deviatoric strain energy decomposition (2.92) done in [Pen14a]; [MR18a].

### 2.3.4 Compressible transversely isotropic hyperelastic models

An alternative approach to avoid the drawback of the volumetric/isochoric multiplicative decomposition of the deformation gradient can be described well by the

fiber reinforced continuum mechanics theory of [RE54]; [Spe84]. To do this, a phenomenological approach is usually adopted and the anisotropic compressible hyperelastic potential is expressed in various functional forms such as a series of polynomials or exponentials within the framework of invariant theory [SN03c]; [SNB05]; [CC19a]; [OAK19a]; [O'S+20a]. An example of compressible transversely isotropic hyperelastic model was done by [JT01] and generalize incompressible models (2.85) and (2.86)

$$W = \sum_{k,l,m,n} C_{klmn}(I_1 - 3)^{a_k}(I_2 - 3)^{b_l}(I_4 - 1)^{c_m}(I_5 - 1)^{d_n} + \Gamma(J), \tag{2.98}$$

$$W = \sum_{k,l,m,n} C_{klmn}(I_1^{a_k} - 3^{a_k})(I_2^{b_l} - 3^{b_l})(I_4^{c_m} - 1)(I_5^{d_n} - 1) + \Gamma(J). \tag{2.99}$$

Here, $\Gamma(J)$ is a convex function with $\Gamma(J = 1) = 0$ and verify the growth conditions: $\Gamma(J)$ tends to infinity if $J$ tends to zero or infinity.

## 2.4 Conclusion

The fiber reinforced composites subject of our study are maid of a rubber material matrix and one family of fibers and have a single preferred direction. This architecture of the material, together with the large deformation involved, lead to an anisotropic transversely hyperelastic behaviour whose main constitutive known laws have been presented in this chapter. Some of the hyperelastic potentials presented in this chapter will be used as homogenized potentials in the next chapters.

# Chapter 3

# Two-scale boundary-value problem homogenization

## 3.1 Introduction

The main objective of this chapter is to propose a computational homogenization strategy for a fiber reinforced layer in large elastic deformation having the best possible compromise in term of computational cost and reliability. For this purpose, we develop à decoupled homogenization methodology which is related to the work of Terada et al. [Ter+13a]. We perform a comparison of some different homogenized transverse isotropic hyperelastic potentials with moderate number of parameters and introduce an iterative method to improve the approximation error. This method, by taking into account the deformation state of the structure at the macroscopic scale, allows to approach the coupled $FE^2$ method while keeping a much lower numerical cost. It is organized as follows. Section 2 introduces the homogenization in large deformations. In section 3, we develop the decoupled computational homogenization. We compare various homogenized potentials in section 4 in terms of a local inaccuracy in regard to the heterogeneous model.

## 3.2 Two-scale boundary-value problem homogenization

In order to introduce the two-scale homogenization for the large deformation of a micro-structured composite material, we describe first the macro-scale description, then the micro-scale one and finally the coupling between the two scales.

### 3.2.1 Macro-scale description

Consider a continuum body that occupies the reference configuration $\tilde{\mathcal{B}}_0$ with the boundary $\partial\tilde{\mathcal{B}}_0$ and the outward unit normal vector $\tilde{N}$ where each point is labeled by the macro-scale reference position vector $X \in \tilde{\mathcal{B}}_0$. It is mapped to the spatial current configuration $\tilde{\mathcal{B}}_t$ with the boundary $\partial\tilde{\mathcal{B}}_t$ and the surface normal unit vector $\tilde{n}$, labeled by its current position $x$ via the nonlinear deformation function $\tilde{\varphi}(X) = \tilde{u}(X) + X$, where $\tilde{u}$ being the macro-scale displacement field, written as $x = \tilde{\varphi}(X) \in \tilde{\mathcal{B}}_t$ (see fig. 3.1).

$$\mathrm{d}x = \tilde{F}.\mathrm{d}X. \tag{3.1}$$

For a macroscopic heterogeneous body, subjected to loading and constraints and in the absence of inertia effects, the macro-scale equilibrium equation is expressed as

$$\nabla_X.\tilde{P} + \tilde{b} = 0 \text{ in } \tilde{\mathcal{B}}_0, \tag{3.2}$$

where $\tilde{P}$ is the macro-scale first Piola–Kirchhoff stress tensor and $\tilde{b}$ is the body forces on the reference configuration $\tilde{\mathcal{B}}_0$. Here, $\nabla_X$ designates the divergence operator with respect to material macro-scale coordinates. The body is subjected to Neumann and Dirichlet boundary conditions

$$\begin{aligned} \tilde{P}.\tilde{N} &= \tilde{T}_0 \text{ on } \partial\tilde{\mathcal{B}}_0^N, \\ \tilde{u} &= \tilde{u}_0 \text{ on } \partial\tilde{\mathcal{B}}_0^D, \end{aligned} \tag{3.3}$$

where $\tilde{T}_0$ is the given applied density on the reference configuration, $\tilde{u}_0$ the prescribed displacement on $\partial\tilde{\mathcal{B}}_0^D$ and $\{\partial\tilde{\mathcal{B}}_0^N, \partial\tilde{\mathcal{B}}_0^D\}$ are partitions of $\partial\tilde{\mathcal{B}}_0$.

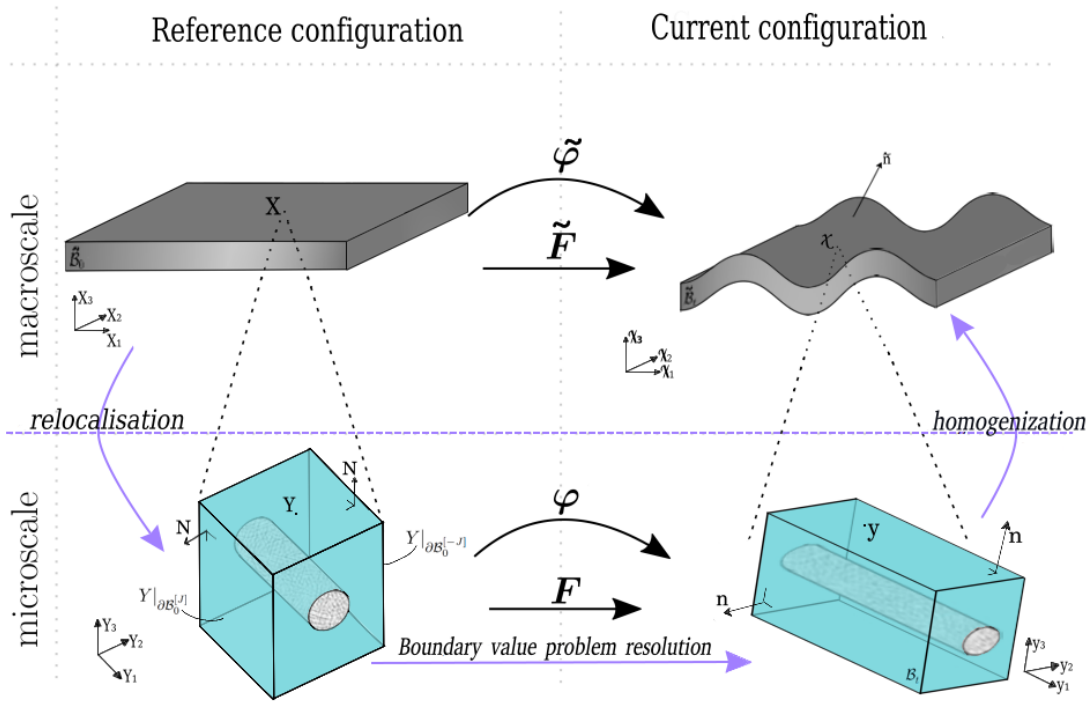


FIGURE 3.1: Two-scale Coupled homogenization

### 3.2.2 Micro-scale description

The mechanical behaviour of the material micro-structure is identified through a representative volume element (RVE). Ideally this RVE has to include a sampling of all micro-structural heterogeneities that occur in the composite at a length scale that should be smaller than the characteristic length of the relevant macroscopic field variation, but sufficiently larger than the micro-scale physics and micro-fluctuations. In particular, it is very important in the homogenization of a fibrous material that the fiber/matrix ratio is maintained on both scales, see classical textbooks on homogenization theory [NNH13b]; [Fis10b].

Due to the scale independence of the equation and boundary conditions, the RVE is usually taken to be the unit cell. The spatial position, denoted $Y$, in the micro-scale reference configuration $\mathcal{B}_0$ of the unit cell domain and the spatial position $y$ in the micro-scale current configuration $\mathcal{B}_t$ are introduced. They are inter-related by the micro-scale deformation as

$$y = \varphi(X; Y) = Y + w(X; Y), \tag{3.4}$$

where

$$w(X;Y) = \tilde{H}(X).Y + u^*(X;Y) + c(X), \tag{3.5}$$

is the micro-scale displacement of the unit cell, $\tilde{H}$ is the macro-scale displacement gradient defined as $\tilde{H}(X) = \nabla_X \tilde{u}(X)$, $u^*$ is the fluctuation displacement, in our case assumed to be exposed to the periodic boundary condition on the RVE external boundary $\partial\mathcal{B}_0$ and $c$ is a constant vector independent of Y, derived from the integration of the micro-scale deformation gradient defined as

$$F(X;Y) = \nabla_Y \varphi(X;Y) = \nabla_Y w(X;Y) + \mathbb{1} = H(X;Y) + \mathbb{1}, \tag{3.6}$$

where $\mathbb{1}$ is the identity (metric) tensor and $H$ is the micro-scale displacement gradient given by

$$H(X;Y) = \nabla_Y w(X;Y) = \tilde{H}(X) + \nabla_Y u^*(X;Y), \tag{3.7}$$

where $\tilde{H} = \frac{1}{|\mathcal{B}_0|}\int_{\mathcal{B}_0} H dV$ and $|\mathcal{B}_0|$ is the reference volume of the RVE (in our case, $|\mathcal{B}_0| = 1$).

The macro-homogeneous deformation tensor $\tilde{F}$ is related to the micro-scale deformation gradient tensor for every point at the micro-scale by

$$F(X;Y) = \tilde{F}(X) + \nabla_Y u^*(X;Y). \tag{3.8}$$

In the absence of body forces, the micro-scale self-equilibrium equation for the unit cell RVE in terms of the micro-scale first Piola–Kirchhoff stress tensor $P$ and its response function $\mathcal{F}(F)$ is given by

$$\begin{cases} \nabla_Y.P = 0 \text{ in } \mathcal{B}_0 \\ P = \mathcal{F}(F) \text{ in } \mathcal{B}_0 \end{cases} \tag{3.9}$$

subjected to periodic boundary conditions

$$w|_{\partial\mathcal{B}_0^{[J]}} - w|_{\partial\mathcal{B}_0^{[-J]}} = w^{[J]} - w^{[-J]} = \tilde{H}.L^{[J]} \text{ on } \partial\mathcal{B}_0^{[J]} \quad (J = 1,2,3), \tag{3.10}$$

where $\partial\mathcal{B}_0^{[J]}$ and $\partial\mathcal{B}_0^{[-J]}$ indicate a pair of opposite external faces of the RVE (see fig. 3.1) and $L$ is called the side vector connecting the material points of a periodic boundary condition defined as

$$L^{[J]} := Y|_{\partial\mathcal{B}_0^{[J]}} - Y|_{\partial\mathcal{B}_0^{[-J]}} \quad (J = 1,2,3). \tag{3.11}$$

Here, $\nabla_Y$ designates the divergence operator with respect to material micro-scale coordinates and $\mathcal{F}$ is a functional defining the constitutive law.

### 3.2.3 Micro-macro coupling

The first order coupling homogenization is based on the idea of computing the overall response of the micro-scale problem, in particular the macro-scale first Piola–Kirchhoff stress tensor $\tilde{P}$, by prescribing the macroscopic deformation gradient $\tilde{F}$ onto the micro-problem. Microscopic quantities are related to their macroscopic counterparts through volume averaging over the RVE [Hil72]; [Ogd74].

The macro-scale deformation gradient can be written as the volume average of the corresponding micro-scale deformation gradient over the RVE derived from (3.6)

$$\tilde{F} = \frac{1}{|\mathcal{B}_0|}\int_{\mathcal{B}_0} F dV = \tilde{H} + \mathbb{1}. \tag{3.12}$$

The insertion of the micro-scale deformation gradient tensor (3.8) into (3.12) leads to

$$\frac{1}{|\mathcal{B}_0|}\int_{\mathcal{B}_0} F dV = \tilde{F} + \frac{1}{|\mathcal{B}_0|}\int_{\mathcal{B}_0} \nabla_Y u^*(X;Y) dV = \tilde{F} + \frac{1}{|\mathcal{B}_0|}\int_{\partial\mathcal{B}_0} u^*(X;Y) \otimes N dA, \tag{3.13}$$

where we use the divergence theorem to transform the volume integral to surface integral over the undeformed boundary $\partial\mathcal{B}_0$ of the RVE with outward normal vector $N$.

It is clear that in order to satisfy the relation between the micro-scale deformation gradient tensor and the macro-scale one (3.8), the contribution of the micro-fluctuation field $u^*(X;Y)$ must vanish at the macro level, which means to prescribe the following adequate boundary conditions

$$u^*|_{\partial\mathcal{B}_0^{[J]}} = u^*|_{\partial\mathcal{B}_0^{[-J]}} \quad (J = 1,2,3). \tag{3.14}$$

The macro-scale first Piola–Kirchhoff stress tensor $\tilde{P}$ can be defined as the volume average of the corresponding micro-scale stress $P$ over the unit cell RVE as

$$\tilde{P} = \frac{1}{|\mathcal{B}_0|}\int_{\mathcal{B}_0} P dV. \tag{3.15}$$

Considering the periodicity condition (3.10), the micro Piola traction vector $T$ satisfies an anti-periodicity conditions on the unit cell boundary $\partial\mathcal{B}_0$ with $N$ being the outward unit normal vector on the corresponding surface in the reference configuration

$$T^{[J]} + T^{[-J]} = 0 \qquad \text{where } T^{[J]} = P.N^{[J]}, \tag{3.16}$$

from which the average Piola traction vector can be derived

$$\tilde{T}_i^{[J]} = \tilde{P}_{iJ} = N^{[i]}.\tilde{T}^{[J]} = N^{[i]}.(\tilde{P}.N^{[J]}) = N^{[i]}.\left(\frac{1}{|\partial\mathcal{B}_0|}\int_{\partial\mathcal{B}_0} P.N^{[J]} dA\right) = \frac{1}{|\partial\mathcal{B}_0^{[J]}|}\int_{\partial\mathcal{B}_0^{[J]}} T_i^{[J]} ds, \tag{3.17}$$

where $|\partial\mathcal{B}_0^{[J]}|$ is the area of the RVE boundary $\partial\mathcal{B}_0^{[J]}$ and $\tilde{P}_{iJ}$ is the iJ component of the macro-scale first Piola–Kirchhoff stress tensor, the area average of the corresponding micro-scale Piola traction vector $T_i^{[J]}$ at the unit cell boundary $\partial\mathcal{B}_0^{[J]}$. This relation is of great interest for the numerical computation of $\tilde{P}$ .

A standard requirement is the satisfaction of the Hill–Mandel condition that requires the volume average of the variation of work performed on the RVE to be equal to the increment of local work on the macro-scale, formulated as

$$\frac{1}{|\mathcal{B}_0|}\int_{\mathcal{B}_0} P : \delta F^T dV = \tilde{P} : \delta\tilde{F}^T. \tag{3.18}$$

The boundary conditions of the RVE that satisfy the Hill-Mandel condition [Hil72]; [Man72] must be determined in order to solve the micro-problem. These

are determined using Hill's lemma

$$\frac{1}{|\mathcal{B}_0|}\int_{\mathcal{B}_0} P:\delta F^T dV - \tilde{P}:\delta\tilde{F}^T = \int_{\partial\mathcal{B}_0}[\delta\varphi - \delta\tilde{F}.Y].[P.N - \tilde{P}.N]dA. \tag{3.19}$$

In our case, the periodic displacement, anti-periodic traction boundary conditions and (3.15) are sufficient to satisfy the Hill–Mandel condition.

The coupled micro-macro homogenized problem can be summarized as follows; the micro-scale BVP is to be solved for each $X \in \tilde{\mathcal{B}}_0$ for the set of solutions $w$,$F$,$H$ that satisfies the micro-scale equilibrium equation (3.9) along with the periodic condition (3.10), while the macro-scale BVP is for $\tilde{F}$, $\tilde{P}$ that satisfies (3.12), (3.15) and (3.2). It is noted that the micro-scale BVP can be solved only if the macro-scale solution is given and vice versa.

This coupled homogenization method allows to define analytical effective behaviour of heterogeneous materials for simple and special classes of uniform boundary conditions and materials constituents models behaviours. These analytic results are of both theoretical and practical importance and will be used in this work. For complexes situations, computational methods were developed (see interesting review in [Gee+17]) but they remain highly expensive for industrial applications.

## 3.3 Micro-macro decoupled computational homogenization

To overcome the computational cost due to the coupled homogenization method, some decoupled numerical approaches for homogenizing heterogeneous materials have been developed [TK95]; [TZO96]; [TW07]; [YGH09]; [CSY12]; [Ter+13a]; [Ter+14b].

The principle of this method, which is related to the work of Terada and his co-workers [Ter+13a], is the decoupling between the microscopic and macroscopic scales carried out by the *a priori* choice of a parametric homogenized law. The parameters of this law are adjusted to minimize the deviation with respect to a series of numerical tests (such as uniform tension, uniform compression, shearing tests and so on) performed on a finite element approximation of the microscopic problem on the RVE. Once the parameters of the law have been optimized, it can be used to compute the deformation at the macroscopic level without solving many microscopic problems simultaneously. This obviously leads to the reduction of computational cost, compared for instance with the $FE^2$ strategy. The quality of the approximation depends of course on the choice of the form of the parametric homogenized law as well as on the strategy of choice of the set of tests (that we will call in the following the training set). In the following sections we describe the details of this method.

### 3.3.1 Selection of a parametrized homogenized law

As shown in the previous sections, the variables exchanged between the scales are the macro displacement gradient $\tilde{H}$ and the average of micro First Piola-Kirchhoff tensor $\tilde{P}$. In order to analyze the micro and macro problems separately, the macro-homogenized constitutive relationship inherent in the micro-structure and its mechanical behaviour is approximated by an appropriate constitutive model. In simple situations, including the fiber reinforced matrix we consider, a possible way to design such constitutive model is to assume that the macroscopic material responses inherit the microscopic ones except for anisotropic behaviour. Consequently, at this stage, and considering large elastic deformation, one has to select a parametrized

elastic law, i.e., the macro-scale second Piola–Kirchhoff stress tensor

$$\tilde{S}_h(p, \tilde{H}),$$

depending on a certain number of parameters

$$p = (p_1, p_2, ..., p_{n_{para}}).$$

In the hyperelastic framework, the elastic law derives from a potential $\tilde{W}_h(p, \tilde{H})$, in the sense that [Ogd97]

$$\tilde{S}_h(p, \tilde{H}) = \frac{\partial \tilde{W}_h}{\partial \tilde{E}}(p, \tilde{H}) = 2\frac{\partial \tilde{W}_h}{\partial \tilde{C}}(p, \tilde{H}), \tag{3.20}$$

where $\tilde{C} = (\tilde{H} + \mathbb{1})^T(\tilde{H} + \mathbb{1})$ is the right Cauchy-Green deformation tensor and $\tilde{E} = \frac{1}{2}(\tilde{C} - \mathbb{1})$ the Green-Lagrange one. Often, for the classical invariants (Table 1), the parametrized law is linear with respect to the material coefficients, which means that it reads

$$\tilde{S}_h(p, \tilde{H}) = \sum_{i=1}^{n_{para}} p_i \tilde{S}_h^i(p, \tilde{H}), \tag{3.21}$$

or

$$\tilde{S}_h(p, \tilde{H}) = 2\sum_{i=1}^{n_{para}} p_i \frac{\partial \tilde{W}_h^i}{\partial \tilde{C}}(p, \tilde{H}), \tag{3.22}$$

in the hyperelastic case, where $\tilde{S}_h^i(\tilde{H}) = 2\frac{\partial \tilde{W}_h^i}{\partial \tilde{C}}(\tilde{H})$.

When the potential $\tilde{W}_h$ is decomposed into volumic and isochoric parts using the isochoric invariants (Table 1 in the appendix of this chapter) and denoting the isochoric Cauchy-Green strain tensor $\underline{\tilde{C}} = J^{-2/3}\tilde{C}$, writting $\tilde{W}_h = \tilde{W}_{vol}(J) + \tilde{W}_{isc}(\underline{\tilde{C}}; \mathbf{A}, \mathbf{B})$ for $\mathbf{A}$ and $\mathbf{B}$ the fibers direction vectors and $J$ the Jacobian of the deformation,

$$\tilde{S}_h(p, \tilde{H}) = 2\frac{\partial \tilde{W}_h}{\partial \tilde{C}} = 2\frac{\partial \tilde{W}_{vol}(J)}{\partial \tilde{C}} + 2\frac{\partial \tilde{W}_{isc}(\underline{\tilde{C}}; \mathbf{A}, \mathbf{B})}{\partial \tilde{C}} = \tilde{S}_{vol}(J) + \tilde{S}_{isc}(\underline{\tilde{C}}; \mathbf{A}, \mathbf{B}), \tag{3.23}$$

where

$$\tilde{S}_{vol}(J) = J\frac{\partial \tilde{W}_{vol}(J)}{\partial J}\tilde{C}^{-1}, \tag{3.24}$$

$$\tilde{S}_{isc}(\underline{\tilde{C}}; \mathbf{A}, \mathbf{B}) = J^{\frac{-2}{3}}\mathbb{Q} : \underline{S}, \tag{3.25}$$

where $\mathbb{Q}$ and $\underline{S}$ are respectively expressed as

$$\mathbb{Q} = \mathbb{I} - \frac{1}{3}\tilde{C}^{-1} \otimes \tilde{C}, \tag{3.26}$$

$$\begin{aligned} \underline{S} = 2\frac{\partial \tilde{W}(\underline{\tilde{C}})}{\partial \underline{\tilde{C}}} = \underline{\gamma}_1\mathbb{1} + \underline{\gamma}_2\underline{\tilde{C}} + \underline{\gamma}_4\mathbf{A} \otimes \mathbf{A} + \underline{\gamma}_5(\mathbf{A} \otimes \underline{\tilde{C}}\mathbf{A} + \underline{\tilde{C}}\mathbf{A} \otimes \mathbf{A}) \\ + \underline{\gamma}_6\mathbf{B} \otimes \mathbf{B} + \underline{\gamma}_7(\mathbf{B} \otimes \underline{\tilde{C}}\mathbf{B} + \underline{\tilde{C}}\mathbf{B} \otimes \mathbf{B}) + \underline{\gamma}_8(\mathbf{A}.\mathbf{B})(\mathbf{A} \otimes \mathbf{B}), \end{aligned} \tag{3.27}$$

along with

$$\left.\begin{aligned} \underline{\gamma}_1 &= 2\left(\frac{\partial \tilde{W}(\underline{\tilde{C}};\mathbf{A},\mathbf{B})}{\partial \underline{I}_1} + \underline{I}_1 \frac{\partial \tilde{W}(\underline{\tilde{C}};\mathbf{A},\mathbf{B})}{\partial \underline{I}_2}\right), \\ \underline{\gamma}_2 &= -2\frac{\partial \tilde{W}(\underline{\tilde{C}};\mathbf{A},\mathbf{B})}{\partial \underline{I}_2}, \quad \underline{\gamma}_4 = 2\frac{\partial \tilde{W}(\underline{\tilde{C}};\mathbf{A},\mathbf{B})}{\partial \underline{I}_4}, \quad \underline{\gamma}_5 = 2\frac{\partial \tilde{W}(\underline{\tilde{C}};\mathbf{A},\mathbf{B})}{\partial \underline{I}_5}, \\ \underline{\gamma}_6 &= 2\frac{\partial \tilde{W}(\underline{\tilde{C}};\mathbf{A},\mathbf{B})}{\partial \underline{I}_6}, \quad \underline{\gamma}_7 = 2\frac{\partial \tilde{W}(\underline{\tilde{C}};\mathbf{A},\mathbf{B})}{\partial \underline{I}_7}, \quad \underline{\gamma}_8 = 2\frac{\partial \tilde{W}(\underline{\tilde{C}};\mathbf{A},\mathbf{B})}{\partial \underline{I}_8}, \end{aligned}\right\}. \tag{3.28}$$

where $\underline{I}_i = J^{-2/3} I_i$ for $i \in \{1,4,6\}$ and $\underline{I}_j = J^{-4/3} I_j$ for $j \in \{2,5,7,8\}$.

Even if this strategy can be applied in the case of fully parametric homogenized laws, as it is presented for instance in [YMH13]; [Gee+17] where interpolation functions are used to describe the homogenized potential, our objective in this study is to consider laws having a restricted number of parameters and allowing a lower cost numerical modelling of the global structure.

### 3.3.2 Numerical material testing, definition of a training set

The idea is to "train" the law (i.e. to fit its parameters) on the response of the microstructure represented on the RVE for a representative set of solicitations. This is done by solving a finite element approximation of the BVP (3.9)-(3.10) for each solicitation. In our case, we select a set of $n_{tests}$ gradients

$$\tilde{H}^{[\alpha]}, \alpha = 1...n_{test}.$$

Then, each gradient $\tilde{H}^{[\alpha]}$ induces a finite element computation (with Lagrange quadratic elements on the mesh represented on fig. 3.2 in our case) which allows in return to calculate the corresponding average of the first Piola-Kirchhoff tensor $\tilde{P}^{[\alpha]}$ through the relation (3.17). Then, the second Piola-Kirchhoff tensor $\tilde{S}^{[\alpha]}$ is obtained using

$$\tilde{S}^{[\alpha]} = (\mathbb{1} + \tilde{H}^{[\alpha]})^{-1} \tilde{P}^{[\alpha]}. \tag{3.29}$$

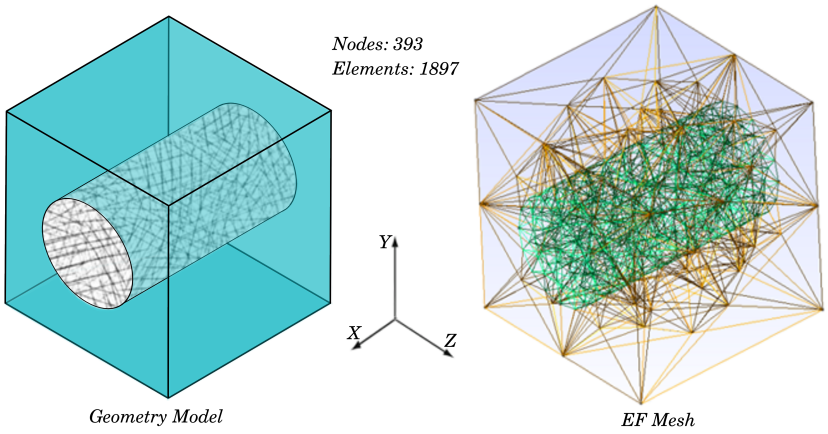


FIGURE 3.2: uni-directional fiber reinforced composite, geometry and finite element mesh

The tests are more or less expensive depending on the complexity of the microstructure represented in the RVE and the refinement of the finite element approximation. As far as we are concerned, the microstructure being relatively simple, the computations on the RVE are relatively cheap although on a three-dimensional RVE.

In our case, the chosen unit cell model for the transverse isotropic material consists of two different materials: the matrix and the fiber. The matrix is assumed to be a cubic sample filling the three dimensional space in $[0,1]^3$ with an inclusion of cylindrical shape. The FE mesh is generated taking into account the interface between the fiber and the matrix, using tetrahedral elements. We employ, for the fibers and matrix, a fixed Poisson's ratio $(\nu_f, \nu_m)$ and Young's modulus defined as

$$E_f = cE_m, \tag{3.30}$$

where $c$ is the contrast constant and $(f, m)$ are indices that refer to the fibers and matrix, respectively.

Finally, we can apply to each solicitation a weight $w^{[\alpha]} > 0$, so that at the end of this step we obtain a training set made of triplets

$$\tilde{H}^{[\alpha]}, \tilde{S}^{[\alpha]}, w^{[\alpha]}, \alpha = 1...n_{test}.$$

For the identification of the coefficients of the chosen potential to be as representative as possible, it is important to give a sufficiently varied panel of solicitations. We apply 6 basic patterns (and some combinations) of macroscopic strains by imposing displacement gradient $\tilde{H}$, introduced in table 3.1. Here, $h$ and $(\varepsilon_1, \varepsilon_2, \varepsilon_3)$ are the specified and unspecified components of the macro-scale displacement gradient $\tilde{H}_i (i = 1, ..., 6)$, respectively. We choose the limiting strain level such that $h \in [-0.5, 0.5]$. The values of $(\varepsilon_1, \varepsilon_2, \varepsilon_3)$ is fixed to $(0, 0, 0)$ in the compressible case and is determined to satisfy the following volume conservation condition in the incompressible case:

$$\det(\tilde{H}(X) + \mathbb{1}) = 1.$$

| | |
|---|---|
| Pattern-1: Uniaxial tension in the direction of x<br>$\tilde{H}_1 = \begin{pmatrix} h & 0 & 0 \\ 0 & \varepsilon_2 & 0 \\ 0 & 0 & \varepsilon_3 \end{pmatrix}$ | Pattern-4: xy shear<br>$\tilde{H}_4 = \begin{pmatrix} \varepsilon_1 & h & 0 \\ h & \varepsilon_2 & 0 \\ 0 & 0 & \varepsilon_3 \end{pmatrix}$ |
| Pattern-2: Uniaxial tension in the direction of y<br>$\tilde{H}_2 = \begin{pmatrix} \varepsilon_1 & 0 & 0 \\ 0 & h & 0 \\ 0 & 0 & \varepsilon_3 \end{pmatrix}$ | Pattern-5: xz shear<br>$\tilde{H}_5 = \begin{pmatrix} \varepsilon_1 & 0 & h \\ 0 & \varepsilon_2 & 0 \\ h & 0 & \varepsilon_3 \end{pmatrix}$ |
| Pattern-3: Uniaxial tension in the direction of z<br>$\tilde{H}_3 = \begin{pmatrix} \varepsilon_1 & 0 & 0 \\ 0 & \varepsilon_2 & 0 \\ 0 & 0 & h \end{pmatrix}$ | Pattern-6: yz shear<br>$\tilde{H}_6 = \begin{pmatrix} \varepsilon_1 & 0 & 0 \\ 0 & \varepsilon_2 & h \\ 0 & h & \varepsilon_3 \end{pmatrix}$ |

TABLE 3.1: Deformation patterns on the RVE

### 3.3.3 Identification of the homogenized law

Once the training set has been determined, the identification of the coefficients of the homogenized law $\tilde{S}_h(p, \tilde{H}^{[\alpha]})$ is performed using a least squares optimization, by minimizing the following quantity:

$$J(p) = \frac{1}{2\omega_*} \sum_{\alpha=1}^{n_{test}} w^{[\alpha]} \frac{\left\| \tilde{S}_h(p, \tilde{H}^{[\alpha]}) - \tilde{S}^{[\alpha]} \right\|^2}{\left\| \tilde{S}^{[\alpha]} \right\|^2}, \tag{3.31}$$

with $\omega_* = \sum_{\beta=1}^{n_{test}} w^{[\beta]}$ the sum of the weights, and $\| \cdot \|$ the Frobenius norm for second order tensors.

This minimization can be performed with or without constraints on the values of the parameters. For instance, most constitutive laws have coefficients that are intended to remain positive and ensure interesting properties (such as polyconvexity) with positive coefficients [SN03a]; [SN03b]. In this case, constraining the coefficients to remain positive can avoid modelling problems (such as spurious zero energy deformations).

In the specific case where the homogenized law $\tilde{S}_h(p, \tilde{H}^{[\alpha]})$ is linear with respect to its coefficients, i.e. in the form (3.20), and if no constraints on the parameters are considered, the minimization of (3.31) leads to the following linear system:

$$A \begin{pmatrix} p_1 \\ \vdots \\ p_{n_{para}} \end{pmatrix} = L, \qquad \text{with} \begin{cases} A_{ll} = \frac{1}{\omega_*} \sum_{j=1}^{n_{test}} w^{[j]} \frac{1}{\left\| \tilde{S}^{[j]} \right\|^2} \tilde{S}_h^l : \tilde{S}_h^l, \\ A_{il} = \frac{1}{2\omega_*} \sum_{j=1}^{n_{test}} w^{[j]} \frac{1}{\left\| \tilde{S}^{[j]} \right\|^2} \tilde{S}_h^l : \tilde{S}_h^i \qquad \forall i \neq l, \\ L_l = \frac{-1}{\omega_*} \sum_{j=1}^{n_{test}} w^{[j]} \frac{1}{\left\| \tilde{S}^{[j]} \right\|^2} \tilde{S}_h^l : \tilde{S}^{[j]}. \end{cases}$$

Of course, the last step of the method, once the homogenized law is identified, is to solve the macro-scale BVP using this constitutive law, generally approximated also by a finite element method. Moreover, since the homogenized law is approximated within the framework of a two-variables boundary value problem derived from homogenization theory, the macro response obtained using this model can be regarded as approximating the data of the micro problem at each material point.

### 3.3.4 Example of the NeoHookean hyperelastic law for both fiber and matrix

The validity of the micro-macro computational decoupled homogenization procedure developed in section 3.3 is investigated by comparison of its predictions with an explicit expression for the effective behaviour of fiber composites [Hil72]; [Ogd74] developed initially for an incompressible transverse isotropic hyperelastic behaviour (i.e. when both $D_{1,m}$ and $D_{1,f}$ goes to infinity) by [DHS06b]. For computational reasons, the fiber and the matrix of the RVE micro-structure are represented by nearly incompressible NeoHookean potential

$$\tilde{W}_{NH,i} = C_{01,i}(\underline{I}_1 - 3) + D_{1,i}(J-1)^2 \quad (i = f, m), \tag{3.32}$$

where $J = \det(\tilde{F})$ is the Jacobian of the deformation, $\underline{I}_1 = \mathrm{tr}(\underline{\tilde{C}})$ is the invariant of the Cauchy-Green strain tensor $\underline{\tilde{C}} = \underline{\tilde{F}}^t.\underline{\tilde{F}} = J^{-2/3}\tilde{F}^t.\tilde{F} = I_3^{-1/3}\tilde{C}$ with $\underline{\tilde{F}} = J^{-1/3}\tilde{F}$ and $I_3 = \det(\tilde{C}) = J^2$, $C_{01,i}$ and $D_{1,i}$ are given coefficients that can be related to Young's modulus and Poisson's ratio by the formula

$$C_{01,i} = \frac{E_i}{4(1+\nu_i)}, \quad D_{1,i} = \frac{E_i}{6(1-2\nu_i)}, \tag{3.33}$$

where we take $E_i$ and $\nu_i$ are the Young modulus and Poisson coefficients of the fiber and the matrix materials with $E_f = 203$GPa and still $E_m = E_f/c$, with $c$ the constrast.

The strain energy decomposition defined by (3.32) governs a slightly compressible material behaviour. If the material behaviour is incompressible, i.e. the coefficients $D_{1,i} \to \infty$, that energy corresponds to the Neo-Hookean potential corresponding to the simplest phenomenological and molecular constitutive model function of rubber like materials [Tre43]. However, its capability to predict experimental data is poor especially at high values of deformation. Nevertheless, the Neo-Hookean strain energy model is the most used model in finite elasticity to deduce analytic solutions of the associated boundary-value problems [Ogd97].

The explicit expression for the effective behaviour of fiber/matrix RVE composite is developed by DeBotton and his co-workers in [DHS06b] exploiting the analytical homogenized method [Hil72]; [Ogd74]. The resulting homogenized law is an incompressible transverse isotropic NeoHookean hyperelastic model [DHS06b]. An extension to a nearly incompressible behaviour will be exploited in this work

$$\tilde{W}_h = \frac{\tilde{\mu}}{2}(\underline{I}_1 - 3) + \frac{\overline{\mu} - \tilde{\mu}}{2}(\underline{I}_4 + \frac{2}{\sqrt{\underline{I}_4}} - 3) + D(J-1)^2, \tag{3.34}$$

where $\underline{I}_4 = \mathbf{A}.\underline{\tilde{C}}\mathbf{A}$, $\mathbf{A}$ is the unit vector along the fiber, and the coefficients $\tilde{\mu}$ and $\overline{\mu}$ are scalar-valued material parameters given by

$$\begin{aligned} \tilde{\mu} = \mu_m \frac{(1+c^f)\mu_f + (1-c^f)\mu_m}{(1-c^f)\mu_f + (1+c^f)\mu_m}, \\ \overline{\mu} = \mu_f c^f + \mu_m c^m, \end{aligned} \tag{3.35}$$

with $0 < c^f < 1$ the volume fraction of fiber, $c^m = 1 - c^f$ the volume of fraction of matrix and $\mu_f, \mu_m$ the shear modulus (Lamé coefficients) of the fiber and matrix, respectively.

For anisotropic hyperelastic behaviour, the decomposition (3.34) was firstly adopted by [WMG96a] and [HGO00] and is also adopted by almost all commercial and open-source Finite Element codes. Notice that the incompressible case is recovered if the coefficient $D$ (proportional to the bulk coefficient) tends to infinity.

The test are performed with $\nu = \nu_f = \nu_m$ varying from 0.49 to 0.4999 and with $c^f = 0.196$. We perform the identification of the parameters of the homogeneized law (3.34) with a training set composed of 50 experiments for each simple pattern and mixed combinations from table 3.1 for a range of deformations up to 50% and compare the results with the theoretical values (3.35).

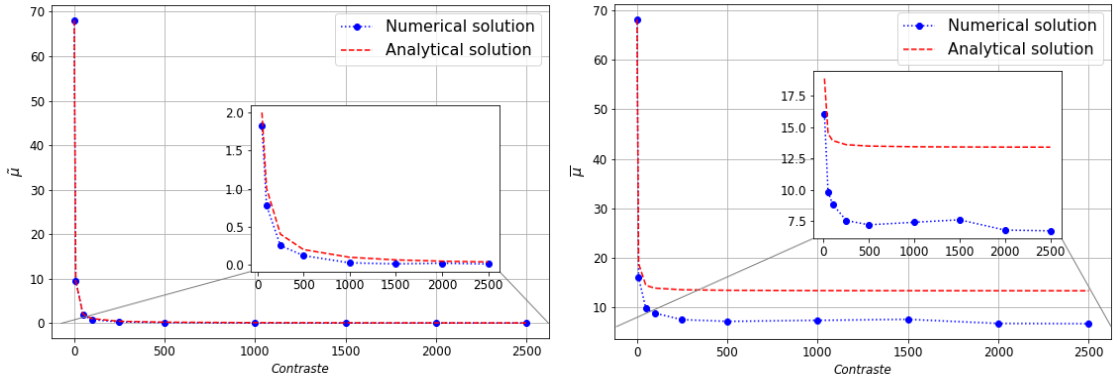


(a) $\tilde{\mu}$ vs contrast (b) $\bar{\mu}$ vs contrast

FIGURE 3.3: Identification of the coefficients $\tilde{\mu}$ and $\bar{\mu}$ for a Poisson coefficient $\nu = 0.49$ and for a contrast $c \in [1, 2500]$.

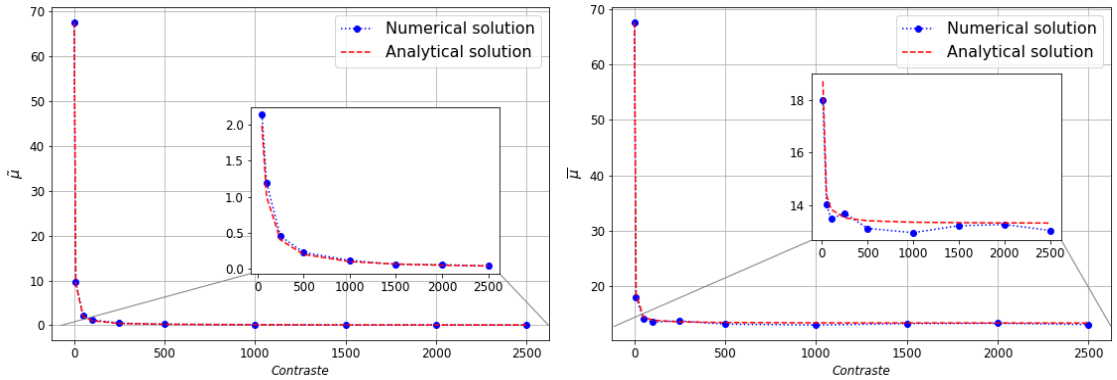


(a) $\tilde{\mu}$ vs contrast (b) $\bar{\mu}$ vs contrast

FIGURE 3.4: Identification of the coefficients $\tilde{\mu}$ and $\bar{\mu}$ for a Poisson coefficient $\nu = 0.4999$ and for a contrast $c \in [1, 2500]$.

The result of the identification, presented on fig. 3.3 for a Poisson coefficient $\nu = \nu_f = \nu_m = 0.49$, shows a relatively good agreement between the identified value of $\tilde{\mu}$ and its theoretical value. On the contrary, there is a significant difference for $\bar{\mu}$. The differences are much smaller on fig. 3.4 for a Poisson coefficient $\nu = \nu_f = \nu_m = 0.4999$ closer of the incompressibility limit for which the theoretical values (3.35) are valid. Overall, these numerical experiments show that the identification based on a training set allows to identify the homogenized law with a good accuracy.

## 3.4 Local error

In the case of the previous section, the homogenized law has been identified exactly and therefore the decoupling does not induce additional approximation. In the general case where this identification cannot be done exactly, the form of the chosen homogenized law corresponds to an additional approximation. One way to measure the approximation made once the identification is done on a particular training set, is to compute the local error between the homogenized law and the average of second Piola-Kirchhoff tensor calculated on the RVE. For this purpose, the following local error is introduced:

$$\mathrm{Err}(\tilde{H}^{[\alpha]}) = \frac{\left\| \tilde{S}_h(p, \tilde{H}^{[\alpha]}) - \tilde{S}^{[\alpha]} \right\|}{\left\| \tilde{S}^{[\alpha]} \right\|}. \tag{3.36}$$

This error must be zero for any $\tilde{H}^{[\alpha]}$ in the case of exact decoupling. In the following sections, we present numerical studies of this local error for different choices of homogenized laws.

For the rest of this study, the fiber is represented by a Saint-Venant Kirchhoff hyper-elastic law which potential reads

$$\tilde{W}_{SVK} = \frac{\lambda_f}{2}[\mathrm{tr}(E)]^2 + \mu_f \mathrm{tr}(E^2), \tag{3.37}$$

with $\lambda_f = \frac{E_f \nu_f}{(1+\nu_f)(1-2\nu_f)}$ and $\mu_f = \frac{E_f}{2(1+\nu_f)}$ and $E_f = 203\mathrm{GPa}$, $\nu_f = 0.3$. This model only extends the geometrically linear Hooke elastic material model to the geometrically nonlinear region as has been presented in [TT60]. Even though it appears to have deficiencies in large strain areas, it has since attracted a lot of interest [Bat98] [Bat01] [Sau+22].

The matrix is represented by a compressible Mooney-Rivlin hyper-elastic law of potential

$$\tilde{W}_{MR} = c_{01,m}(\underline{I}_1 - 3) + c_{10,m}(\underline{I}_2 - 3) + d_{1,m}(J-1)^2, \tag{3.38}$$

with $c_{01,i} = \frac{E_m}{4(1+\nu_m)}$, $c_{10,i} = 0.15 c_{01,i}$, $d_{1,i} = \frac{E_m}{6(1-2\nu_m)}$ and $\nu_m = 0.49$ and for different values of $E_m$ corresponding to different contrasts $c = \frac{E_f}{E_m}$.

The incompressible version of the hyperelastic model (3.38) was first published by Melvin Mooney in [Moo40b] and Ronald Rivlin later defined it in terms of invariants [Riv48b]. It is also to be noted that the Mooney-Rivlin (MR) model is an extension of the NeoHookean model that attempts to improve the accuracy by including a linear dependence on the second invariant $\underline{I}_2$ in strain energy [HS12].

As an experimental training set, we use 50 experiments for each of the 6 simple patterns of table 3.1 and also for 9 additional patterns which are combinations of the simple ones as $\tilde{H}_i + \tilde{H}_j$ for $i \in \{1,2,3\}$ and $j \in \{4,5,6\}$. The 50 experiments are regularly distributed in a logarithmic scale up to a deformation of 30% and we use uniform weights ($\omega^{[\alpha]} = 1$ in (3.31)).

In both of the homogenized potentials bellow, we will study the difference between the local error results of the identified coefficients of the homogenized law using the Sequential Least Squares Programming (SLSQP) method with constraints on positivity of the coefficients to preserve the consistency of the law and also without these constraints.

### 3.4.1 Slightly compressible hyperelastic model : original decoupled Kaliske's transverse isotropic law

One way to develop hyperelastic models is to extend existing incompressible hyperelastic models to compressible behaviour. This is done by assuming an additive split of the strain energy into two parts: a volumetric $W_{vol}$ strain energy depending on volume change invariant $J$ and a isochoric (deviatoric) $W_{isc}$ one function of isochoric strain $\underline{C}$. This is inspired by the decomposition of the deformation gradient introduced in [Flo61b]:

$$\tilde{W}_h(\underline{\tilde{C}}, J; \mathbf{A}) = W_{vol}(J) + W_{isc}(\underline{\tilde{C}}; \mathbf{A}), \tag{3.39}$$

This decomposition (3.39), originally proposed for isotropic behaviour when the hydrostatic Cauchy stress is a function only of $J$ [Ogd78b], should satisfy some constraint. For incompressible behaviour $J = 1$, the strain energy $\tilde{W}_h(J = 1, \underline{\tilde{C}}; \mathbf{A})$ should recover a known incompressible hyperelastic model with the constraint $W_{vol}(J = 1) = 0$. In the case of small transformations, the strain energy should be compatible with the linear elasticity theory. Notice that the split into bulk and deviatoric strain energies has the convenience of facilitating material identification through bulk and shear responses. This decoupled sum of strain energies is also crucial for improving the finite element implementation to avoid numerical locking problems for nearly incompressible analysis [STP85b]. Attention should be made for material behaviour that is not nearly incompressible, the decomposition leads to unphysical responses [EE98b].

The key question addressed here is if this decomposition (3.39) is also available for anisotropic behaviour. For the moment, the strain energy decoupled form is adopted.

In this work, the homogenized material is modelled by a hyperelastic potential as a summation of a volumetric energy function of the Jacobian $W_{vol}$ which is the response of the material to volume changes and an isochoric energy function $W_{isc}$ depends only on the distortional part of the deformation which can be divided into $W_{iso}$ and $W_{aniso}$ for the energy contributions of the matrix as domineering ground substance and and the fibers, respectively:

$$W_{vol} = D(J-1)^2, \tag{3.40}$$

$$W_{isc} = W_{iso}(\underline{I}_1, \underline{I}_2) + W_{aniso}(\underline{I}_4, \underline{I}_5; \mathbf{A}), \tag{3.41}$$

where the isochoric invariants of $\underline{\tilde{C}}$ are defined as $\underline{I}_2 = \frac{1}{2}(\mathrm{tr}^2(\underline{\tilde{C}}) - \mathrm{tr}(\underline{\tilde{C}}^2))$, for the first layer $\underline{I}_4 = \mathbf{A}.\underline{\tilde{C}}\mathbf{A}$, $\underline{I}_5 = \mathbf{A}.\underline{\tilde{C}}^2\mathbf{A}$ and $\mathbf{A}$ still being a unit vector along the layer fiber.

The isochoric strain energy density function of Kaliske, as presented in [Kal00a] and in particular used in a similar context for periodic unidirectional composite layer in [Ter+13a], reduces to

$$W_{iso} = \sum_{i=1}^{3} a_i(\underline{I}_1 - 3)^i + \sum_{j=1}^{3} b_j(\underline{I}_2 - 3)^j, \tag{3.42}$$

$$W_{aniso} = \sum_{k=2}^{6} c_k(\underline{I}_4 - 1)^k + \sum_{l=2}^{6} d_l(\underline{I}_5 - 1)^l. \tag{3.43}$$

and the second Piola Kirchoff tensor is

$$\tilde{S}_h = S_{vol} + S_{isc} = S_{vol} + S_{iso} + S_{aniso}, \tag{3.44}$$

$$S_{vol} = 2(J-1)J\tilde{C}^{-1}, \tag{3.45}$$

$$\begin{aligned} S_{iso} = I_3^{\frac{-1}{3}}((2a_1 + 4a_2(\underline{I}_1 - 3) + 6a_3(\underline{I}_1 - 3)^2)(\mathbb{1} - \frac{1}{3}\tilde{C}^{-1}(\tilde{C} : \mathbb{1})) \\ +(2b_1 + 4b_2(\underline{I}_2 - 3) + 6b_3(\underline{I}_2 - 3)^2)((\underline{I}_1\mathbb{1} - \underline{\tilde{C}}) - \frac{1}{3}\tilde{C}^{-1}(\tilde{C} : (\underline{I}_1\mathbb{1} - \underline{\tilde{C}})))), \end{aligned} \tag{3.46}$$

$$
\begin{aligned}
S_{aniso} = I_3^{\frac{-1}{3}}\,((4c_2(\underline{I}_4-1)+6c_3(\underline{I}_4-1)^2+8c_4(\underline{I}_4-1)^3+10c_5(\underline{I}_4-1)^4 \\
+12c_6(\underline{I}_4-1)^5)(\mathbf{A}\otimes\mathbf{A}-\frac{1}{3}\tilde{C}^{-1}(\tilde{C}:(\mathbf{A}\otimes\mathbf{A})))+(4d_2(\underline{I}_4-1) \\
+6c_3(\underline{I}_4-1)^2+8d_4(\underline{I}_4-1)^3+10d_5(\underline{I}_4-1)^4+12d_6(\underline{I}_4-1)^5) \\
((\mathbf{A}\otimes(\underline{\tilde{C}}.\mathbf{A})+(\underline{\tilde{C}}.\mathbf{A})\otimes\mathbf{A})-\frac{1}{3}\tilde{C}^{-1}(\tilde{C}:(\mathbf{A}\otimes(\underline{\tilde{C}}.\mathbf{A})+(\underline{\tilde{C}}.\mathbf{A})\otimes\mathbf{A})))).
\end{aligned}
\tag{3.47}
$$

The tests are performed for a range of deformations up to 30% and for three different contrast values ($c = 10$, $c = 150$ and $c = 2000$).

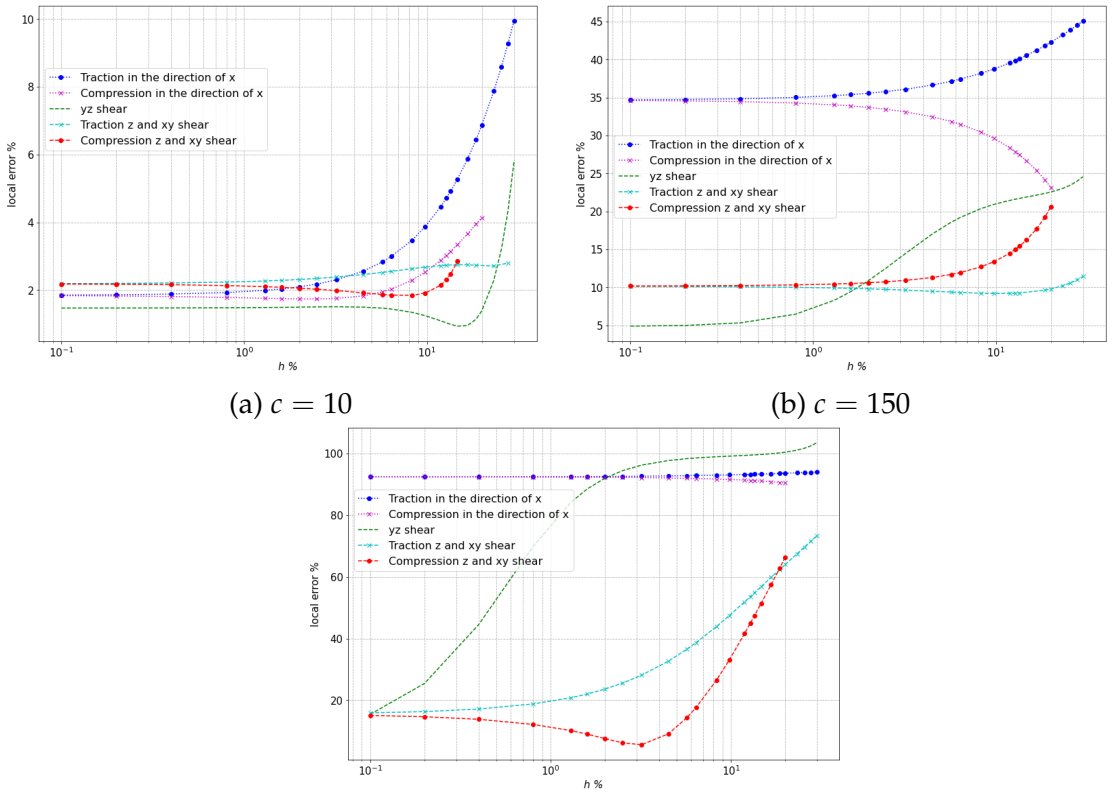


(a) $c = 10$ (b) $c = 150$

(c) $c = 2000$

FIGURE 3.5: Local error for Kaliske's transverse isotropic law with respect to the deformation and three different contrasts, with constraints on positivity of the coefficients

The local errors shown on fig. 3.5 are quite large, except for the lowest contrast value ($c = 10$) and even for small deformations. Our interpretation of this very poor approximation for a high value of the contrast is that isochoric invariants $\underline{I}_1$, $\underline{I}_2$, and especially $\underline{I}_4$ and $\underline{I}_5$ being insensitive to uniform compression, the only term in Kaliske's law which is responsible for the response to a uniform compression is the volumic one. This means in particular that a uniform compression result in an isotropic response, even for a high value of the contrast, which is not the expected behaviour. Our conclusion is that Kaliske's law cannot be used for a high value of contrast in the context of our study (nearly incompressible matrix and compressible fiber) and therefore we propose a variant for the anisotropic part in the next section.

The analysis done above is corroborated by theoretical and numerical works. In fact, it seems that the decomposition was generalized to anisotropic behaviour [WMG96a] and [Hol02] without theoretical, numerical and experimental analysis. Firstly, it is shown that the fibers play no role for a cube or a sphere under hydrostatic tension [Hel+10b] [NA+13b] [Ver+13b] [Nol+14b] [Gil+14b] [Pie+16b]. Secondly, the decomposition is not compatible with anisotropic linear elastic theory [San08b] [Fed10b] [Pen14b] [MR18b] as it is expected to be for any nonlinear theory [QS07b].

The recent works of Annaidh et al. [NA+13b] and Gilchrist et al. [Gil+14b] have shown that this uncoupled form was not only physically unrealistic but also gave erroneous results; for instance, a transversely isotropic cube under hydrostatic tension deforms into another cube instead of a rectangular cuboid. The mathematical reasons of this issue have been demonstrated by Gilchrist et al. [Gil+14b], and may be roughly explained by the fact that the dilational component $W_{vol}$ depends only on $J$ (or $I_3$), which does not account for anisotropy of volumetric deformations.

### 3.4.2 Modified slightly compressible hyperelastic model : First Variant of Kaliske's transverse isotropic law

In order to address this issue, Gilchrist et al. [Gil+14b] proposed an alternative variant in which the isochoric (deviatoric) part of $W$ remains unchanged but the volumetric (dilatational) part is a function of $J$ and $I_4$ which ensures a non-homogeneous deformation of the VER and according to Helfenstein et al. (2010), it weakens the principle of the uncoupled form and allows the fibers to highly contribute in the energy according to the total deformation.

The new form for the volumetric part (3.40) of the strain energy density function may therefore be expressed as

$$W_{vol} = W_{vol}(I_4, J) = D(J-1)^2 + D_1 J(3I_4^{1/2} - 4 + I_4^{-3/2}) \tag{3.48}$$

$$S_{vol} = 2DJ(J-1)\tilde{C}^{-1} + D_1 J((3I_4^{1/2} - 4 + I_4^{-3/2})\tilde{C}^{-1} + 3(I_4^{-1/2} - I_4^{-5/2})\mathbf{A}\otimes\mathbf{A}) \tag{3.49}$$

**First Variant of Kaliske's law**

$$\tilde{W}_{FKV} = W_{vol}(I_4, J) + W_{iso}(\underline{I}_1, \underline{I}_2) + W_{aniso}(\underline{I}_4, \underline{I}_5),$$

$$W_{vol} = W_{vol}(I_4, J) = D(J-1)^2 + D_1 J(3I_4^{1/2} - 4 + I_4^{-3/2})$$

$$W_{iso} = \sum_{i=1}^{3} a_i(\underline{I}_1 - 3)^i + \sum_{j=1}^{3} b_j(\underline{I}_2 - 3)^j$$

$$W_{aniso} = \sum_{k=2}^{6} c_k(\underline{I}_4 - 1)^k + \sum_{l=2}^{6} d_l(\underline{I}_5 - 1)^l$$

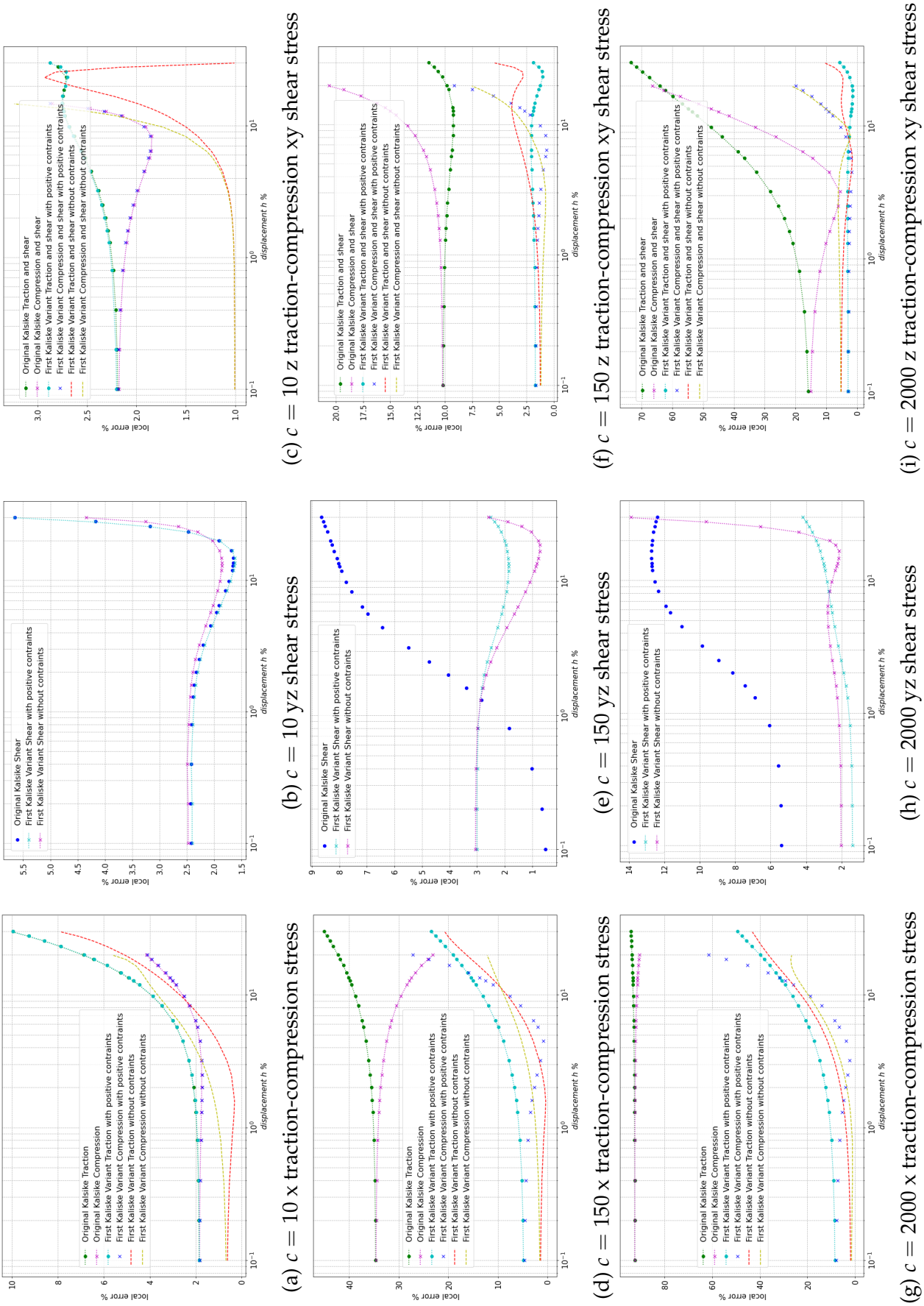


(a) $c = 10$ x traction-compression stress (b) $c = 10$ yz shear stress (c) $c = 10$ z traction-compression xy shear stress

(d) $c = 150$ x traction-compression stress (e) $c = 150$ yz shear stress (f) $c = 150$ z traction-compression xy shear stress

(g) $c = 2000$ x traction-compression stress (h) $c = 2000$ yz shear stress (i) $c = 2000$ z traction-compression xy shear stress

FIGURE 3.6: Local error for the original vs the first variant of Kaliske's law

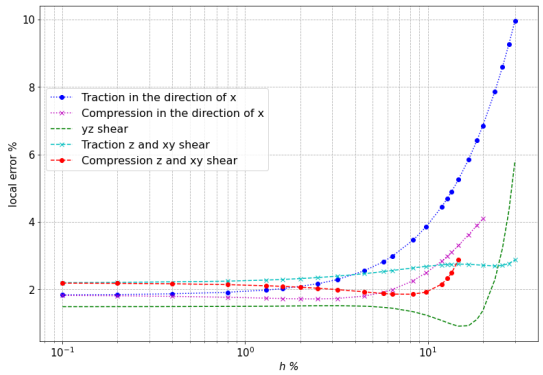


(a) $c = 10$

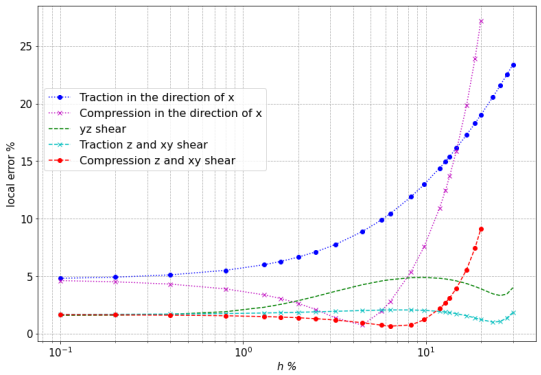


(b) $c = 150$

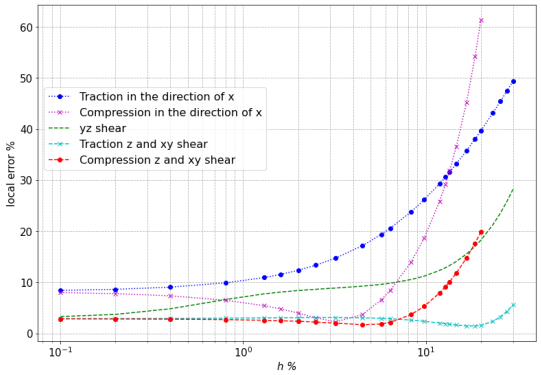


(c) $c = 2000$

FIGURE 3.7: Local error for the first variant of Kaliske's transverse isotropic law with respect to the deformation and three different contrasts, with constraints on positivity of the coefficients

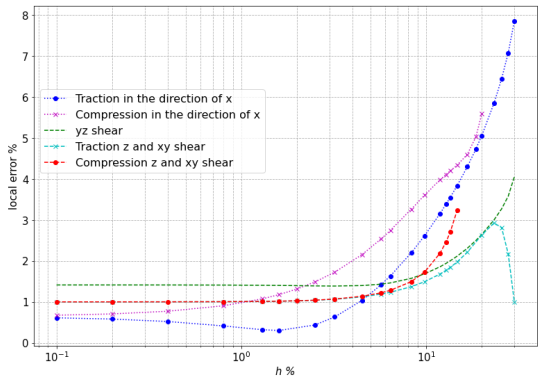


(a) $c = 10$

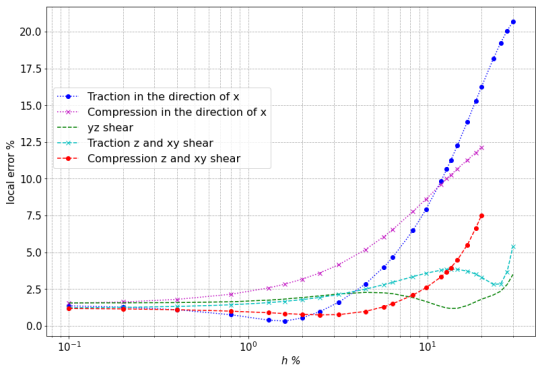


(b) $c = 150$

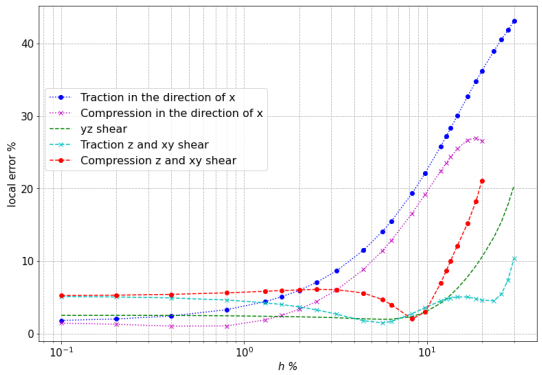


(c) $c = 2000$

FIGURE 3.8: Local error for the first variant of Kaliske's transverse isotropic law with respect to the deformation and three different contrasts without constraints

The modified first variant of Kaliske's law (3.4.2) allows a significant reduction in local error fig. 3.7 with positivity constraints and fig. 3.8 without constraints when compared to the original Kaliske's law fig. 3.5. It shows that for high contrasts and moderated deformations, the local error is greatly reduced. For combined pattern z tension-compression and xy shear and for low contrasts (c=10), the modified first variant of the Kaliske model allows to obtain relatively low error rates (of the order of 1%) for deformation rates of 90%. The error does not exceed 3% even for deformation rates exceeding 200%. An increase in the error rates is observed when the contrast increases significantly. Nevertheless, these rates, for the first Kaliske variant, remain lower than the rates obtained by the original model fig. 3.6 (a)-(d)-(g). The same trend is observed for simple shear fig. 3.6 (c)-(f)-(i) and traction-compression fig. 3.6 (b)-(e)-(h) stresses, which confirms that this first variant of the Kaliske model provides a better approximation of the behaviour of the fibrous layer.

### 3.4.3 Modified slightly compressible hyperelastic model : Second Variant of Kaliske's transverse isotropic law

Following the conclusion of section 3.4.1 that the deficiency of Kaliske's law comes from the fact that isochoric invariants are used even for the anisotropic part, which does not fit well with the numerical experiments on the RVE, we propose a second variant of this law replacing the strain energy density function (3.43) for the anisotropic part by the following one which uses standard invariants:

$$W_{aniso} = \sum_{k=2}^{6} c_k (I_4 - 1)^k + \sum_{l=2}^{6} d_l (I_5 - 1)^l. \tag{3.50}$$

$$\begin{aligned} S_{aniso} = {} & (2c_1 + 4c_2(I_4 - 1) + 6c_3(I_4 - 1)^2 + 8c_4(I_4 - 1)^3 + 10c_5(I_4 - 1)^4 \\ & + 12c_6(I_4 - 1)^5)(\mathbf{A} \otimes \mathbf{A}) + (2d_1 + 4d_2(I_5 - 1) + 6d_3(I_5 - 1)^2 + 8d_4(I_5 - 1)^3 \\ & + 10d_5(I_5 - 1)^4 + 12d_6(I_5 - 1)^5)(\mathbf{A} \otimes (\tilde{C}.\mathbf{A}) + (\tilde{C}.\mathbf{A}) \otimes \mathbf{A}) \end{aligned} \tag{3.51}$$

This enrichment of the anisotropic part of hyperelastic model (3.43) was first proposed in [Nol+14b] [WL20] and its prediction capability was attested in [NM16b].

There are also others theoretical contributions to overcome the drawback of the volumetric/deviatoric strain energy decomposition done in [Pen14b][MR18b].

**Second Variant of Kaliske's law**

$$\tilde{W}_{SKV} = W_{vol}(J) + W_{iso}(\underline{I}_1, \underline{I}_2) + W_{aniso}(I_4, I_5),$$

$$W_{vol} = D(J-1)^2$$

$$W_{iso} = \sum_{i=1}^{3} a_i(\underline{I}_1 - 3)^i + \sum_{j=1}^{3} b_j(\underline{I}_2 - 3)^j$$

$$W_{aniso} = \sum_{k=2}^{6} c_k(I_4 - 1)^k + \sum_{l=2}^{6} d_l(I_5 - 1)^l$$

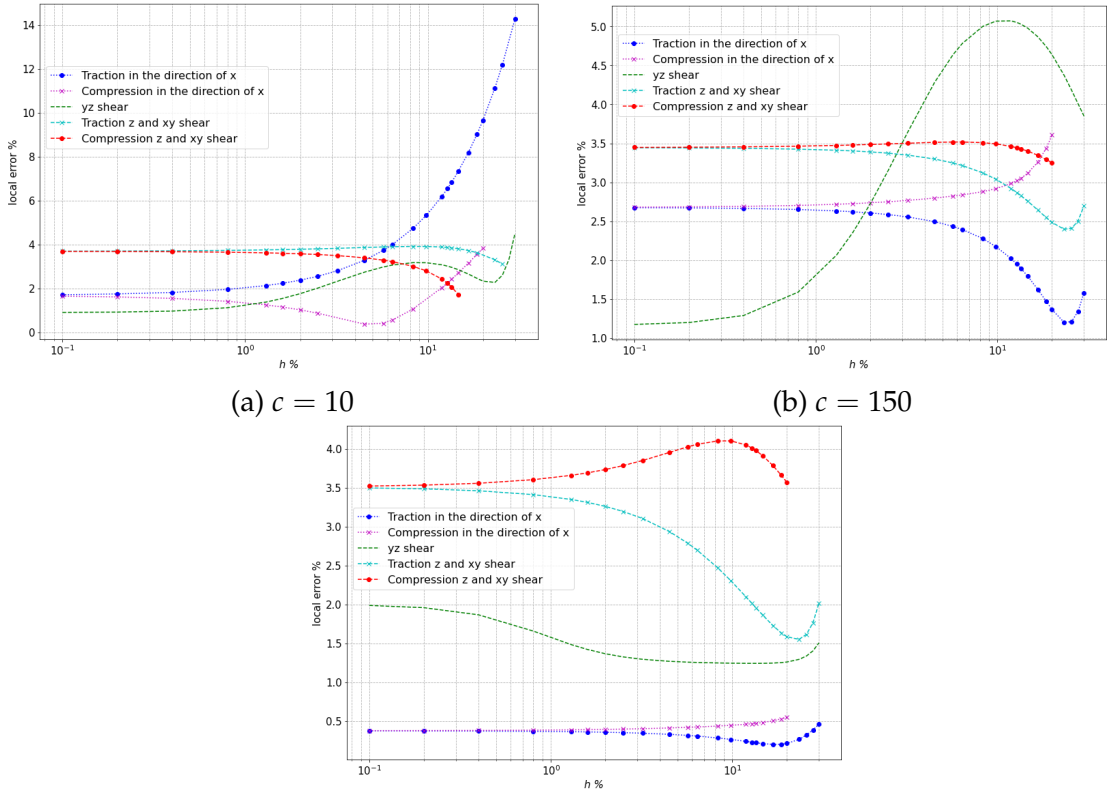


(a) $c = 10$ (b) $c = 150$

(c) $c = 2000$

FIGURE 3.9: Local error for the second variant of Kaliske's transverse isotropic law with respect to the deformation and three different contrasts with positivity constraints

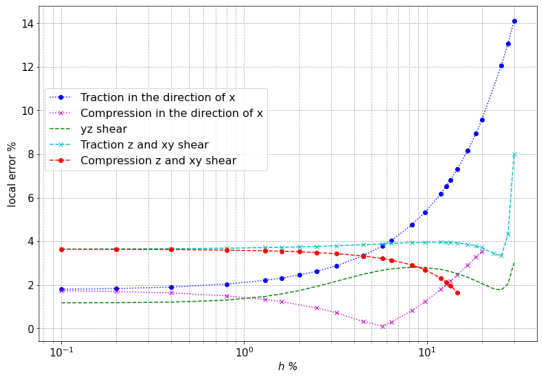


(a) $c = 10$

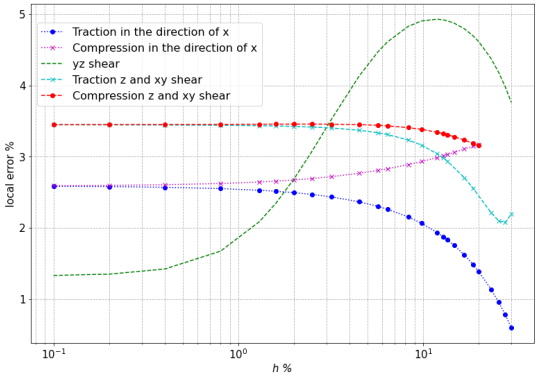


(b) $c = 150$

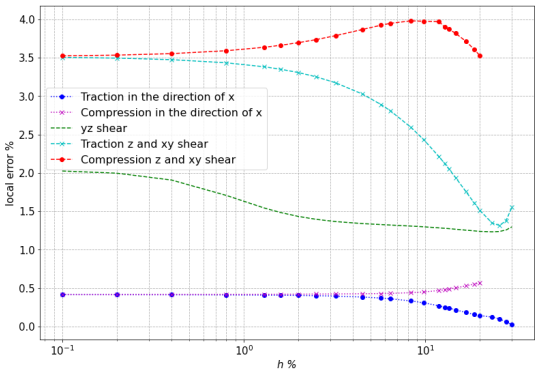


(c) $c = 2000$

FIGURE 3.10: Local error for the second variant of Kaliske's transverse isotropic law with respect to the deformation and three different contrasts without constraints

The corresponding local errors can be seen on fig. 3.9 for the optimisation with positivity constraints on the coefficients and fig. 3.10 for the optimisation without. The error level is slightly higher for the contrast ($c = 10$) for moderate deformations compared to fig. 3.5 for original Kaliske law. Along with this, there is a huge improvement of the approximation for high values of contrast, with less than 5% of error and no degradation for large deformations, even compared to second variant of Kaliske [Gil+14b]. For combined pattern z tension-compression and xy shear fig. 3.11 (a)-(d)-(g) and for simple yz shear fig. 3.11 (c)-(f)-(i) stresses for high contrasts (c=2000) , the modified second variant of Kaliske's law shows relatively low error rates (of the order of 2.5%) for deformation rates of 90%. The error does not exceed 4% even for deformation rates exceeding 200%. An increase in the error rates is observed when the contrast decreases significantly. Nevertheless, these rates, for the second Kaliske variant, remain lower than the rates obtained by the original model and first Kaliske variant. The same trend is observed for simple traction-compression fig. 3.11 (b)-(e)-(h) stresses, which confirms that this second variant of the Kaliske model provides a better approximation of the behaviour of the fibrous layer. In the context of the rest of our study, we will focus on a high value of contrast ($c = 2000$) compatible with a couple of material such as rubber and steel. Consequently, we will consider only this variant of Kaliske's law instead of the original and first variant ones.

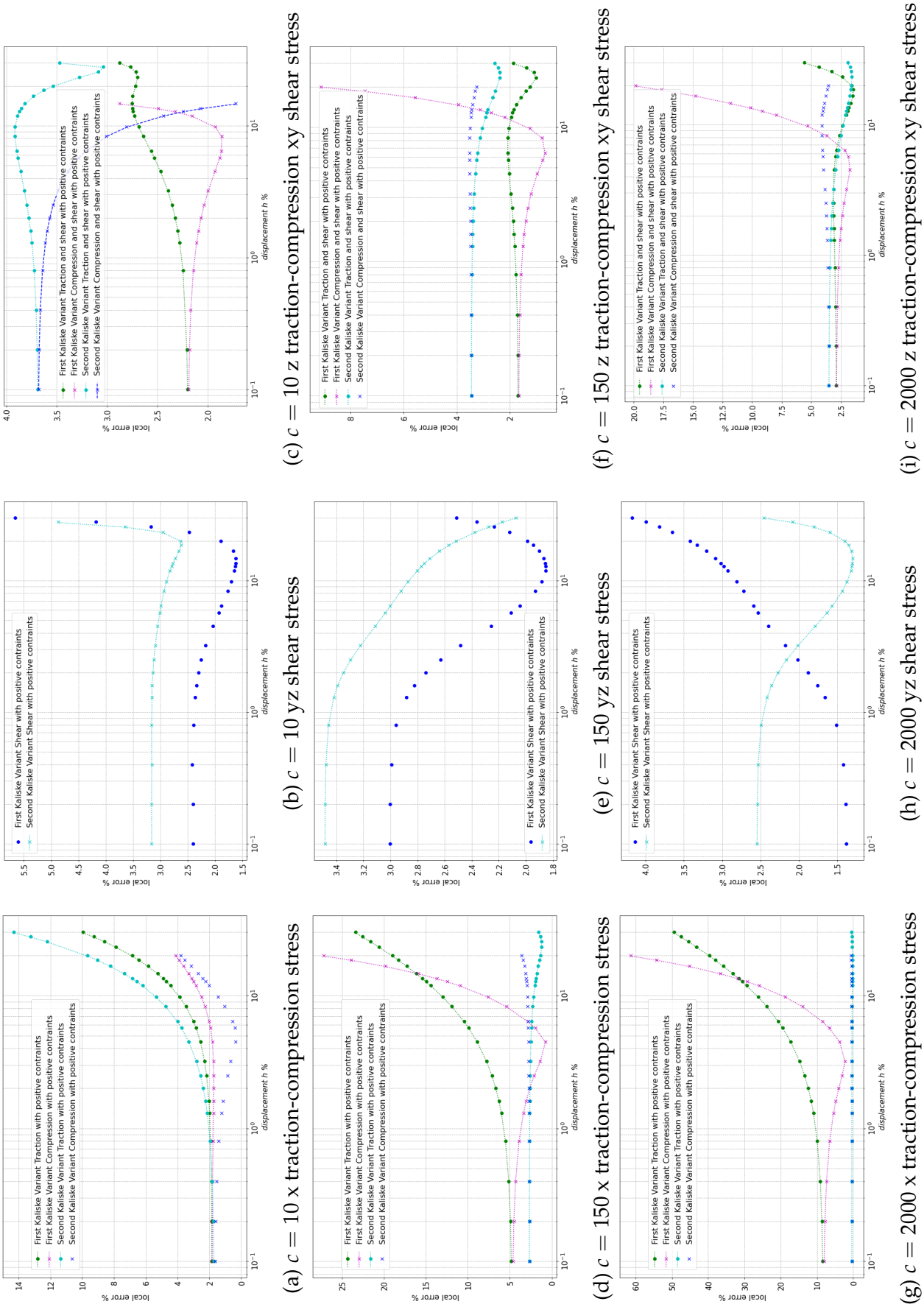


(a) $c = 10$ x traction-compression stress (b) $c = 10$ yz shear stress (c) $c = 10$ z traction-compression xy shear stress

(d) $c = 150$ x traction-compression stress (e) $c = 150$ yz shear stress (f) $c = 150$ z traction-compression xy shear stress

(g) $c = 2000$ x traction-compression stress (h) $c = 2000$ yz shear stress (i) $c = 2000$ z traction-compression xy shear stress

FIGURE 3.11: Local error for the first vs the second variants of Kaliske's law

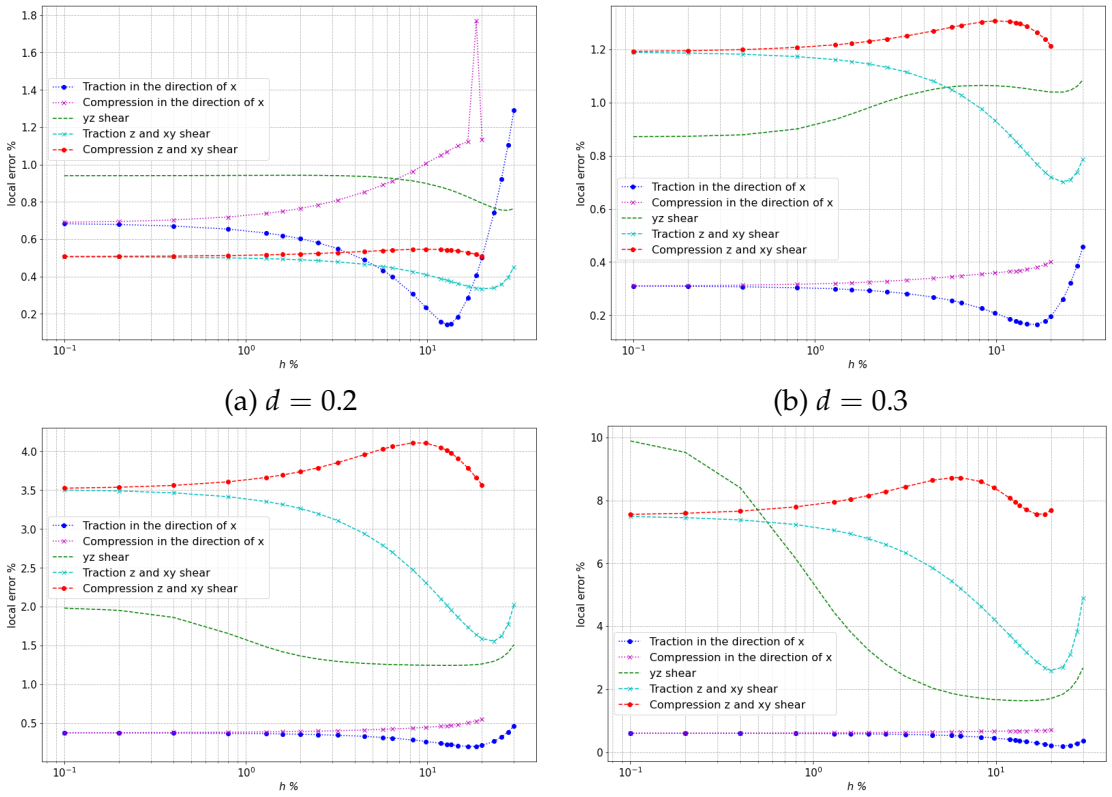


(a) $d = 0.2$ (b) $d = 0.3$

(c) $d = 0.5$ (d) $d = 0.7$

FIGURE 3.12: Local error for second variant of Kaliske's law with respect to the deformation and four different fiber diameters for contrast = 2000 with positivity constraints

Finally, on fig. 3.12, we observe slight deterioration of the local error with the augmentation of the fiber diameter, but still with a good approximation.

### 3.4.4 Compressible hyperelastic model: Bonet's transverse isotropic law

An alternative approach to avoid the drawback of the volumetric/isochoric multiplicative decomposition of the deformation gradient can be described well by the fiber-reinforced continuum mechanics theory of [ER97]; [Spe85]. To do this, a phenomenological approach is usually adopted and the anisotropic compressible hyperelastic potential is expressed in various functional forms such as a series of polynomials or exponentials within the framework of invariant theory [SN03b]; [SNB05]; [CC19b]; [OAK19b]; [O'S+20b].

In this work, Bonet's transverse isotropic potential [BB98] is considered, which is a combination of an isotropic strain energy density function $W_{iso}$ characterising the rubber type of materials in the large strain (Neo-Hookean potential), and a transverse one $W_{trn}$ defined as follows:

$$\tilde{W}_h = W_{iso} + W_{trn}, \tag{3.52}$$

$$W_{iso} = \mu_{iso}(\frac{1}{2}(I_1 - 3) - \ln(J)) + \frac{\lambda_{iso}}{2}(\ln(J))^2, \tag{3.53}$$

$$W_{trn} = (a_{tr} + b_{tr}\ln(J) + c_{tr}(I_4 - 1))(I_4 - 1) - (\frac{1}{2}a_{tr} + d_{tr}\ln(J))(I_5 - 1), \tag{3.54}$$

and the second Piola Kirchoff tensor is

$$S_{iso} = \mu_{iso}(\mathbb{1} - \tilde{C}^{-1}) + \lambda_{iso}\ln(J)\tilde{C}^{-1}, \tag{3.55}$$

$$S_{trn} = 2a_{tr}(\mathbf{A}\otimes\mathbf{A} - \frac{1}{2}(\mathbf{A}\otimes(\tilde{C}.\mathbf{A}) + (\tilde{C}.\mathbf{A})\otimes\mathbf{A})) + 2b_{tr}(\frac{1}{2}\tilde{C}^{-1}(I_4-1) + \ln(J)\mathbf{A}\otimes\mathbf{A})$$
$$+4c_{tr}(I_4-1)\mathbf{A}\otimes\mathbf{A} - 2d_{tr}(\frac{1}{2}\tilde{C}^{-1}(I_5-1) + \ln(J)(\mathbf{A}\otimes(\tilde{C}.\mathbf{A}) + (\tilde{C}.\mathbf{A})\otimes\mathbf{A})), \tag{3.56}$$

where $I_1 = \mathrm{tr}(\tilde{C})$, $I_4 = \mathbf{A}.\tilde{C}\mathbf{A}$, $I_5 = \mathbf{A}.\tilde{C}^2\mathbf{A}$, and $\mathbf{A}$ still being a unit vector along the fiber. Note that we consider the improved version of [NTT19] instead of the original one in [BB98] where $b_{tr}\ln(J)$ replaces $b_{tr}(I_1-3)$ and $d_{trn}\ln(J)(I_5-1)$ is added to improve the identification of the homogenized material parameters. This strain energy decomposition (3.52) into isotropic (3.53) and anisotropic (3.54) parts was suggested by [HGO00] to simplify the model complexity and to facilitate model's parameters experimental identification. This hyperelastic model decoupled assumption is motivated by physical arguments coming from the fiber and matrix behaviour which are assumed isotropic. At small deformation, the fibres, which are more rigid then the matrix, are less active and then the behaviour is governed by isotropic strain energy part. At large deformation, the fibres come into play (it is their roles), the anisotropic strain energy part pilots the mechanical behaviour.

**Bonet's law**

$$\tilde{W}_h = W_{iso}(I_1;J) + W_{trn}(I_4,I_5;J),$$
$$W_{iso} = \mu_{iso}(\tfrac{1}{2}(I_1-3) - \ln(J)) + \tfrac{\lambda_{iso}}{2}(\ln(J))^2$$
$$W_{trn} = (a_{tr} + b_{tr}\ln(J) + c_{tr}(I_4-1))(I_4-1) - (\tfrac{1}{2}a_{tr} + d_{tr}\ln(J))(I_5-1)$$

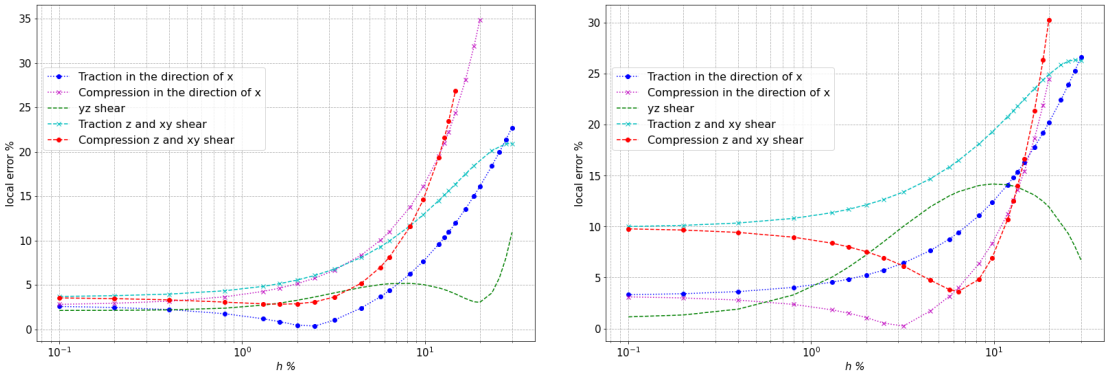


(a) $c = 10$ (b) $c = 150$

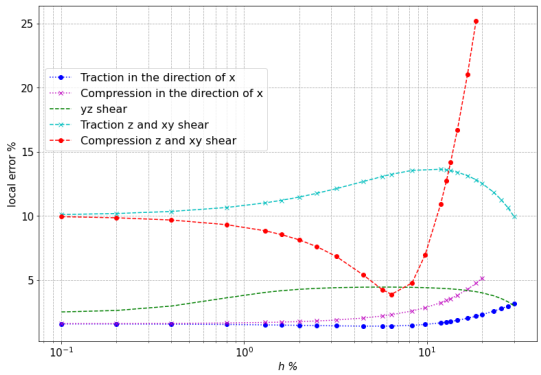


(c) $c = 2000$

FIGURE 3.13: Local error for Bonet's transverse isotropic law with respect to the deformation and three different contrasts with positivity constraints

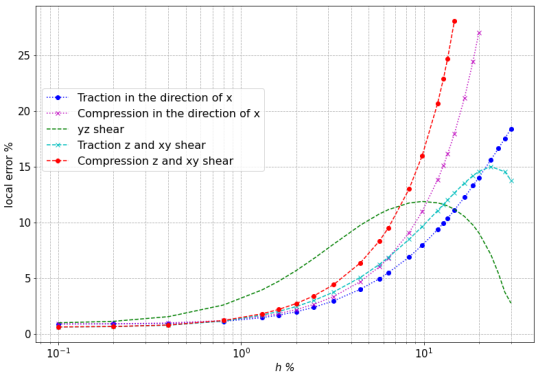


(a) $c = 10$

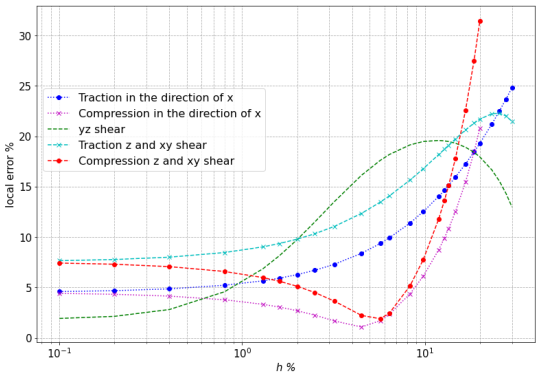


(b) $c = 150$

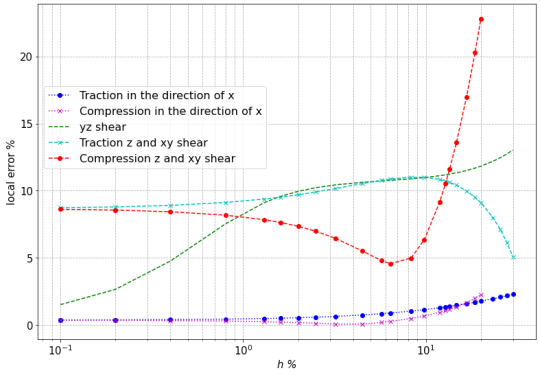


(c) $c = 2000$

FIGURE 3.14: Local error for Bonet's transverse isotropic law with respect to the deformation and three different contrasts without constraints

The numerical tests are identical to those performed for Kaliske's traditional decoupled model law in the previous section. After identification, the local errors are shown on fig. 3.13 for three selected deformation patterns of table 3.1 and two additional mixed ones. A local error less than 5%, for optimisation with positivity constraints, is only obtained for a low contrast ($c = 10$) and for small deformation

(less than 1%). Moreover, for that contrast, there is an important degradation of the approximation for large deformations. For a high contrast ($c = 150$ and c=2000) the maximal local error is about 10% for moderate deformation. The degradation for large deformations is less important, except for the last mixed deformation pattern (compression z and xy shear). As for the optimisation without constraints as shown on fig. 3.14 for the chosen deformation patterns, the local error is remarkably lower than that with positivity constraints for high contrast ($c = 150$ and c=2000) but remains higher for lower contrasts ($c = 10$) and for moderate deformation. The results are a little better but the polyconvex character is not assured in this case.

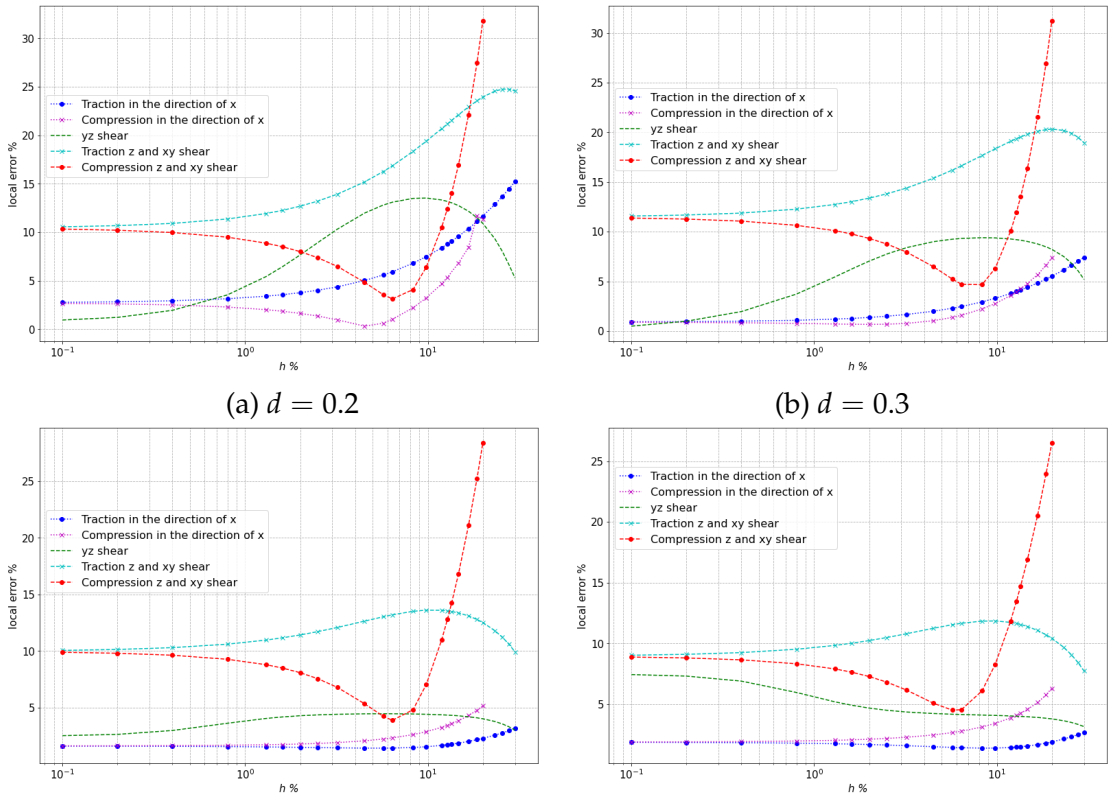


(a) $d = 0.2$ (b) $d = 0.3$

(c) $d = 0.5$ (d) $d = 0.7$

FIGURE 3.15: Local error for Bonet's transverse isotropic law with respect to the deformation and four different fiber diameters for contrast = 2000

Despite same variation, the maximal local error is globally stable when the diameter of fiber vary, meaning that Bonet's law equally approximate these differents situations.

**Micro-macro decoupled computational homogenization**

1. Select a macroscopic anisotropic constitutive law (Homogenized Potential)
2. Conduct numerical tests on a heterogeneous (Matrix/Fiber) representative volume element (RVE) approximated by finite elements (FE) to build a training set:
   - Choose a set of macroscopic deformations $H^{[\alpha]}$, and the number of tests to perform (type and intensity).
   - Compute the average of $2^{nd}$ Piola-Kirchhoff tensor ($S^{[\alpha]}$) by solving the corresponding boundary problem by integration on the heterogeneous RVE.
3. Macroscopic identification of the coefficients of the chosen potential:
   - Express the $2^{nd}$ Piola-Kirchhoff tensor as a function of the chosen homogenized potential and the $p^{[k]}$ coefficients of the material. In the case of a potential which is linear with respect to its coefficients, we have:
   $$\tilde{S}_h(p, H^{[\alpha]}) = \sum_{k}^{n_{para}} p^{[k]} g^{[k]}(\tilde{H}^{[\alpha]})$$
   where $g^{[k]}$ are the derivatives of the different terms of the potential.
   - Identify the macroscopic coefficients using a least squares optimization method, by minimizing:
   $$\chi(p) = \frac{1}{2} \sum_{\alpha=1}^{n_{test}} \frac{w^{[\alpha]}}{\sum_{\beta=1}^{n_{test}} w^{[\beta]}} \frac{\left\| \tilde{S}_h^{[\alpha]}(p, \tilde{H}^{[\alpha]}) - \tilde{S}^{[\alpha]}(\tilde{H}^{[\alpha]}) \right\|^2}{\left\| \tilde{S}^{[\alpha]}(\tilde{H}^{[\alpha]}) \right\|^2}$$
4. Calculate the local error of the RVEs between $\tilde{S}_h^{[\alpha]}(p, \tilde{H}^{[\alpha]})$ and $\tilde{S}^{[\alpha]}(\tilde{H}^{[\alpha]})$ on the training set to evaluate the capacity of the chosen potential to approximate the RVE behaviour on the desired range of deformation.

## 3.5 Conclusion

In this chapter, we have illustrated the ability of the decoupled homogenization method to approximate the homogenization problem of a fiber reinforced layer using two different potentials: Kaliske and Bonet potentials. We also validated the method on NeoHookean hyperelastic potential for which the homogenized law is known in the incompressible case. In spite of a reduced number of coefficients, Bonet's potential allows to reach a local error which can be in some range of deformation competitive compared to Kaliske's one, including for the modified variant that we have proposed. It can therefore be more computationally efficient to use in that cases. A better approximation can however be achieved, especially for large deformations, with the second variant of Kaliske's potential that we have proposed.

# Chapter 4

# Correction method for two-scale homogenization problem

## 4.1 Introduction

In this chapter, we test the ability of the decoupled homogenization method to approximate the deformation of a fiber reinforced layer in large deformation. To do so, we carry out a number of tests on the deformation of such a layer by comparing the deformation of a finite element method using the homogenized law obtained thanks to the method developed in the previous chapter with the deformation obtained on a (very expansive) finite element approximation of a complete heterogeneous model with a mesh taking into account the fibers.

In order to improve the approximation obtained and to get closer to a coupled homogenization method, we propose a new iterative correction method which allows to improve the homogenized laws, Bonet's law and second varaint of Kaliske's law, in the deformation regime of the fiber reinforced layer, with a much lower cost than the $FE^2$ method.

## 4.2 Test on a complete fiber reinforced layer

In order to test the relevance of the homogenization procedure developed in chapter 3, a comparative test between the deformation of a fully meshed fiber reinforced layer and of the same structure using the homogenized law is performed in the following sections. The tests are done using quadratic Lagrange elements on our finite element library GetFEM++ [RP20].

Denoting $\tilde{U}_e$ the approximated displacement of the complete FE fiber reinforced model and $\tilde{U}_h$ the one which uses the homogenized law, the following relative global error is considered

$$\mathrm{Err}_g = \frac{\left\|\tilde{U}_h - \tilde{U}_e\right\|}{\left\|\tilde{U}_e\right\|}, \qquad \text{where } \left\|\tilde{U}_e\right\| = \left(\int_{\tilde{\mathcal{B}}_0} |\tilde{U}_e|^2 d\tilde{V}\right)^{1/2}. \tag{4.1}$$

Of course, this error reflects several approximations: the finite element one, the homogenization principle itself and finally, what's interest us, the approximation due to the choice of parametric constitutive law in the decoupled homogenization.

Additionnally to this global error, we compute also some local error in the same manner as in chapter 3 with formula (3.36) except that instead of using a deformation gradient $\tilde{H}$ from the training set, we use the average of deformation on a certain number of predefined volume elements of the homogenized layer (see section 4.3 for more details).

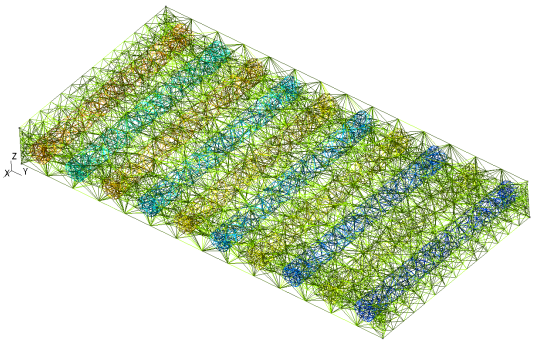

(a) Full 10 fibers mesh

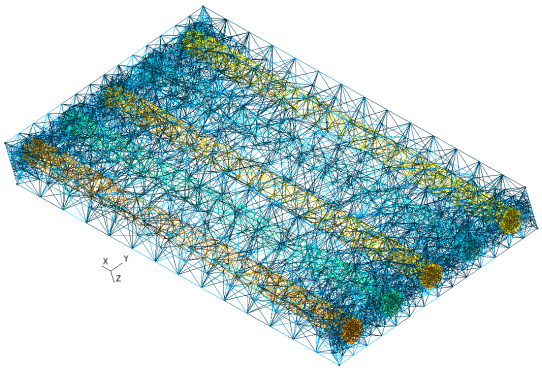

(b) Full 5 fibers mesh

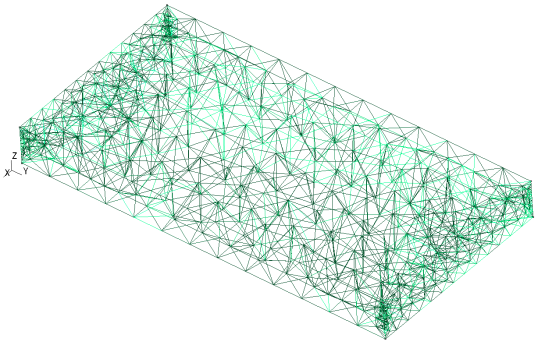

(c) Mesh for the homogenized layer

FIGURE 4.1: Meshes for the fiber reinforced layer: (a)-(b) mesh of the fibers and matrix for the full computation and (c) simpler mesh for the homogenized law

We conduct two types of numerical experiments on two different fiber reinforced layers: we consider a transversal flexion in the direction of the fibers on a layer with 5 fibers and a longitudinal flexion transverse to the direction of the fibers on a layer with 5 and 10 fibers.

### 4.2.1 Test on fiber reinforced layer with 5 fibers

The meshes used for the heterogenous computation and the homogenized one are represented on fig. 4.1(b)-(c). The size of the domain is 1cm $\times$ 5cm $\times$ 10cm with regularly spaced fibers of diameter 0.5cm

#### 4.2.1.1 A longitudinal flexion transverse to the direction of the fibers

The longitudinal flexion transverse deformation obtained for the fully 5 fibers meshed model (c), the homogenized one using Bonet's law (3.4.4) (a) and the homogenized one using second variant of Kaliske's law (3.4.3) (b) can be seen on fig. 4.2 for comparison.

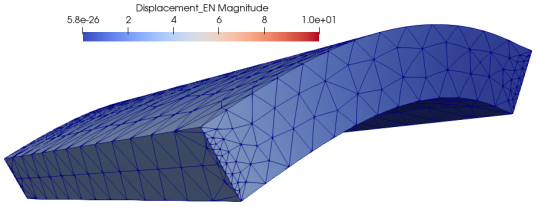


(a) Bonet's law

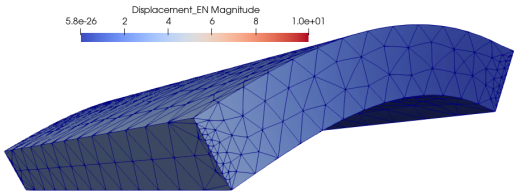


(b) $2^{nd}$ variant of Kaliske's law

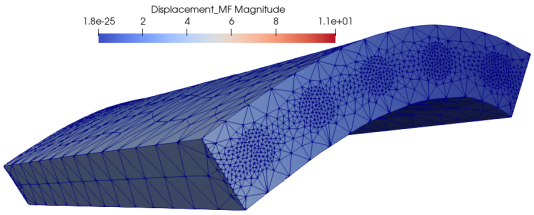


(c) fully 5 fibers meshed model

FIGURE 4.2: Comparison of the layer's deformation obtained after homogenization with Bonets's law (a), $2^{nd}$ variant of Kaliske (b) and without homogenization with the fully 5 fibers meshed model (c).

We recall

**Bonet's law**

$$\tilde{W}_h = W_{iso}(I_1; J) + W_{trn}(I_4, I_5; J),$$

$$W_{iso} = \mu_{iso}(\tfrac{1}{2}(I_1 - 3) - \ln(J)) + \tfrac{\lambda_{iso}}{2}(\ln(J))^2$$
$$W_{trn} = (a_{tr} + b_{tr}\ln(J) + c_{tr}(I_4 - 1))(I_4 - 1) - (\tfrac{1}{2}a_{tr} + d_{tr}\ln(J))(I_5 - 1)$$

**Second Variant of Kaliske's law**

$$\tilde{W}_{SKV} = W_{vol}(J) + W_{iso}(\underline{I}_1, \underline{I}_2) + W_{aniso}(I_4, I_5),$$

$$W_{vol} = D(J-1)^2$$
$$W_{iso} = \sum_{i=1}^{3} a_i(\underline{I}_1 - 3)^i + \sum_{j=1}^{3} b_j(\underline{I}_2 - 3)^j$$
$$W_{aniso} = \sum_{k=2}^{6} c_k(I_4 - 1)^k + \sum_{l=2}^{6} d_l(I_5 - 1)^l$$

The global error obtained for Bonet's law is about 3% compared to 15.96% for the average local error on the layer's volume elements, since for second variant of Kaliske's law, the global error is about 5% and 16.67% for the average local error.

A zoom of a superposition of the three deformations is also presented on fig. 4.3 where it is possible to see that the Bonet's law allow a slightly better approximation than second variant of Kaliske's law.

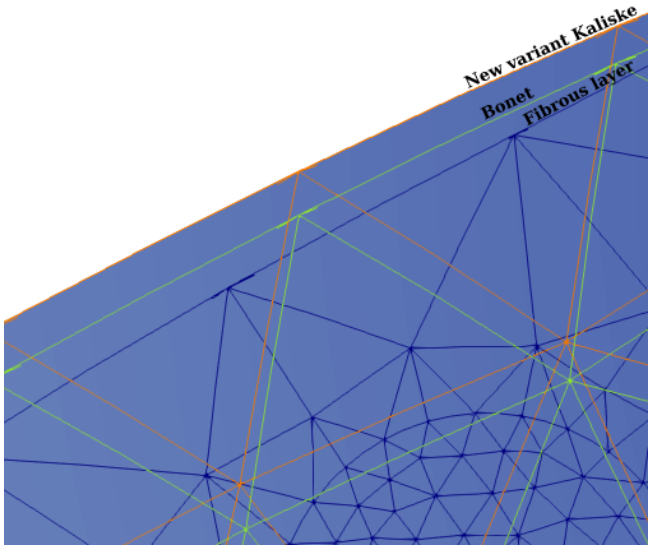


FIGURE 4.3: Zoom of the superposition of the deformation for the three situations: full model, homogenized one with Bonet's law, homogenized one with $2^{nd}$ variant of Kaliske's law

#### 4.2.1.2 A transversal flexion in the direction of the fibers with two fixed edges

The deformation obtained for the fully 5 fibers meshed model (c), the homogenized one using Bonet's law (a) and the homogenized one using $2^{nd}$ variant of Kaliske's law (b) can be seen on fig. 4.4 for comparison.

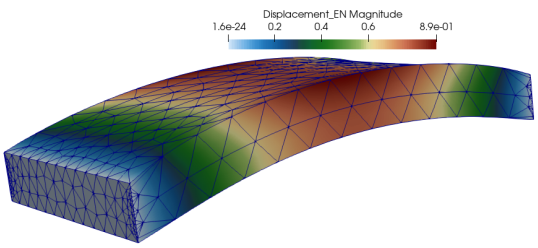


(a) Bonet's law

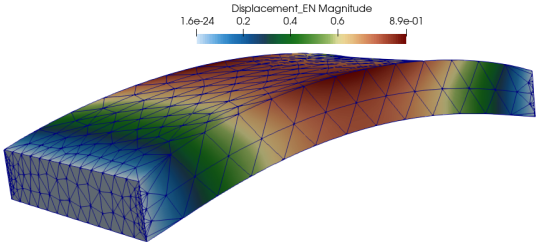


(b) $2^{nd}$ variant of Kaliske's law

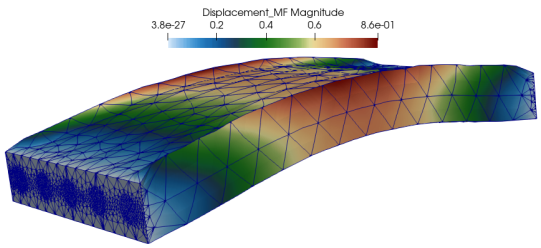


(c) fully 5 fibers meshed model

FIGURE 4.4: Comparison of the layer's deformation obtained after homogenization with Bonets's law (a), $2^{nd}$ variant of Kaliske (b) and without homogenization with the fully 5 fibers meshed model (c).

For this experiment, the global error found on the displacement for Bonet's law is about 31.5% and the local error on the average of deformation on the layer volume elements doesn't exceed 2%.

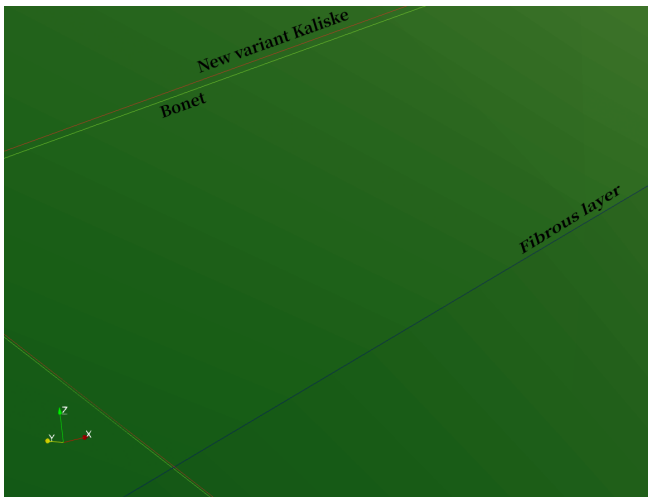


FIGURE 4.5: Zoom of the superposition of the deformation for the three situations: full model, homogenized one with Bonet's law, homogenized one with $2^{nd}$ variant of Kaliske's law

The same observation is noted for Kaliske's second variant law where the global error is about 32.1% and the local errors are less than 0.75%. The important global error obtained despite rather small local errors, is probably due to the important fluctuations that can be noted on the deformation fig. 4.4 on the full model while the local errors of the elementary volumes of the layer eliminate them by averaging. A zoom of a superposition of the three deformations is also presented on fig. 4.5 where it is possible to see that Bonet's law allow a slightly better approximation than the second variant of Kaliske's law.

### 4.2.2 Test on fiber reinforced layer with 10 fibers

The meshes used for the heterogenous computation and the homogenized one are represented on fig. 4.1(a)-(c). The size of the domain is 1cm $\times$ 4cm $\times$ 10cm with still some regularly spaced fibers of diameter 0.5cm

#### 4.2.2.1 A longitudinal flexion transverse to the direction of the fibers

The longitudinal flexion transverse deformation obtained for the fully 10 fibers meshed model (c), the homogenized one using Bonet's law (a) and the homogenized one using $2^{nd}$ variant of Kaliske's law (b) can be seen on fig. 4.6 for comparison.

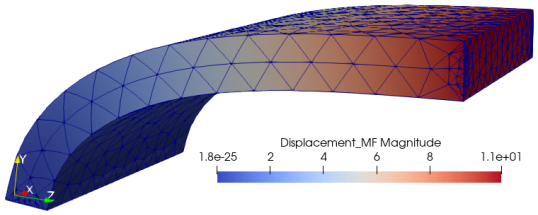


(a) Bonet's law

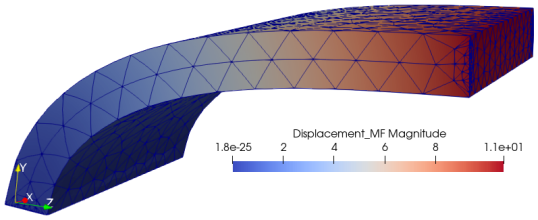


(b) $2^{nd}$ variant of Kaliske's law

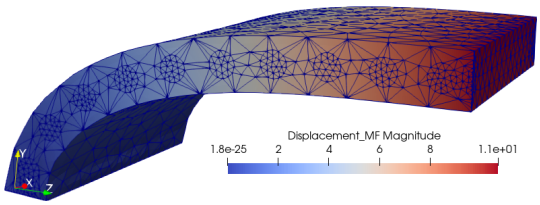


(c) fully 10 fibers meshed model

FIGURE 4.6: Comparison of the layer's deformation obtained after homogenization with Bonets's law (a), $2^{nd}$ variant of Kaliske (b) and without homogenization with the fully 10 fibers meshed model (c).

The global error for Bonet's law is about 3.88% compared to 20% for the average local error on the layer's volume elements, as for second variant of Kaliske law, the global error is about 5.08% against 18.17% for the average local error.

A zoom of a superposition of the three deformations is also presented on fig. 4.7 where it is possible to see that the Bonet's law allow a slightly better approximation than second variant of Kaliske's law.

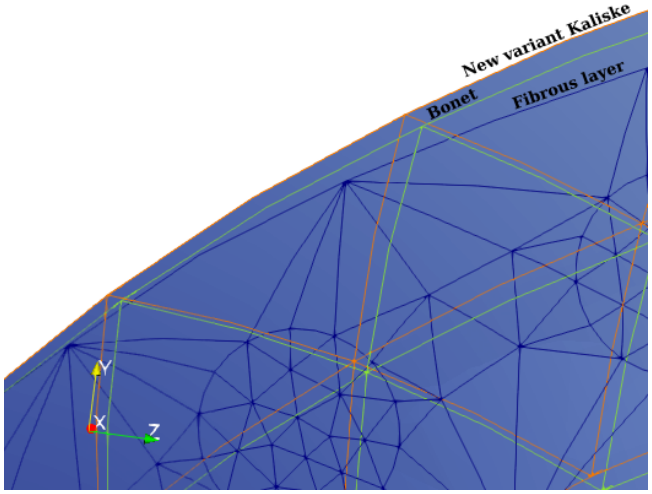


FIGURE 4.7: Zoom of the superposition of the deformation for the three situations: full model, homogenized one with Bonet's law, homogenized one with $2^{nd}$ variant of Kaliske's law

#### 4.2.2.2 A longitudinal flexion transverse to the direction of the fibers with two fixed edges

The deformation obtained for the fully 10 fibers meshed model (c), the homogenized one using Bonet's law (a) and the homogenized one using Kaliske's law (b) can be seen on fig. 4.8 for comparison.

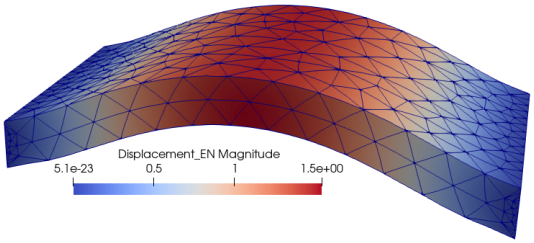


(a) Bonet's law

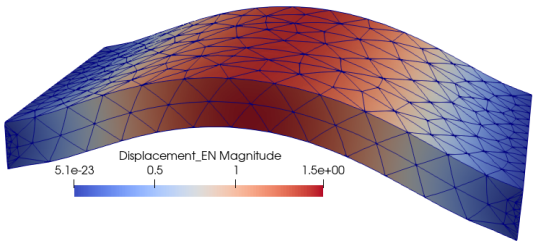


(b) $2^{nd}$ variant of Kaliske's law

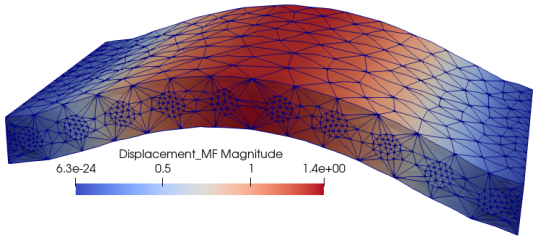


(c) fully 10 fibers meshed model

FIGURE 4.8: Comparison of the layer's deformation obtained after homogenization with Bonets's law (a), $2^{nd}$ variant of Kaliske (b) and without homogenization with the fully 10 fibers meshed model (c).

The global error for Bonet's law is about 10.14% compared to 18.3% for the average local error on the layer's volume elements as shown in table 4.13, as for second variant of Kaliske law, the global error is about 8.32% against 18.05% for the average local error as presented in table 4.15.

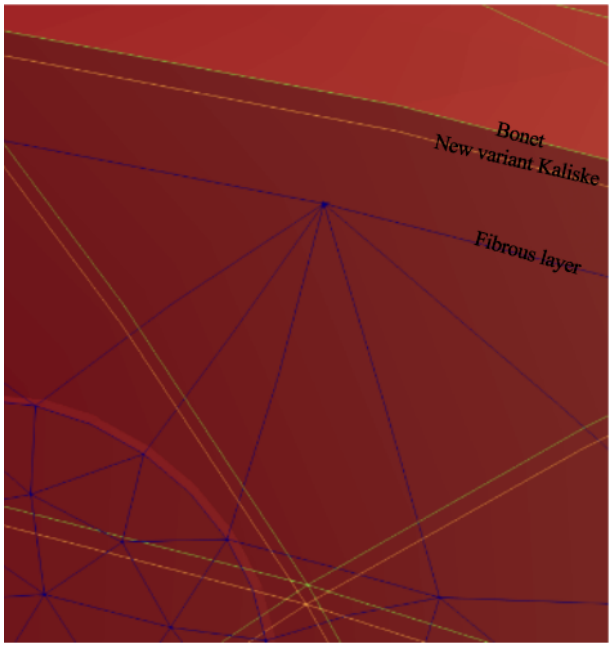


FIGURE 4.9: Zoom of the superposition of the deformation for the three situations: full model, homogenized one with Bonet's law, homogenized one with $2^{nd}$ variant of Kaliske's law

A zoom of a superposition of the three deformations is also presented on fig. 4.9 where it is possible to see that, for this case, the second variant of Kaliske's law allow a slightly better approximation than Bonet's law.

For this case, we tested also a change in the diameter of the fibers (both for the layer and the RVE). It can be seen in table 4.11 and table 4.12 that there is a certain increase of global and local error with respect to the diameter of the fibers (and for both the two laws), meaning that both the two laws have difficulties to model the deformation of the RVE and the layer when the ratio of fiber to matrix increase.

| | d=0.2 | d=0.3 | d=0.5 | d=0.7 |
|---|---|---|---|---|
| $Err_g$ | 2.793% | 3.835% | 10.14% | 45.29% |
| $Err_{al}$ | 6.58% | 7.504% | 18.275% | 31.664% |

TABLE 4.11: Layer's global and local error for Bonet's potential and four different fiber diameters for a contrast $c = 2000$, 10 Fibers case and with constraints of positivity on coefficients and four different fiber diameters (in cm)

| | d=0.2 | d=0.3 | d=0.5 | d=0.7 |
|---|---|---|---|---|
| $Err_g$ | 2.5256% | 3.507% | 8.223% | 26.899% |
| $Err_{al}$ | 3.025% | 4.721% | 18.027% | 56.099% |

TABLE 4.12: Layer's global and local error for Kaliske's potential second variant for a contrast $c = 2000$ Flex Matrix 10 Fibers with constraints and four different fiber diameters (in cm)

For the rest of the chapter, we will be considering the 10 fibers layer deformation results only with fibers of diameter 0.5cm.

## 4.3 Correction method

In order to improve the quality of the approximation provided by the decoupled method, we develop a new iterative method whose objective is to adapt the optimization of the homogenized law to the considered structural computation at a much lower computational cost than the $FE^2$ method.

The reference configuration $\tilde{\mathcal{B}}_0$ of the macroscopic structure is divided into a certain number of parallelepipedic element volumes

$$\mathcal{B}_p^{[\alpha]}, \quad \alpha = 1...n_{vol},$$

distributed all over the structure. As far as possible, the chosen volumes should be representative of the micro-structure. However, this does not seem mandatory and their number should not be excessive in order not to penalize the calculation time. These volumes can also be placed in zones of interest of the considered structure. The proposed method can then be divided into the following steps:

1. Determine a training set by the choice of $\tilde{H}^{[\beta]}, \beta = 1...n_{test}$ deformation patterns and the computation of the corresponding $\tilde{S}^{[\beta]}$ by $n_{test}$ computations on the micro-scale BVP. Choose a set of weights $w^{[\beta]}, \beta = 1...n_{test}$.

2. Perform the identification of the coefficient of the homogenized law with the considered training set by minimization of (3.31).

3. Compute a finite element approximation $u^h$ of the displacement of the structure by solving numerically the decoupled macro-scale BVP using the homogenized law.

4. On each volume $\mathcal{B}_p^{[\alpha]}$, compute numerically the average of deformation

$$\tilde{H}_p^{[\alpha]} = \frac{1}{|\mathcal{B}_p^{[\alpha]}|} \int_{\mathcal{B}_p^{[\alpha]}} \nabla u^h dV,$$

and the corresponding average of second Piola-Kirchhoff tensor $\tilde{S}_p^{[\alpha]}$ by $n_{vol}$ computations on the micro-scale BVP.

5. Loop to step 2 with the initial training set completed by $\tilde{H}_p^{[\alpha]}$, $\tilde{S}_p^{[\alpha]}$, $\alpha = 1...n_{vol}$ with some chosen weights $w_p^{[\alpha]}, \alpha = 1...n_{vol}$.

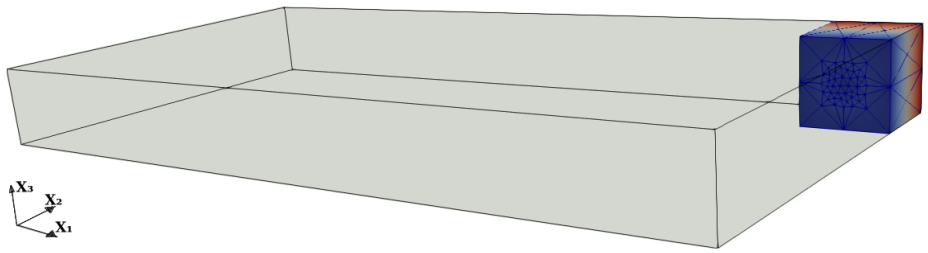


FIGURE 4.10: The element volumes of the 10 Fibred layer

In order to test the correction method, we use different weights $\omega = 1, 10, 100$ for the deformation test flexion with two fixed edges with a deformation force density of 2MPa and in our case the number of parallelepipedic element volumes of the layer is $n_{vol} = 50$ (the weights for the initial training set are kept uniform to the value $\omega = 1$),

### 4.3.1 Test with Bonet's law

Fig. 4.11 shows the error distribution between the heterogeneous reference solution and the homogenized problem solution before and after a correction step with constraints of positivity of the coefficients using Bonet's potential. The global error and the local errors on the element volumes of the layer are reported in table 4.13. We can see a significant improvement from the first iteration for all considered weights, whether on the global error or on the local errors. In the considered case, the weight of $w_p^{[\alpha]} = 10$ for the layer volumes seems to be the best compromise, a weight of $w_p^{[\alpha]} = 100$ degrades a little the results. We can also notice that the next iterations (2 and 3) do not allow to improve the errors, either global or local. These errors remain very close or even with a slight degradation. We can conclude that the main part of the correction in this case is done at the first iteration of correction.

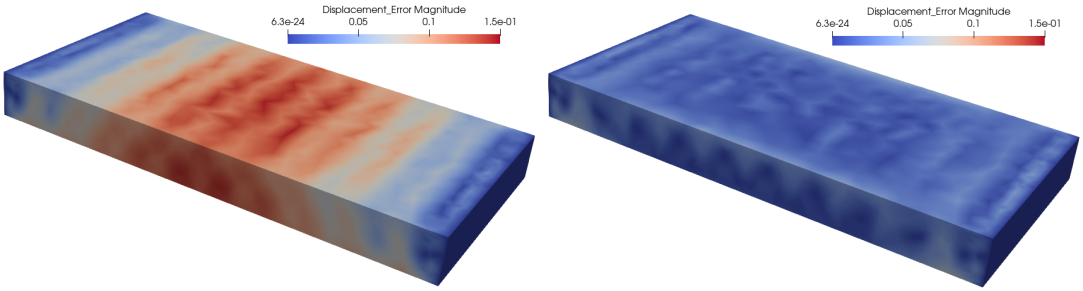


FIGURE 4.11: Error distribution before correction for Bonet's potential (left) and after correction (right)

| Before correction | weight | After correction | | |
|---|---|---|---|---|
| | | 1 iteration | 2 iterations | 3 iterations |
| Global error | 1 | 4.356% | 4.784% | 4.746% |
| $Err_g = 10.14\%$ | 10 | 1.659% | 1.805% | 1.779% |
| | 100 | 1.809% | 1.674% | 1.683% |
| Average local error on | 1 | 12.508% | 12.821% | 12.79% |
| layer volume elements | 10 | 10.247% | 10.098% | 10.091% |
| $Err_{al} = 18.275\%$ | 100 | 9.341% | 9.26% | 9.241% |

TABLE 4.13: Layer's global and local error for Bonet's potential for a contrast $c = 2000$ Flex Matrix 10 Fibers with constraint of positivity on the coefficients

In the case of homogenization without constraints, the global error and the local errors on the element volumes of the layer are reported in table 4.14. We can see that the results are slightly degraded before correction compared to the ones with positivity constraints (even though the local error measured on the training set is necessary a bit better). Nevertheless, the results after correction are slightly better that the ones on table 4.13. This means that globally, it is possible to have a slightly better approximation without considering the constraint of positivity on the coefficients, at the risk to obtain a non consistant homogenized law.

| Before correction | weight | After correction | | |
|---|---|---|---|---|
| | | 1 iteration | 2 iterations | 3 iterations |
| Global error | 1 | 4.102% | 4.613% | 4.565% |
| $Err_g = 11.067\%$ | 10 | 1.658% | 1.747% | 1.728% |
| | 100 | 1.856% | 1.681% | 1.692% |
| Average local error on | 1 | 12.004% | 12.448% | 12.399% |
| layer volume elements | 10 | 9.828% | 9.8% | 9.791% |
| $Err_{al} = 19.582\%$ | 100 | 9.359% | 9.265% | 9.241% |

TABLE 4.14: Layer's global and local error for Bonet's potential for a contrast $c = 2000$ Flex Matrix 10 Fibers without constraints

### 4.3.2 Test with second variant of Kaliske's law

Fig. 4.12 and table 4.15 show the same experiments but using the second variant of Kaliske's potential with positivity constraints. Overall, it can be seen that the error

level is comparable and slightly lower than for Bonet's potential, although this does not represent a significant advantage.

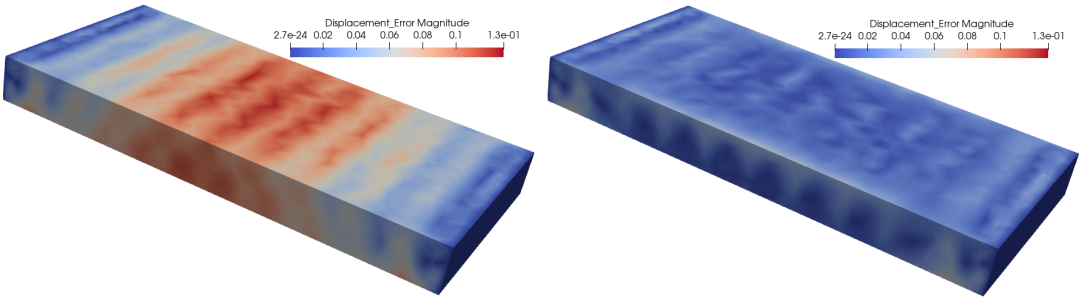


FIGURE 4.12: Error distribution before correction for the second variant of Kaliske's potential (left) and after correction (right)

| Before correction | weight | After correction | | |
|---|---|---|---|---|
| | | 1 iteration | 2 iterations | 3 iterations |
| Global error $Err_g = 8.223\%$ | 1 | 3.233% | 3.503% | 3.48% |
| | 10 | 1.661% | 1.799% | 1.716% |
| | 100 | 1.727% | 1.661% | 1.663% |
| Average local error on layer volume elements $Err_{al} = 18.027\%$ | 1 | 12.988% | 13.125% | 13.124% |
| | 10 | 9.695% | 9.783% | 9.827% |
| | 100 | 9.14% | 9.351% | 9.274% |

TABLE 4.15: Layer's global and local error for Kaliske's potential second variant for a contrast $c = 2000$ Flex Matrix 10 Fibers with positivity constraints

For Kaliske's second variant law correction without constraints, the global error and the local errors on the element volumes of the layer are reported in table 4.14. We can see that the results, in this case, are very slightly upgraded from the ones with positivity constraints. The corrected results have the same sensitivity as the ones above, gives best results from the first iteration of correction with one exception; the global error for a weight of $w_p^{[\alpha]} = 100$.

| Before correction | weight | After correction | | |
|---|---|---|---|---|
| | | 1 iteration | 2 iterations | 3 iterations |
| Global error $Err_g = 8.117\%$ | 1 | 2.459% | 2.823% | 2.788% |
| | 10 | 5.679% | 4.531% | 5.044% |
| | 100 | 15.592% | 2.31% | 14.594% |
| Average local error on layer volume elements $Err_{al} = 18.008\%$ | 1 | 12.968% | 13.109% | 13.081% |
| | 10 | 8.286% | 8.452% | 8.491% |
| | 100 | 8.163% | 7.664% | 8.262% |

TABLE 4.16: Layer's global and local error for Kaliske's potential second variant for a contrast $c = 2000$, 10 Fibers case and without constraints of positivity on coefficients

### 4.3.3 Special test: incompressible training set

In the tests presented in the tables 4.17 and 4.18, the starting training set contains only incompressible deformations, as was used in Section 3.3.4 for the NeoHokean case. Since the material of the matrix is quasi-incompressible and occupies most of the volume of the RVE, this would make sense.

| Before correction | weight | After correction | | |
|---|---|---|---|---|
| | | 1 iteration | 2 iterations | 3 iterations |
| Global error $Err_g = 32.167\%$ | 1 | 8.756% | 1.769% | 2.149% |
| | 10 | 8.709% | 1.846% | 1.666% |
| | 100 | 8.264% | 1.918% | 1.705% |
| Average local error on layer volume elements $Err_{al} = 41.272\%$ | 1 | 24.288% | 10.159% | 10.195% |
| | 10 | 24.18% | 9.628% | 9.321% |
| | 100 | 23.726% | 9.6% | 9.229% |

TABLE 4.17: Layer's global and local error for Bonet's potential for a contrast $c = 2000$ Flex Matrix 10 Fibers with positivity constraints

| Before correction | weight | After correction | | |
|---|---|---|---|---|
| | | 1 iteration | 2 iterations | 3 iterations |
| Global error $Err_g = 106.537\%$ | 1 | 8.683% | 2.48% | 2.815% |
| | 10 | 8.429% | 1.655% | 1.725% |
| | 100 | 4.128% | 1.686% | 1.662% |
| Average local error on layer volume elements $Err_{al} = 99.761\%$ | 1 | 17.382% | 12.196% | 11.839% |
| | 10 | 17.153% | 9.411% | 9.603% |
| | 100 | 14.806% | 9.213% | 9.269% |

TABLE 4.18: Layer's global and local error for Kaliske's potential second variant for a contrast $c = 2000$ Flex Matrix 10 Fibers with positivity constraints

However, both the global error and the average of local error are pretty high before the correction, which means that the deformations of the RVE are not sufficiently close to incompressible ones and the fact that the homogenized law is not trained in the compressible regime do not allow to have a good approximation.

It is remarkable that the correction method, by adding deformations which are not strictly incompressible, allows to rapidly correct this bias (mainly in two iterations).

## 4.4 Conclusion

The tests carried out in this chapter allow to evaluate the approximation made using the decoupled homogenization method presented in chapter 3 together with the proposed correction method. The results on the considered experiments, show that quite low levels of error can be reached with both Bonet and second varian of Kaliske potential with the proposed method, at the considered deformation level. Even if Bonet's potential gives slightly larger errors, it can be a good compromise since the number of parameters to be identified is lower than for the second varian of Kaliske potential (5 instead of 16) which leads to a lower computational cost.

# General conclusion and outlook

The main objective of this thesis is to propose a numerical homogenisation strategy for a fiber reinforced layer in nonlinear hyperelastic framework with the best possible compromise in terms of computational cost and reliability. To this end, we have developed a new decoupled and correction methodology based on the decoupled method of Terada et al. [Ter+13a]. We have performed a comparison of two different transverse isotropic homogenised hyperelastic potentials with a moderate number of parameters and introduce an iteration method to improve the approximation error. This method takes into account the deformation state of the structure at the macroscopic scale, allows to approach the coupled $FE^2$ [Fey99] method while keeping a much lower numerical cost.

The original Kaliske [Kal00a] and Bonet [BB98] hyperelastic potentials were used to demonstrate how the decoupled homogenization approach proposed may approximate the homogenization issue of a fiber reinforced layer. The Neo-Hookean hyperelastic potential [DHS06b], for which the homogenized law is known in the incompressible case, was also used to further confirm the proposed technique. Despite having fewer coefficients, Bonet's potential still enables one to achieve a local error that, given the modified second variation that we have suggested, can be competitive with Kaliske's one in specific deformation ranges. Therefore, using it in certain circumstances may be more computationally efficient. But using the Kaliske's potential second variant we've suggested, especially for significant deformations, a better approximation may be made.

A number of tests on the deformation of a fiber reinforced layer was performed by contrasting the deformation obtained on a (very expansive) finite element approximation of a complete heterogeneous model with a mesh taking into account the fibers with the deformation obtained on a finite element method using the homogenized law obtained thanks to the method developed. A new correction method is proposed to overcome the lack of robustness of the proposed homogenisation method. The results on the considered experiments, show that quite low levels of error can be reached with both Bonet and Kaliske potential with the proposed method, at the considered deformation level. Even if Bonet's potential gives slightly larger errors, it can be a good compromise since the number of parameters to be identified is lower than for the Kaliske potential (5 instead of 16) which leads to a lower computational cost.

This work can be completed by the generalization of the different constitutive formulations for the hyperelastic potentials (threshold law, double layers laws ...) to take account of the inner anisotropy and more complex behaviours (plasticity, viscosity ...). Moreover, in order to better adaptation of the non-linear material behaviour, neural networks can be considered to make an adaptative approximation of the behaviour of the heterogeneous layer. Also, different boundary conditions can be considered for micro-macro transitions. Focusing on the identification part, the presented approach can be tested and ameliorated for more complex models. The methodology developed in this work can be adapted to be used with experimental data.

# Bibliography


[Aça21] Alp Kağan Açan. "A comparative study of anisotropic hyperelastic models of biological soft tissues". MA thesis. Middle East Technical University, 2021.

[AR55] John Edward Adkins and Ronald Samuel Rivlin. "Large elastic deformations of isotropic materials X. Reinforcement by inextensible cords". In: *Philosophical Transactions of the Royal Society of London. Series A, Mathematical and Physical Sciences* 248.944 (1955), pp. 201–223.

[Bal+06] Daniel Balzani et al. "A polyconvex framework for soft biological tissues. Adjustment to experimental data". In: *International journal of solids and structures* 43.20 (2006), pp. 6052–6070.

[Bat01] RC Batra. "Comparison of results from four linear constitutive relations in isotropic finite elasticity". In: *International Journal of Non-Linear Mechanics* 36.3 (2001), pp. 421–432.

[Bat98] RC Batra. "Linear constitutive relations in isotropic finite elasticity". In: *Journal of Elasticity* 51.3 (1998), pp. 243–245.

[BB98] J Bonet and AJ0944 Burton. "A simple orthotropic, transversely isotropic hyperelastic constitutive equation for large strain computations". In: *Computer methods in applied mechanics and engineering* 162.1-4 (1998), pp. 151–164.

[Bea87] Millard F Beatty. "Topics in finite elasticity: hyperelasticity of rubber, elastomers, and biological tissues—with examples". In: (1987).

[BG10] Andrea Bacigalupo and Luigi Gambarotta. "Second-order computational homogenization of heterogeneous materials with periodic microstructure". In: *ZAMM-Journal of Applied Mathematics and Mechanics/Zeitschrift für Angewandte Mathematik und Mechanik* 90.10-11 (2010), pp. 796–811.

[BK62] P.J. Blatz and W.L. Ko. "Application of finite elastic theory to the deformation of rubbery materials". In: *Journal of Rheology* 6 (1962), pp. 223–252. ISSN: 0148-6055.

[BKG15] E Bosco, VG Kouznetsova, and MGD3340087 Geers. "Multi-scale computational homogenization–localization for propagating discontinuities using X-FEM". In: *International Journal for Numerical Methods in Engineering* 102.3-4 (2015), pp. 496–527.

[BLP11] Alain Bensoussan, Jacques-Louis Lions, and George Papanicolaou. *Asymptotic analysis for periodic structures*. Vol. 374. American Mathematical Soc., 2011.

[BLS08] Ted Belytschko, Stefan Loehnert, and Jeong-Hoon Song. "Multiscale aggregating discontinuities: a method for circumventing loss of material stability". In: *International journal for numerical methods in engineering* 73.6 (2008), pp. 869–894.

[BO13] Gal de Botton and Tal Oren. "Analytical and numerical analyses of the micromechanics of soft fibrous connective tissues". In: *Biomechanics and modeling in mechanobiology* 12.1 (2013), pp. 151–166.

[Boe79] Jean-Paul Boehler. "A simple derivation of representations for non-polynomial constitutive equations in some cases of anisotropy". In: *ZAMM-Journal of Applied Mathematics and Mechanics/Zeitschrift für Angewandte Mathematik und Mechanik* 59.4 (1979), pp. 157–167.

[Bos+14] Emanuela Bosco et al. "A multiscale framework for localizing microstructures towards the onset of macroscopic discontinuity". In: *Computational Mechanics* 54.2 (2014), pp. 299–319.

[BS86] MILLIARD F Beatty and DO Stalnaker. "The Poisson function of finite elasticity". In: 53.108 (1986), pp. 807–813.

[BW08] J. Bonnet and R.D. Wood. *Nonlinear continuum mechanics for finite element analysis*. 2nd. Cambridge university press, 2008. ISBN: 9780521838702.

[CC19a] Krit Chaimoon and Prinya Chindaprasirt. "An anisotropic hyperelastic model with an application to soft tissues". In: *European Journal of Mechanics-A/Solids* 78 (2019), p. 103845.

[CC19b] Krit Chaimoon and Prinya Chindaprasirt. "An anisotropic hyperelastic model with an application to soft tissues". In: *European Journal of Mechanics-A/Solids* 78 (2019), p. 103845.

[CH71] TY Chu and Zvi Hashin. "Plastic behavior of composites and porous media under isotropic stress". In: *International Journal of Engineering Science* 9.10 (1971), pp. 971–994.

[Cha+17] Grégory Chagnon et al. "Hyperelasticity modeling for incompressible passive biological tissues". In: *Biomechanics of living organs*. Elsevier, 2017, pp. 3–30.

[CKG10] Erica WC Coenen, Varvara G Kouznetsova, and Marc GD Geers. "Computational homogenization for heterogeneous thin sheets". In: *International Journal for Numerical Methods in Engineering* 83.8-9 (2010), pp. 1180–1205.

[CKG12a] EWC Coenen, VG Kouznetsova, and MGD Geers. "Multi-scale continuous–discontinuous framework for computational-homogenization–localization". In: *Journal of the Mechanics and Physics of Solids* 60.8 (2012), pp. 1486–1507.

[CKG12b] EWC Coenen, VG Kouznetsova, and MGD2904244 Geers. "Novel boundary conditions for strain localization analyses in microstructural volume elements". In: *International Journal for Numerical Methods in Engineering* 90.1 (2012), pp. 1–21.

[CMO22] Carlos Castillo-Méndez and Armando Ortiz. "Role of anisotropic invariants in numerically modeling soft biological tissues as transversely isotropic hyperelastic materials: A comparative study". In: *International Journal of Non-Linear Mechanics* 138 (2022), p. 103833.

[Coe+12] EWC Coenen et al. "A multi-scale approach to bridge microscale damage and macroscale failure: a nested computational homogenization-localization framework". In: *International journal of fracture* 178.1 (2012), pp. 157–178.

[Con+15] Yu Cong et al. "Multiscale computational homogenization of heterogeneous shells at small strains with extensions to finite displacements and buckling". In: *International Journal for Numerical Methods in Engineering* 104.4 (2015), pp. 235–259.

[CRF15] Grégory Chagnon, Marie Rebouah, and Denis Favier. "Hyperelastic energy densities for soft biological tissues: a review". In: *Journal of Elasticity* 120.2 (2015), pp. 129–160.

[CS14] Jacopo Ciambella and Giuseppe Saccomandi. "A continuum hyperelastic model for auxetic materials". In: *Proceedings of the Royal Society A: Mathematical, Physical and Engineering Sciences* 470.2163 (2014), p. 20130691.

[CSY12] A Clément, Christian Soize, and Julien Yvonnet. "Computational nonlinear stochastic homogenization using a nonconcurrent multiscale approach for hyperelastic heterogeneous microstructures analysis". In: *International Journal for Numerical Methods in Engineering* 91.8 (2012), pp. 799–824.

[Dal+22] Hüsnü Dal et al. "An in silico-based review on anisotropic hyperelastic constitutive models for soft biological tissues". In: *arXiv preprint arXiv:2207.13985* (2022).

[DEGA16] Issam Doghri, Marieme Imene El Ghezal, and Laurent Adam. "Finite strain mean-field homogenization of composite materials with hyperelastic-plastic constituents". In: *International Journal of Plasticity* 81 (2016), pp. 40–62.

[DHS06a] G DeBotton, I Hariton, and EA Socolsky. "Neo-Hookean fiber-reinforced composites in finite elasticity". In: *Journal of the Mechanics and Physics of Solids* 54.3 (2006), pp. 533–559.

[DHS06b] G DeBotton, I Hariton, and EA Socolsky. "Neo-Hookean fiber-reinforced composites in finite elasticity". In: *Journal of the Mechanics and Physics of Solids* 54.3 (2006), pp. 533–559.

[DLW13] Laura De Lorenzis and Peter Wriggers. "Computational homogenization of rubber friction on rough rigid surfaces". In: *Computational Materials Science* 77 (2013), pp. 264–280.

[EE98a] Wolfgang Ehlers and G16349840904 Eipper. "The simple tension problem at large volumetric strains computed from finite hyperelastic material laws". In: *Acta Mechanica* 130.1 (1998), pp. 17–27.

[EE98b] Wolfgang Ehlers and G16349840904 Eipper. "The simple tension problem at large volumetric strains computed from finite hyperelastic material laws". In: *Acta Mechanica* 130.1 (1998), pp. 17–27.

[Ehl+03] W Ehlers et al. "From particle ensembles to Cosserat continua: homogenization of contact forces towards stresses and couple stresses". In: *International Journal of Solids and Structures* 40.24 (2003), pp. 6681–6702.

[Ekr+22] Fredrik Ekre et al. "Numerical Model Reduction with error estimation for computational homogenization of non-linear consolidation". In: *Computer Methods in Applied Mechanics and Engineering* 389 (2022), p. 114334.

[ER97] JL Ericksen and RS Rivlin. "Large elastic deformations of homogeneous anisotropic materials". In: *Collected Papers of RS Rivlin*. Springer, 1997, pp. 467–487.

[ESD05] T Ebinger, H Steeb, and S Diebels. "Modeling macroscopic extended continua with the aid of numerical homogenization schemes". In: *Computational materials science* 32.3-4 (2005), pp. 337–347.

[Esh57] John Douglas Eshelby. "The determination of the elastic field of an ellipsoidal inclusion, and related problems". In: *Proceedings of the royal society of London. Series A. Mathematical and physical sciences* 241.1226 (1957), pp. 376–396.

[Esh59] John Douglas Eshelby. "The elastic field outside an ellipsoidal inclusion". In: *Proceedings of the Royal Society of London. Series A. Mathematical and Physical Sciences* 252.1271 (1959), pp. 561–569.

[FC00] Frédéric Feyel and Jean-Louis Chaboche. "FE2 multiscale approach for modelling the elastoviscoplastic behaviour of long fibre SiC/Ti composite materials". In: *Computer methods in applied mechanics and engineering* 183.3-4 (2000), pp. 309–330.

[Fed10a] Salvatore Federico. "Volumetric-distortional decomposition of deformation and elasticity tensor". In: *Mathematics and mechanics of solids* 15.6 (2010), pp. 672–690.

[Fed10b] Salvatore Federico. "Volumetric-distortional decomposition of deformation and elasticity tensor". In: *Mathematics and mechanics of solids* 15.6 (2010), pp. 672–690.

[Fen+16] Yuan Feng et al. "On the accuracy and fitting of transversely isotropic material models". In: *journal of the mechanical behavior of biomedical materials* 61 (2016), pp. 554–566.

[Fey99] Frédéric Feyel. "Multiscale FE2 elastoviscoplastic analysis of composite structures". In: *Computational Materials Science* 16.1-4 (1999), pp. 344–354.

[FFF15] Jacob Fish, Vasilina Filonova, and Dimitrios Fafalis. "Computational continua revisited". In: *International Journal for Numerical Methods in Engineering* 102.3-4 (2015), pp. 332–378.

[FHL14] Felix Fritzen, Max Hodapp, and Matthias Leuschner. "GPU accelerated computational homogenization based on a variational approach in a reduced basis framework". In: *Computer Methods in Applied Mechanics and Engineering* 278 (2014), pp. 186–217.

[Fis06] Jacob Fish. "Bridging the scales in nano engineering and science". In: *Journal of Nanoparticle Research* 8.5 (2006), pp. 577–594.

[Fis10a] Jacob Fish. *Multiscale methods: bridging the scales in science and engineering*. Oxford University Press on Demand, 2010.

[Fis10b] Jacob Fish. *Multiscale methods: bridging the scales in science and engineering*. Oxford University Press on Demand, 2010.

[FK10] Jacob Fish and Sergey Kuznetsov. "Computational continua". In: *International Journal for Numerical Methods in Engineering* 84.7 (2010), pp. 774–802.

[FL13] Felix Fritzen and Matthias Leuschner. "Reduced basis hybrid computational homogenization based on a mixed incremental formulation". In: *Computer Methods in Applied Mechanics and Engineering* 260 (2013), pp. 143–154.

[Flo61a] PJ128117 Flory. "Thermodynamic relations for high elastic materials". In: *Transactions of the Faraday Society* 57 (1961), pp. 829–838.

[Flo61b] PJ128117 Flory. "Thermodynamic relations for high elastic materials". In: *Transactions of the Faraday Society* 57 (1961), pp. 829–838.

[FMS15] Sebastian Fillep, Julia Mergheim, and Paul Steinmann. "Computational homogenization of rope-like technical textiles". In: *Computational Mechanics* 55.3 (2015), pp. 577–590.

[Fun13] Yuan-cheng Fung. *Biomechanics: mechanical properties of living tissues*. Springer Science & Business Media, 2013.

[Fun67] YC Fung. "Elasticity of soft tissues in simple elongation". In: *American Journal of Physiology–Legacy Content* 213.6 (1967), pp. 1532–1544.

[GAS08] Inna M Gitman, Harm Askes, and LJ Sluys. "Coupled-volume multiscale modelling of quasi-brittle material". In: *European Journal of Mechanics-A/Solids* 27.3 (2008), pp. 302–327.

[GCK07] Marc GD Geers, Erica WC Coenen, and Varvara G Kouznetsova. "Multi-scale computational homogenization of structured thin sheets". In: *Modelling and Simulation in Materials Science and Engineering* 15.4 (2007), S393.

[Gee+17] Marc GD Geers et al. "Homogenization methods and multiscale modeling: nonlinear problems". In: *Encyclopedia of Computational Mechanics Second Edition* (2017), pp. 1–34.

[Gen96] AN Gent. "A new constitutive relation for rubber". In: *Rubber chemistry and technology* 69.1 (1996), pp. 59–61.

[Gil+14a] MD Gilchrist et al. "Modelling the slight compressibility of anisotropic soft tissue". In: *International Journal of Solids and Structures* 51.23-24 (2014), pp. 3857–3865.

[Gil+14b] MD Gilchrist et al. "Modelling the slight compressibility of anisotropic soft tissue". In: *International Journal of Solids and Structures* 51.23-24 (2014), pp. 3857–3865.

[GKB01] Marc GD Geers, Varvara Kouznetsova, and WAM Brekelmans. "Gradient-enhanced computational homogenization for the micro-macro scale transition". In: *Le Journal de Physique IV* 11.PR5 (2001), Pr5–145.

[GKB03] Marc Geers, Varvara G Kouznetsova, and WAM Brekelmans. "Multi-scale first-order and second-order computational homogenization of microstructures towards continua". In: *International Journal for Multiscale Computational Engineering* 1.4 (2003), 371—386.

[GKB10] Marc GD Geers, Varvara G Kouznetsova, and WAM1402 Brekelmans. "Multi-scale computational homogenization: Trends and challenges". In: *Journal of computational and applied mathematics* 234.7 (2010), pp. 2175–2182.

[GLM96] Somnath Ghosh, Kyunghoon Lee, and Suresh Moorthy. "Two scale analysis of heterogeneous elastic-plastic materials with asymptotic homogenization and Voronoi cell finite element model". In: *Computer methods in applied mechanics and engineering* 132.1-2 (1996), pp. 63–116.

[GLR01] Somnath Ghosh, Kyunghoon Lee, and Prasanna Raghavan. "A multi-level computational model for multi-scale damage analysis in composite and porous materials". In: *International journal of solids and structures* 38.14 (2001), pp. 2335–2385.

[HD14] Cécile E Helfen and Stefan Diebels. "Computational homogenisation of composite plates: consideration of the thickness change with a modified projection strategy". In: *Computers & Mathematics with Applications* 67.5 (2014), pp. 1116–1129.

[He99] Q-C He. "Uniform strain fields and microstructure-independent relations in nonlinear elastic fibrous composites". In: *Journal of the Mechanics and Physics of Solids* 47.8 (1999), pp. 1781–1793.

[Hel+10a] J Helfenstein et al. "On non-physical response in models for fiber-reinforced hyperelastic materials". In: *International Journal of Solids and Structures* 47.16 (2010), pp. 2056–2061.

[Hel+10b] J Helfenstein et al. "On non-physical response in models for fiber-reinforced hyperelastic materials". In: *International Journal of Solids and Structures* 47.16 (2010), pp. 2056–2061.

[Her+14] JA Hernández et al. "High-performance model reduction techniques in computational multiscale homogenization". In: *Computer Methods in Applied Mechanics and Engineering* 276 (2014), pp. 149–189.

[HG03] Jacques Hadamard and Georges Guadet. *Cours du Collège de France. Leçons sur la propagation des ondes et les équations de l'hydrodynamique, par Jacques Hadamard*. A. Hermann, 1903.

[HGO00] Gerhard A Holzapfel, Thomas C Gasser, and Ray W Ogden. "A new constitutive framework for arterial wall mechanics and a comparative study of material models". In: *Journal of elasticity and the physical science of solids* 61.1 (2000), pp. 1–48.

[HGO04] Gerhard A Holzapfel, Thomas C Gasser, and Ray W Ogden. "Comparison of a multi-layer structural model for arterial walls with a Fung-type model, and issues of material stability". In: *Journal of biomechanical engineering* 126.2 (2004), pp. 264–275.

[HHR08] Thomas Hettich, Andrea Hund, and Ekkehard Ramm. "Modeling of failure in composites by X-FEM and level sets within a multiscale framework". In: *Computer Methods in Applied Mechanics and Engineering* 197.5 (2008), pp. 414–424.

[Hil63] Rodney Hill. "Elastic properties of reinforced solids: some theoretical principles". In: *Journal of the Mechanics and Physics of Solids* 11.5 (1963), pp. 357–372.

[Hil72] Rodney Hill. "On constitutive macro-variables for heterogeneous solids at finite strain". In: *Proceedings of the Royal Society of London. A. Mathematical and Physical Sciences* 326.1565 (1972), pp. 131–147.

[HLQF06] Q-C He, Hung Le Quang, and Z-Q Feng. "Exact results for the homogenization of elastic fiber-reinforced solids at finite strain". In: *Journal of Elasticity* 83.2 (2006), pp. 153–177.

[HM09] Cornelius O Horgan and Jeremiah G Murphy. "Constitutive modeling for moderate deformations of slightly compressible rubber". In: *Journal of Rheology* 53.1 (2009), pp. 153–168.

[HM21] CO Horgan and JG Murphy. "Incompressible transversely isotropic hyperelastic materials and their linearized counterparts". In: *Journal of Elasticity* 143.1 (2021), pp. 187–194.

[HMS18] CO Horgan, JG Murphy, and G Saccomandi. "The complex mechanical response of anisotropic materials in simple experiments". In: *International Journal of Non-Linear Mechanics* 106 (2018), pp. 274–279.

[HO10] Gerhard A Holzapfel and Ray W Ogden. "Constitutive modelling of arteries". In: *Proceedings of the Royal Society A: Mathematical, Physical and Engineering Sciences* 466.2118 (2010), pp. 1551–1597.

[Hol02] Gerhard A Holzapfel. "Nonlinear solid mechanics: a continuum approach for engineering science". In: *Meccanica* 37.4 (2002), pp. 489–490.

[HS05] Cornelius O Horgan and Giuseppe Saccomandi. "A new constitutive theory for fiber-reinforced incompressible nonlinearly elastic solids". In: *Journal of the Mechanics and Physics of Solids* 53.9 (2005), pp. 1985–2015.

[HS12] Cornelius O Horgan and Michael G Smayda. "The importance of the second strain invariant in the constitutive modeling of elastomers and soft biomaterials". In: *Mechanics of Materials* 51 (2012), pp. 43–52.

[HS63] Zvi Hashin and Shmuel Shtrikman. "A variational approach to the theory of the elastic behaviour of multiphase materials". In: *Journal of the Mechanics and Physics of Solids* 11.2 (1963), pp. 127–140.

[HSY90] JD Humphrey, RK Strumpf, and FCP Yin. "Determination of a constitutive relation for passive myocardium: I. A new functional form". In: (1990).

[HY87] JD Humphrey and FC Yin. "A new constitutive formulation for characterizing the mechanical behavior of soft tissues". In: *Biophysical journal* 52.4 (1987), pp. 563–570.

[Ilt+15] Alexandre Iltchev et al. "Computational homogenisation of periodic cellular materials: application to structural modelling". In: *International Journal of Mechanical Sciences* 93 (2015), pp. 240–255.

[JCS13] A Javili, Georges Chatzigeorgiou, and P Steinmann. "Computational homogenization in magneto-mechanics". In: *International Journal of Solids and Structures* 50.25-26 (2013), pp. 4197–4216.

[JK88] Qing Jiang and James K Knowles. *A class of compressible elastic materials capable of sustaining finite anti-plane shear*. Tech. rep. CALIFORNIA INST OF TECH PASADENA DIV OF ENGINEERING and APPLIED SCIENCE, 1988.

[Joh66] Fritz John. "Plane elastic waves of finite amplitude. Hadamard materials and harmonic materials". In: *Communications on Pure and Applied Mathematics* 19.3 (1966), pp. 309–341.

[JT01] S Jemioło and JJ Telega. "Transversely isotropic materials undergoing large deformations and application to modelling of soft tissues". In: *Mechanics Research Communications* 28.4 (2001), pp. 397–404.

[Kal00a] M Kaliske. "A formulation of elasticity and viscoelasticity for fibre reinforced material at small and finite strains". In: *Computer methods in applied mechanics and engineering* 185.2-4 (2000), pp. 225–243.

[Kal00b] M Kaliske. "A formulation of elasticity and viscoelasticity for fibre reinforced material at small and finite strains". In: *Computer methods in applied mechanics and engineering* 185.2-4 (2000), pp. 225–243.

[Kal+22] Karl A Kalina et al. "Automated constitutive modeling of isotropic hyperelasticity based on artificial neural networks". In: *Computational Mechanics* 69.1 (2022), pp. 213–232.

[Kan+03] Toufik Kanit et al. "Determination of the size of the representative volume element for random composites: statistical and numerical approach". In: *International Journal of solids and structures* 40.13-14 (2003), pp. 3647–3679.

[Kan+06] Toufik Kanit et al. "Apparent and effective physical properties of heterogeneous materials: representativity of samples of two materials from food industry". In: *Computer Methods in Applied Mechanics and Engineering* 195.33-36 (2006), pp. 3960–3982.

[KBB01] Varvara Kouznetsova, WAM Brekelmans, and FPT1005 Baaijens. "An approach to micro-macro modeling of heterogeneous materials". In: *Computational mechanics* 27.1 (2001), pp. 37–48.

[KGB02] Varvara Kouznetsova, Marc GD Geers, and WA Marcel Brekelmans. "Multi-scale constitutive modelling of heterogeneous materials with a gradient-enhanced computational homogenization scheme". In: *International journal for numerical methods in engineering* 54.8 (2002), pp. 1235–1260.

[KGB04a] Varvara G Kouznetsova, Marc Geers, and WAM Brekelmans. "Size of a representative volume element in a second-order computational homogenization framework". In: *International Journal for Multiscale Computational Engineering* 2.4 (2004), 575—598.

[KGB04b] VG Kouznetsova, Marc GD Geers, and WAM1112 Brekelmans. "Multi-scale second-order computational homogenization of multi-phase materials: a nested finite element solution strategy". In: *Computer methods in applied Mechanics and Engineering* 193.48-51 (2004), pp. 5525–5550.

[Kno77] J.K. Knowles. "The finite anti-plane shear field near the tip of a crack for a class of incompressible elastic solids". In: *International Journal of Fracture* 13.5 (1977), pp. 611–639. ISSN: 0376-9429.

[KOS06] ZF Khisaeva and M Ostoja-Starzewski. "On the size of RVE in finite elasticity of random composites". In: *Journal of elasticity* 85.2 (2006), pp. 153–173.

[Kou04] Varvara Gennadyevna Kouznetsova. "Computational homogenization for the multi-scale analysis of multi-phase materials." In: (2004).

[KPB08] Łukasz Kaczmarczyk, Chris J Pearce, and Nenad Bićanić. "Scale transition and enforcement of RVE boundary conditions in second-order computational homogenization". In: *International Journal for Numerical Methods in Engineering* 74.3 (2008), pp. 506–522.

[KPB10] Łukasz Kaczmarczyk, Chris J Pearce, and Nenad Bićanić. "Studies of microstructural size effect and higher-order deformation in second-order computational homogenization". In: *Computers & structures* 88.23-24 (2010), pp. 1383–1390.

[KRB14] Pierre Kerfriden, Juan-José Ródenas, and SP-A Bordas. "Certification of projection-based reduced order modelling in computational homogenisation by the constitutive relation error". In: *International Journal for Numerical Methods in Engineering* 97.6 (2014), pp. 395–422.

[KSS14] Marc-André Keip, Paul Steinmann, and Jörg Schröder. "Two-scale computational homogenization of electro-elasticity at finite strains". In: *Computer Methods in Applied Mechanics and Engineering* 278 (2014), pp. 62–79.

[Lar+11] Fredrik Larsson et al. "Computational homogenization based on a weak format of micro-periodicity for RVE-problems". In: *Computer Methods in Applied Mechanics and Engineering* 200.1-4 (2011), pp. 11–26.

[LB07] Stefan Loehnert and Ted Belytschko. "A multiscale projection method for macro/microcrack simulations". In: *International Journal for Numerical Methods in Engineering* 71.12 (2007), pp. 1466–1482.

[Li+14] Xikui Li et al. "A mixed finite element procedure of gradient Cosserat continuum for second-order computational homogenisation of granular materials". In: *Computational Mechanics* 54.5 (2014), pp. 1331–1356.

[Lig11] Eric Lignon. "Modélisation multi-échelles de nappes fibrées en compression". PhD thesis. Ecole Polytechnique X, 2011.

[LPI10] Oscar Lopez-Pamies and Martín I Idiart. "Fiber-reinforced hyperelastic solids: a realizable homogenization constitutive theory". In: *Journal of Engineering Mathematics* 68.1 (2010), pp. 57–83.

[LRS10] Fredrik Larsson, Kenneth Runesson, and Fang Su. "Variationally consistent computational homogenization of transient heat flow". In: *International Journal for Numerical Methods in Engineering* 81.13 (2010), pp. 1659–1686.

[LYH15] BA Le, Julien Yvonnet, and Q-C He. "Computational homogenization of nonlinear elastic materials using neural networks". In: *International Journal for Numerical Methods in Engineering* 104.12 (2015), pp. 1061–1084.

[Man72] J. Mandel. *Plasticité Classique Et Viscoplasticité: Course Held at the Department of Mechanics of Solids, September-October, 1971*. Springer, 1972. URL: https://books.google.es/books?id=zvHaoAEACAAJ.

[MB07] Christian Miehe and CG2344771 Bayreuther. "On multiscale FE analyses of heterogeneous structures: from homogenization to multigrid solvers". In: *International Journal for Numerical Methods in Engineering* 71.10 (2007), pp. 1135–1180.

[MH94] J.E. Marsden and T.J.R. Hughes. *Mathematical foundations of elasticity*. Dover Publications, 1994. ISBN: 0486678652.

[MHY11] E Monteiro, Q-C He, and Julien Yvonnet. "Hyperelastic large deformations of two-phase composites with membrane-type interface". In: *International journal of engineering science* 49.9 (2011), pp. 985–1000.

[Mie02] Christian Miehe. "Strain-driven homogenization of inelastic microstructures and composites based on an incremental variational formulation". In: *International Journal for numerical methods in engineering* 55.11 (2002), pp. 1285–1322.

[MK02] Christian Miehe and Andreas Koch. "Computational micro-to-macro transitions of discretized microstructures undergoing small strains". In: *Archive of Applied Mechanics* 72.4 (2002), pp. 300–317.

[MKG08] Karel Matouš, Mohan G Kulkarni, and Philippe H Geubelle. "Multiscale cohesive failure modeling of heterogeneous adhesives". In: *Journal of the Mechanics and Physics of Solids* 56.4 (2008), pp. 1511–1533.

[MM15] Matthew Mosby and Karel Matouš. "Hierarchically parallel coupled finite strain multiscale solver for modeling heterogeneous layers". In: *International Journal for Numerical Methods in Engineering* 102.3-4 (2015), pp. 748–765.

[MO02] J Merodio and RW Ogden. "Material instabilities in fiber-reinforced nonlinearly elastic solids under plane deformation". In: *Archives of Mechanics* 54.5-6 (2002), pp. 525–552.

[Moo40a] M. Mooney. "A theory of large elastic deformation". In: *Journal of applied physics* 11.9 (1940), pp. 582–592.

[Moo40b] Melvin Mooney. "A theory of large elastic deformation". In: *Journal of applied physics* 11.9 (1940), pp. 582–592.

[MP05] Sinisa Dj Mesarovic and Jagan Padbidri. "Minimal kinematic boundary conditions for simulations of disordered microstructures". In: *Philosophical Magazine* 85.1 (2005), pp. 65–78.

[MPG07a] TJ Massart, RHJ Peerlings, and MGD Geers. "Structural damage analysis of masonry walls using computational homogenization". In: *International journal of damage mechanics* 16.2 (2007), pp. 199–226.

[MPG07b] TJ Massart, RHJ Peerlings, and MGD1194 Geers. "An enhanced multiscale approach for masonry wall computations with localization of damage". In: *International journal for numerical methods in engineering* 69.5 (2007), pp. 1022–1059.

[MR18a] JG Murphy and GA Rogerson. "Modelling slight compressibility for hyperelastic anisotropic materials". In: *Journal of Elasticity* 131.2 (2018), pp. 171–181.

[MR18b] JG Murphy and GA Rogerson. "Modelling slight compressibility for hyperelastic anisotropic materials". In: *Journal of Elasticity* 131.2 (2018), pp. 171–181.

[MS15] JG Murphy and G Saccomandi. "Exploitation of the linear theory in the non-linear modelling of soft tissue". In: *Mathematics and Mechanics of Solids* 20.2 (2015), pp. 190–203.

[MSS99a] Christian Miehe, Jan Schotte, and Jörg Schröder. "Computational micro–macro transitions and overall moduli in the analysis of polycrystals at large strains". In: *Computational Materials Science* 16.1-4 (1999), pp. 372–382.

[MSS99b] Christian Miehe, Jörg Schröder, and Jan Schotte. "Computational homogenization analysis in finite plasticity simulation of texture development in polycrystalline materials". In: *Computer methods in applied mechanics and engineering* 171.3-4 (1999), pp. 387–418.

[Mur13] JG3107472 Murphy. "Transversely isotropic biological, soft tissue must be modelled using both anisotropic invariants". In: *European Journal of Mechanics-A/Solids* 42 (2013), pp. 90–96.

[MYH08] E Monteiro, Julien Yvonnet, and Qi-Chang He. "Computational homogenization for nonlinear conduction in heterogeneous materials using model reduction". In: *Computational Materials Science* 42.4 (2008), pp. 704–712.

[NA+13a] Aisling Ní Annaidh et al. "Deficiencies in numerical models of anisotropic nonlinearly elastic materials". In: *Biomechanics and modeling in mechanobiology* 12.4 (2013), pp. 781–791.

[NA+13b] Aisling Ní Annaidh et al. "Deficiencies in numerical models of anisotropic nonlinearly elastic materials". In: *Biomechanics and modeling in mechanobiology* 12.4 (2013), pp. 781–791.

[Nez+09] S Nezamabadi et al. "A multilevel computational strategy for handling microscopic and macroscopic instabilities". In: *Computer Methods in Applied Mechanics and Engineering* 198.27-29 (2009), pp. 2099–2110.

[Ngu+12] Vinh Phu Nguyen et al. "Computational homogenization for multiscale crack modeling. Implementational and computational aspects". In: *International Journal for Numerical Methods in Engineering* 89.2 (2012), pp. 192–226.

[Nil+14] Filip Nilenius et al. "Computational homogenization of diffusion in three-phase mesoscale concrete". In: *Computational Mechanics* 54.2 (2014), pp. 461–472.

[Niy+14] Innocent Niyonzima et al. "Nonlinear computational homogenization method for the evaluation of eddy currents in soft magnetic composites". In: *IEEE transactions on magnetics* 50.2 (2014), pp. 61–64.

[NM16a] DR Nolan and JP McGarry. "On the compressibility of arterial tissue". In: *Annals of biomedical engineering* 44.4 (2016), pp. 993–1007.

[NM16b] DR Nolan and JP McGarry. "On the compressibility of arterial tissue". In: *Annals of biomedical engineering* 44.4 (2016), pp. 993–1007.

[NN14] V-D Nguyen and Ludovic Noels. "Computational homogenization of cellular materials". In: *International Journal of Solids and Structures* 51.11-12 (2014), pp. 2183–2203.

[NNH13a] Siavouche Nemat-Nasser and Muneo Hori. *Micromechanics: overall properties of heterogeneous materials*. Elsevier, 2013.

[NNH13b] Siavouche Nemat-Nasser and Muneo Hori. *Micromechanics: overall properties of heterogeneous materials*. Elsevier, 2013.

[Nol+14a] David R Nolan et al. "A robust anisotropic hyperelastic formulation for the modelling of soft tissue". In: *Journal of the mechanical behavior of biomedical materials* 39 (2014), pp. 48–60.

[Nol+14b] David R Nolan et al. "A robust anisotropic hyperelastic formulation for the modelling of soft tissue". In: *Journal of the mechanical behavior of biomedical materials* 39 (2014), pp. 48–60.

[NTT19] S Nishi, K Terada, and I396376807073975 Temizer. "Isogeometric analysis for numerical plate testing of dry woven fabrics involving frictional contact at meso-scale". In: *Computational Mechanics* 64.1 (2019), pp. 211–229.

[NZY11] Saeid Nezamabadi, Hamid Zahrouni, and Julien Yvonnet. "Solving hyperelastic material problems by asymptotic numerical method". In: *Computational mechanics* 47.1 (2011), pp. 77–92.

[OAK19a] Daniel J O'Shea, Mario M Attard, and David C Kellermann. "Hyperelastic constitutive modelling for transversely isotropic composites and orthotropic biological tissues". In: *International Journal of Solids and Structures* 169 (2019), pp. 1–20.

[OAK19b] Daniel J O'Shea, Mario M Attard, and David C Kellermann. "Hyperelastic constitutive modelling for transversely isotropic composites and orthotropic biological tissues". In: *International Journal of Solids and Structures* 169 (2019), pp. 1–20.

[ÖBG08a] I Özdemir, WAM Brekelmans, and MGD2376223 Geers. "Computational homogenization for heat conduction in heterogeneous solids". In: *International journal for numerical methods in engineering* 73.2 (2008), pp. 185–204.

[ÖBG08b] I Özdemir, WAM Brekelmans, and MGD2479126 Geers. "FE2 computational homogenization for the thermo-mechanical analysis of heterogeneous solids". In: *Computer Methods in Applied Mechanics and Engineering* 198.3-4 (2008), pp. 602–613.

[Ogd72] Raymond William Ogden. "Large deformation isotropic elasticity–on the correlation of theory and experiment for incompressible rubberlike solids". In: *Proceedings of the Royal Society of London. A. Mathematical and Physical Sciences* 326.1567 (1972), pp. 565–584.

[Ogd73] RW Ogden. "Large deformation isotropic elasticity-on the correlation of theory and experiment for incompressible rubberlike solids". In: *Rubber Chemistry and Technology* 46.2 (1973), pp. 398–416.

[Ogd74] RW Ogden. "On the overall moduli of non-linear elastic composite materials". In: *Journal of the Mechanics and Physics of Solids* 22.6 (1974), pp. 541–553.

[Ogd78a] RW Ogden. "Nearly isochoric elastic deformations: application to rubberlike solids". In: *Journal of the Mechanics and Physics of Solids* 26.1 (1978), pp. 37–57.

[Ogd78b] RW Ogden. "Nearly isochoric elastic deformations: application to rubberlike solids". In: *Journal of the Mechanics and Physics of Solids* 26.1 (1978), pp. 37–57.

[Ogd97] Raymond W Ogden. *Non-linear elastic deformations*. Courier Corporation, 1997.

[ÖLR13] Mikael Öhman, Fredrik Larsson, and Kenneth Runesson. "Computational homogenization of liquid-phase sintering with seamless transition from macroscopic compressibility to incompressibility". In: *Computer Methods in Applied Mechanics and Engineering* 266 (2013), pp. 219–228.

[OOM18] Fermin Otero, Sergio Oller, and Xavier Martinez. "Multiscale computational homogenization: review and proposal of a new enhanced-first-order method". In: *Archives of Computational Methods in Engineering* 25.2 (2018), pp. 479–505.

[O'S+20a] Daniel J O'Shea et al. "Nonlinear finite element formulation based on invariant-free hyperelasticity for orthotropic materials". In: *International Journal of Solids and Structures* 185 (2020), pp. 191–201.

[O'S+20b] Daniel J O'Shea et al. "Nonlinear finite element formulation based on invariant-free hyperelasticity for orthotropic materials". In: *International Journal of Solids and Structures* 185 (2020), pp. 191–201.

[PD15] JA Plews and CA Duarte. "Bridging multiple structural scales with a generalized finite element method". In: *International Journal for Numerical Methods in Engineering* 102.3-4 (2015), pp. 180–201.

[Pen14a] Thomas J Pence. "Distortion of anisotropic hyperelastic solids under pure pressure loading: compressibility, incompressibility and near-incompressibility". In: *Journal of Elasticity* 114.2 (2014), pp. 251–273.

[Pen14b] Thomas J Pence. "Distortion of anisotropic hyperelastic solids under pure pressure loading: compressibility, incompressibility and near-incompressibility". In: *Journal of Elasticity* 114.2 (2014), pp. 251–273.

[Per+11] D Perić et al. "On micro-to-macro transitions for multi-scale analysis of non-linear heterogeneous materials: unified variational basis and finite element implementation". In: *International Journal for Numerical Methods in Engineering* 87.1-5 (2011), pp. 149–170.

[Pie+16a] B Pierrat et al. "Finite element implementation of a new model of slight compressibility for transversely isotropic materials". In: *Computer methods in biomechanics and biomedical engineering* 19.7 (2016), pp. 745–758.

[Pie+16b] B Pierrat et al. "Finite element implementation of a new model of slight compressibility for transversely isotropic materials". In: *Computer methods in biomechanics and biomedical engineering* 19.7 (2016), pp. 745–758.

[PKG13] Kim Pham, Varvara G Kouznetsova, and Marc GD Geers. "Transient computational homogenization for heterogeneous materials under dynamic excitation". In: *Journal of the Mechanics and Physics of Solids* 61.11 (2013), pp. 2125–2146.

[PSK20] Martyna Poreba-Sebastjan and Wacław Kuś. "Decoupled homogenization of hyperelastic composite with carbon black inclusion". In: *Computer Methods in Materials Science* 20.1 (2020), pp. 14–21.

[QS07a] Ramon Quintanilla and Giuseppe Saccomandi. "The importance of the compatibility of nonlinear constitutive theories with their linear counterparts". In: (2007).

[QS07b] Ramon Quintanilla and Giuseppe Saccomandi. "The importance of the compatibility of nonlinear constitutive theories with their linear counterparts". In: (2007).

[RE54] RS Rivlin and JL Ericksen. "Large elastic deformations of homogeneous anis-tropic materials". In: *Jour. Rat. Mech. Anal* 3 (1954), pp. 281–301.

[Riv48a] Ronald S Rivlin. "Large elastic deformations of isotropic materials. II. Some uniqueness theorems for pure, homogeneous deformation". In: *Philosophical Transactions of the Royal Society of London. Series A, Mathematical and Physical Sciences* 240.822 (1948), pp. 491–508.

[Riv48b] Ronald S Rivlin. "Large elastic deformations of isotropic materials IV. Further developments of the general theory". In: *Philosophical transactions of the royal society of London. Series A, Mathematical and physical sciences* 241.835 (1948), pp. 379–397.

[Riv48c] R.S. Rivlin. "Large elastic deformations of isotropic materials. I. Fundamental concepts". In: *Philosophical Transactions of the Royal Society of London. Series A, Mathematical and Physical Sciences* 240.822 (1948), pp. 459–490.

[Riv49a] Ronald Samuel Rivlin. "Large elastic deformations of isotropic materials. V. The problem of flexure". In: *Proceedings of the Royal Society of London A: Mathematical, Physical and Engineering Sciences*. Vol. 195. 1043. The Royal Society. 1949, pp. 463–473.

[Riv49b] Ronald Samuel Rivlin. "Large elastic deformations of isotropic materials. VI. Further results in the theory of torsion, shear and flexure". In: *Philosophical Transactions of the Royal Society of London A: Mathematical, Physical and Engineering Sciences* 242.845 (1949), pp. 173–195.

[Riv51] RS Rivlin. "Mechanics of large elastic deformations with special reference to rubber". In: *Nature* 167.4250 (1951), pp. 590–591.

[RM87] J Renard and MF Marmonier. "Etude de l'initiation de l'endommagement dans la matrice d'un matériau composite par une méthode d'homogénéisation". In: *La Recherche aérospatiale* 6 (1987), pp. 43–51.

[RP20] Yves Renard and Konstantinos Poulios. "GetFEM: Automated FE modeling of multiphysics problems based on a generic weak form language". In: *ACM Transactions on Mathematical Software (TOMS)* 47.1 (2020), pp. 1–31.

[RS51a] Ronald S Rivlin and DW Saunders. "Large elastic deformations of isotropic materials. VII. Experiments on the deformation of rubber". In: *Philosophical Transactions of the Royal Society of London A: Mathematical, Physical and Engineering Sciences* 243.865 (1951), pp. 251–288.

[RS51b] RS Rivlin and DW Saunders. "Experiments on the deformation of rubber large elastic deformations of isotropic materials VII". In: *Phil. Trans. R. Soc. Lond. A* 243 (1951), pp. 251–88.

[Sac15] Giuseppe Saccomandi. "Nonlinear elasticity for soft fibrous materials". In: *Nonlinear mechanics of soft fibrous materials*. Springer, 2015, pp. 121–173.

[Sai+21] Risa Saito et al. "A decoupling scheme for two-scale finite thermo-viscoelasticity with thermal and cure-induced deformations". In: *International Journal for Numerical Methods in Engineering* 122.4 (2021), pp. 1133–1166.

[San08a] Carlo Sansour. "On the physical assumptions underlying the volumetric-isochoric split and the case of anisotropy". In: *European Journal of Mechanics-A/Solids* 27.1 (2008), pp. 28–39.

[San08b] Carlo Sansour. "On the physical assumptions underlying the volumetric-isochoric split and the case of anisotropy". In: *European Journal of Mechanics-A/Solids* 27.1 (2008), pp. 28–39.

[Sau+22] Klaus Bernd Sautter et al. "Limitations of the St. Venant-Kirchhoff material model in large strain regimes". In: *International Journal of Non-Linear Mechanics* (2022), p. 104207.

[SBG14] A Salvadori, E Bosco, and D31750491323 Grazioli. "A computational homogenization approach for Li-ion battery cells: Part 1–formulation". In: *Journal of the Mechanics and Physics of Solids* 65 (2014), pp. 114–137.

[SBM98] Robert JM Smit, WA Marcel Brekelmans, and Han EH Meijer. "Prediction of the mechanical behavior of nonlinear heterogeneous systems by multi-level finite element modeling". In: *Computer methods in applied mechanics and engineering* 155.1-2 (1998), pp. 181–192.

[SL13] Javier Segurado and Javier Llorca. "Simulation of the deformation of polycrystalline nanostructured Ti by computational homogenization". In: *Computational Materials Science* 76 (2013), pp. 3–11.

[SLR11] Fang Su, Fredrik Larsson, and Kenneth Runesson. "Computational homogenization of coupled consolidation problems in micro-heterogeneous porous media". In: *International journal for numerical methods in engineering* 88.11 (2011), pp. 1198–1218.

[Slu+00] O Van der Sluis et al. "Overall behaviour of heterogeneous elastovisco-plastic materials: effect of microstructural modelling". In: *Mechanics of Materials* 32.8 (2000), pp. 449–462.

[SN03a] J Schröder and P Neff. "On the construction of polyconvex anisotropic free energy functions". In: *IUTAM Symposium on Computational Mechanics of Solid Materials at Large Strains*. Springer. 2003, pp. 171–180.

[SN03b] Jörg Schröder and Patrizio Neff. "Invariant formulation of hyperelastic transverse isotropy based on polyconvex free energy functions". In: *International journal of solids and structures* 40.2 (2003), pp. 401–445.

[SN03c] Jörg Schröder and Patrizio Neff. "Invariant formulation of hyperelastic transverse isotropy based on polyconvex free energy functions". In: *International journal of solids and structures* 40.2 (2003), pp. 401–445.

[SNB05] Jörg Schröder, Patrizio Neff, and Daniel Balzani. "A variational approach for materially stable anisotropic hyperelasticity". In: *International journal of solids and structures* 42.15 (2005), pp. 4352–4371.

[SP80] Enrique Sánchez-Palencia. "Non-homogeneous media and vibration theory". In: *Lecture notes in physics* 127 (1980).

[SP83] E Sanchez-Palencia. "Homogenization method for the study of composite media". In: *Asymptotic Analysis II—*. Springer, 1983, pp. 192–214.

[Spe72] Anthony James Merrill Spencer. "Deformations of fibre-reinforced materials". In: (1972).

[Spe84] Anthony James Merrill Spencer. "Constitutive theory for strongly anisotropic solids". In: *Continuum theory of the mechanics of fibre-reinforced composites*. Springer, 1984, pp. 1–32.

[Spe85] Anthony JM Spencer. *Continuum theory of the mechanics of fibre-reinforced composites*. 1985.

[STP85a] JC Simo, Robert L Taylor, and KS822744 Pister. "Variational and projection methods for the volume constraint in finite deformation elasto-plasticity". In: *Computer methods in applied mechanics and engineering* 51.1-3 (1985), pp. 177–208.

[STP85b] JC Simo, Robert L Taylor, and KS822744 Pister. "Variational and projection methods for the volume constraint in finite deformation elasto-plasticity". In: *Computer methods in applied mechanics and engineering* 51.1-3 (1985), pp. 177–208.

[Suq85] PM Suquet. *Local and global aspects in the mathematical theory of plasticity, Plasticity Today, Sawczuk, A. et al. eds*. 1985.

[Tem14a] I Temizer. "Computational homogenization of soft matter friction: isogeometric framework and elastic boundary layers". In: *International Journal for Numerical Methods in Engineering* 100.13 (2014), pp. 953–981.

[Tem14b] I Temizer. "Multiscale thermomechanical contact: Computational homogenization with isogeometric analysis". In: *International journal for numerical methods in engineering* 97.8 (2014), pp. 582–607.

[Ter+00] Kenjiro Terada et al. "Simulation of the multi-scale convergence in computational homogenization approaches". In: *International Journal of Solids and Structures* 37.16 (2000), pp. 2285–2311.

[Ter+13a] K Terada et al. "A method of two-scale analysis with micro-macro decoupling scheme: application to hyperelastic composite materials". In: *Computational Mechanics* 52.5 (2013), pp. 1199–1219.

[Ter+13b] K Terada et al. "A method of two-scale analysis with micro-macro decoupling scheme: application to hyperelastic composite materials". In: *Computational Mechanics* 52.5 (2013), pp. 1199–1219.

[Ter+14a] K Terada et al. "An adaptive method for homogenization in orthotropic nonlinear elasticity". In: *Advanced Composite Materials* 23.5-6 (2014), pp. 421–450.

[Ter+14b] Kenjiro Terada et al. "Applicability of micro–macro decoupling scheme to two-scale analysis of fiber-reinforced plastics". In: *Advanced Composite Materials* 23.5-6 (2014), pp. 421–450.

[TK01] Kenjiro Terada and Noboru Kikuchi. "A class of general algorithms for multi-scale analyses of heterogeneous media". In: *Computer methods in applied mechanics and engineering* 190.40-41 (2001), pp. 5427–5464.

[TK95] Kenjiro Terada and Noboru Kikuchi. "Nonlinear homogenization method for practical applications". In: *American Society of Mechanical Engineers, Applied Mechanics Division, AMD* 212 (1995), pp. 1–16.

[TN04] Clifford Truesdell and Walter Noll. *The non-linear field theories of mechanics*. Springer, 2004.

[Tra+11] AB Tran et al. "A simple computational homogenization method for structures made of linear heterogeneous viscoelastic materials". In: *Computer Methods in Applied Mechanics and Engineering* 200.45-46 (2011), pp. 2956–2970.

[Tre43] LRG Treloar. "The elasticity of a network of long-chain molecules. I". In: *Transactions of the Faraday Society* 39 (1943), pp. 36–41.

[Tru52] Clifford Truesdell. "The mechanical foundations of elasticity and fluid dynamics". In: *Journal of Rational Mechanics and Analysis* 1 (1952), pp. 125–300.

[TT60] Clifford Truesdell and Richard Toupin. "The classical field theories". In: *Principles of classical mechanics and field theory/Prinzipien der Klassischen Mechanik und Feldtheorie*. Springer, 1960, pp. 226–858.

[TW07] I Temizer and P Wriggers. "An adaptive method for homogenization in orthotropic nonlinear elasticity". In: *Computer Methods in Applied Mechanics and Engineering* 196.35-36 (2007), pp. 3409–3423.

[TZO96] Naoki Takano, Masaru Zako, and Yoshihiro Ohnishi. "Macro-micro uncoupled homogenization procedure for microscopic nonlinear behavior analysis of composites". In: *Journal of the Society of Materials Science, Japan* 45.6Appendix (1996), pp. 81–86.

[VE07] Eric Vanden-Eijnden. "Heterogeneous multiscale methods: a review". In: *Communications in Computational Physics2 (3)* (2007), pp. 367–450.

[Ver+10] Clemens V Verhoosel et al. "Computational homogenization for adhesive and cohesive failure in quasi-brittle solids". In: *International Journal for Numerical Methods in Engineering* 83.8-9 (2010), pp. 1155–1179.

[Ver+13a] Luigi Vergori et al. "On anisotropic elasticity and questions concerning its finite element implementation". In: *Computational Mechanics* 52.5 (2013), pp. 1185–1197.

[Ver+13b] Luigi Vergori et al. "On anisotropic elasticity and questions concerning its finite element implementation". In: *Computational Mechanics* 52.5 (2013), pp. 1185–1197.

[VL67] KC Valanis and RF Landel. "The Strain-Energy Function of a Hyperelastic Material in Terms of the Extension Ratios". In: *Journal of Applied Physics* 38.7 (1967), pp. 2997–3002.

[Wei11] E Weinan. *Principles of multiscale modeling*. Cambridge University Press, 2011.

[Wie+14] Marcin Wierszycki et al. "A two-scale approach for trabecular bone microstructure modeling based on computational homogenization procedure". In: *Computational Mechanics* 54.2 (2014), pp. 287–298.

[WL18] Monan Wang and Fengjie Liu. "Compressible hyperelastic models for soft biological tissue: a review". In: *Journal of Biomaterials and Tissue Engineering* 8.10 (2018), pp. 1375–1389.

[WL20] MN Wang and FJ Liu. "A compressible anisotropic hyperelastic model with $I_5$ and $I_7$ strain invariants". In: *Computer Methods in Biomechanics and Biomedical Engineering* 23.16 (2020), pp. 1277–1286.

[WMG96a] Jeffrey A Weiss, Bradley N Maker, and Sanjay Govindjee. "Finite element implementation of incompressible, transversely isotropic hyperelasticity". In: *Computer methods in applied mechanics and engineering* 135.1-2 (1996), pp. 107–128.

[WMG96b] Jeffrey A Weiss, Bradley N Maker, and Sanjay Govindjee. "Finite element implementation of incompressible, transversely isotropic hyperelasticity". In: *Computer methods in applied mechanics and engineering* 135.1-2 (1996), pp. 107–128.

[WW03] Jay R Walton and J Patrick Wilber. "Sufficient conditions for strong ellipticity for a class of anisotropic materials". In: *International journal of non-linear mechanics* 38.4 (2003), pp. 441–455.

[Yeo90] O.H. Yeoh. "Characterization of elastic properties of carbon-black-filled rubber vulcanizates". In: *Rubber chemistry and technology* 63.5 (1990), pp. 792–805.

[YGH09] Julien Yvonnet, D Gonzalez, and Q-C He. "Numerically explicit potentials for the homogenization of nonlinear elastic heterogeneous materials". In: *Computer Methods in Applied Mechanics and Engineering* 198.33-36 (2009), pp. 2723–2737.

[YH07] Julien Yvonnet and Q-C He. "The reduced model multiscale method (R3M) for the non-linear homogenization of hyperelastic media at finite strains". In: *Journal of Computational Physics* 223.1 (2007), pp. 341–368.

[YMH13] Julien Yvonnet, Eric Monteiro, and Qi-Chang He. "Computational homogenization method and reduced database model for hyperelastic heterogeneous structures". In: *International Journal for Multiscale Computational Engineering* 11.3 (2013).

[Yua+14] Zheng Yuan et al. "Reduced-order multiscale-multiphysics model for heterogeneous materials". In: *International Journal for Multiscale Computational Engineering* 12.1 (2014).

[Yvo19] Julien Yvonnet. *Computational homogenization of heterogeneous materials with finite elements*. Vol. 258. Solid Mechanics and Its Applications. London: Springer, 2019.

[ZM13] Dominic Zäh and Christian Miehe. "Computational homogenization in dissipative electro-mechanics of functional materials". In: *Computer Methods in Applied Mechanics and Engineering* 267 (2013), pp. 487–510.

[ZWZ15] Xiaoying Zhuang, Qing Wang, and Hehua Zhu. "A 3D computational homogenization model for porous material and parameters identification". In: *Computational Materials Science* 96 (2015), pp. 536–548.

FOLIO ADMINISTRATIF

THÈSE DE L'INSA LYON, MEMBRE DE L'UNIVERSITÉ DE LYON

NOM : KAROUI
(avec précision du nom de jeune fille, le cas échéant)

DATE de SOUTENANCE : 06/12/2022

Prénoms : Sarra

TITRE : Contribution à l'homogénéisation d'une nappe fibrée en grande déformation: une méthode itérative découplée

NATURE : Doctorat

Numéro d'ordre : 2022INSAL0116

École doctorale : MEGA

Spécialité : Ingénierie Mécanique

RÉSUME : Nous proposons une approximation des grandes déformations élastiques d'une nappe hyper-élastique fibrée par une procédure numérique d'homogénéisation découplée à deux échelles. Les échelles non linéaires micro et macroscopiques sont fortement couplées dans la plupart des méthodes d'homogénéisation. Notre méthode est dérivée de celle proposée par Terada et al. qui consiste à découpler les échelles micro et macro en considérant des problèmes de valeurs limites séparés et une loi constitutive anisotrope intermédiaire optimisée sur un ensemble de tests. Nous proposons une procédure itérative basée sur cette méthode qui permet d'améliorer la qualité de l'approximation pour se rapprocher de l'homogénéisation couplée et garder un coût de calcul raisonnable. Nous réalisons des études numériques représentatives pour une couche avec un matériau hyper-élastique hétérogène afin de démontrer la capacité et la fiabilité de la méthode proposée et de tester plusieurs lois de comportements. La méthode peut être utilisée soit avec des lois homogénéisées simples, dans le cas où une telle loi simple spécifique peut être attendue, soit avec des lois plus complexes ou même entièrement paramétriques. Une optimisation des paramètres de la loi homogénéisée est effectuée hors ligne sur un ensemble de tests composé d'expériences numériques provenant d'une approximation par éléments finis du problème de la valeur limite (PVL) défini à l'échelle micro sur le VER. La forme de la loi homogénéisée choisie est évidemment cruciale pour le bon fonctionnement et l'efficacité de la méthode. Une fois les paramètres de la loi homogénéisée identifiés, celle-ci peut être utilisée pour représenter la réponse à micro-échelle et ensuite pour évaluer la réponse à macro-échelle. Afin d'améliorer la qualité de l'approximation fournie par la méthode découplée, nous proposons une méthode itérative dont l'objectif est d'adapter l'optimisation de la loi homogénéisée au calcul structurel considéré à un coût de calcul beaucoup plus faible que la méthode EF2.

MOTS-CLÉS : hyper-élasticité, méthode d'homogénéisation itérative découplée, nappe fibrée, composite, grande déformation

Laboratoire (s) de recherche : LaMCoS

Directeur de thèse: Yves RENARDS

Président de jury :

Composition du jury : Mikaël BARBOTEU - Rapporteur
Adnane BOUKAMEL - Rapporteur
Moez CHAFRA - Examinateur
Olfa TRABELSI - Examinatrice
Yves RENARD - Directeur
Makrem ARFAOUI - Co-Directeur

**Abstract**

In this thesis, we propose a procedure to approximate the large elastic deformations of a fiber reinforced layer by a two-scale decoupled homogenization numerical procedure. The nonlinear micro and macroscopic scales are strongly coupled in most homogenization methods. Our method is derived from the one proposed by Terada et al.which consists in decoupling the micro and macro scales by considering separate boundary value problems and an intermediate anisotropic constitutive law optimised over a training set. We propose an iterative procedure based on this method which allows to improve the quality of the approximation to get closer to the coupled homogenization and keeping a reasonable computational cost. We perform representative numerical studies for a layer with heterogeneous hyperelastic material in order to demonstrate the capability and reliability of the proposed method and test several intermediate constitutive laws. The method can be used either with simple homogenized laws, in the case such a specific simple law can be expected, or either with more complex or even fully parametric laws. An optimization of the homogenized law parameters is performed off-line on a training set composed of numerical experiments coming from a finite element approximation of the boundary value problem (BVP) defined at the micro-scale on the RVE. The shape of the chosen homogenized law is obviously crucial for the proper functioning and efficiency of the method. Once the parameters of the homogenized law have been identified, it can be used to represent the micro-scale response and then to evaluate the macro-scale response. In order to improve the quality of the approximation provided by the decoupled method, we propose an iterative method whose objective is to adapt the optimization of the homogenized law to the considered structural computation at a much lower computational cost than the $FE^2$ method.

**Résumé**

Dans cette thèse, nous proposons une approximation des grandes déformations élastiques d'une nappe hyperélastique fibrée par une procédure numérique d'homogénéisation découplée à deux échelles. Les échelles non linéaires micro et macroscopiques sont fortement couplées dans la plupart des méthodes d'homogénéisation. Notre méthode est dérivée de celle proposée par Terada et al.qui consiste à découpler les échelles micro et macro en considérant des problèmes de valeurs limites séparés et une loi constitutive anisotrope intermédiaire optimisée sur un ensemble de tests. Nous proposons une procédure itérative basée sur cette méthode qui permet d'améliorer la qualité de l'approximation pour se rapprocher de l'homogénéisation couplée et garder un coût de calcul raisonnable. Nous réalisons des études numériques représentatives pour une couche avec un matériau hyperélastique hétérogène afin de démontrer la capacité et la fiabilité de la méthode proposée et de tester plusieurs lois de comportements. La méthode peut être utilisée soit avec des lois homogénéisées simples, dans le cas où une telle loi simple spécifique peut être attendue, soit avec des lois plus complexes ou même entièrement paramétriques. Une optimisation des paramètres de la loi homogénéisée est effectuée hors ligne sur un ensemble de tests composé d'expériences numériques provenant d'une approximation par éléments finis du problème de la valeur limite (PVL) défini à l'échelle micro sur le VER. La forme de la loi homogénéisée choisie est évidemment cruciale pour le bon fonctionnement et l'efficacité de la méthode. Une fois les paramètres de la loi homogénéisée identifiés, celle-ci peut être utilisée pour représenter la réponse à micro-échelle et ensuite pour évaluer la réponse à macro-échelle. Afin d'améliorer la qualité de l'approximation fournie par la méthode découplée, nous proposons une méthode itérative dont l'objectif est d'adapter l'optimisation de la loi homogénéisée au calcul structurel considéré à un coût de calcul beaucoup plus faible que la méthode $EF^2$.